

---

# MECHANISMS OF TYROSINASE MEDIATED CROSSLINKING REACTIONS ENABLING THE SYNTHESIS OF HYDROGELS WITH POTENTIAL FOR PHARMACEUTICAL APPLICATIONS

---

Inaugural-Dissertation  
to obtain the academic degree  
Doctor rerum naturalium (Dr. rer. nat.)

submitted to the Department of Biology, Chemistry and Pharmacy  
of Freie Universität Berlin

by

Miroslava Racheva  
from Plovdiv, Bulgaria

2017

Aus dem Institut für Biomaterialforschung des Helmholtz-Zentrums Geesthacht unter  
Leitung von Herrn Prof. Dr. Andreas Lendlein, 2011-2017.

- 1. Gutachter: Prof. Dr. A. Lendlein
- 2. Gutachter: Prof. Dr. D. Klinger

Disputation am: 11.12.2017

# Acknowledgement

I would like to express my sincere gratitude to my supervisor Prof. Dr. Andreas Lendlein for giving me the opportunity to carry out the work for this thesis at the Institute of Biomaterial Science of HZG and for his valuable guidance and numerous scientific discussions. Prof. Lendlein is also especially thanked for the great support and particular consideration of my demanding personal situation throughout the last years.

I would like to gratefully acknowledge Prof. Dr. Daniel Klinger for reading and evaluating the thesis.

I would like to thank my mentor Dr. Christian Wischke for his continuous widespread support for all concerns, for helpful suggestions, advice and scientific discussions, which always brought me some steps further. I also thank Dr. Wischke for his talent and persistence in reviewing manuscripts, presentations, posters and the thesis. I am thankful to Dr. Axel Neffe, who always helped me with useful advices through chemical matters.

I am very thankful to Dr. Konstanze Julich-Gruner for her support in the chemical set-up of my work, introduction to chemical syntheses and some analytical methods, as well as for helpful discussions. I thank Dr. Julich-Gruner for her availability throughout these years, and for her ever-present positive spirit. My thank goes to Dr. Paul Hommes-Schattmann for introduction into semi-preparative HPLC and column chromatography. I would also like to thank Elen Bähr, who carried out a research internship and her master thesis with us, for the studies of enzyme kinetics, repetition of gelation kinetics experiments and the mTyr immobilization approaches. I am grateful to Frau Pfeiffer for technical support, helpful practical advices and her special kindness.

My particular thank goes to all current and former members of BWF and HZG, whom I had the pleasure to know and work with. A special thank goes to Dr. Fabian Frieß and Florian Störmann, with whom I sheared long times in the lab and outside and who made my work much more enjoyable. I wish to thank all PhD students of HZG for sharing knowledge, experience and exchanging loads of motivation.

A special thank goes to my partner and my family for providing mental support, standing my discouragement phases and devoting some extra time to our daughter in the last few months.



# Table of Contents

1	Introduction .....	1
1.1	Hydrogels.....	1
1.1.1	Structural aspects of hydrogels .....	1
1.1.2	Characterization of structure-property relationship .....	2
1.1.3	Applications for controlled release .....	4
1.2	Enzymes as biocatalysts in chemical syntheses .....	6
1.3	Enzymatically crosslinked hydrogels .....	7
1.4	Overview on tyrosinase catalyzed hydrogel synthesis .....	8
1.5	Biocatalysis by mushroom tyrosinase.....	10
2	Motivation, aims and hypotheses .....	15
2.1	Motivation .....	15
2.2	Aims and hypotheses .....	15
3	Concept and strategies.....	17
4	Biocatalysis by mTyr: synthesis of polymeric substrates and studies of enzyme activity.....	21
4.1	Synthesis of monofunctional DAT-IOEG <sub>OMe</sub> as model polymeric substrate .....	21
4.2	Synthesis and characterization of DAT and DATT functionalized four-arm sOEG .....	26
4.3	Selection of conditions for mTyr biocatalytic studies .....	28
4.4	Analysis of mTyr activity with DAT and DATT as substrates.....	33
4.5	Summary .....	38
5	Mechanistic analysis of mTyr catalyzed crosslinking of DAT and DAT-functionalized polymers .....	39
5.1	Overview on proposed crosslinking mechanisms and relevance for the selected system....	39
5.1.1	Factors affecting mTyr catalysis.....	40
5.1.2	Factors affecting non-enzymatic crosslinking.....	41
5.2	Investigation of mTyr catalyzed crosslinking by UV-Vis spectroscopy .....	43
5.3	Study of netpoint chemical structure by FT-IR spectroscopy.....	48
5.4	Study of netpoint chemical structure by NMR spectroscopy .....	50
5.5	Analysis of netpoint structure and functionality by MALDI-ToF .....	57
5.6	Analysis of netpoint structure and functionality by LC-ESI-MS.....	64
5.7	Evaluation of the influence of primary amines on the netpoint structure by model reactions and MS67	
5.8	Investigation of netpoint structure after hydrogel hydrolysis .....	71
5.9	Summary and rationale for selection of hydrogel precursors.....	77
6	Synthesis and characterization of hydrogels from DAT- and DATT-sOEG crosslinked by mTyr catalysis.....	79
6.1	Parameters to control bulk hydrogel formation .....	80
6.1.1	Control on gelation kinetics by precursor properties and mTyr concentration.....	81
6.1.2	Influence of degree of DATT functionalization on hydrogel properties.....	84

6.2	Physicochemical hydrogel characterization.....	86
6.2.1	Hydrogel analysis by NMR spectroscopy .....	86
6.2.2	Hydrogel Analysis by FT-IR spectroscopy .....	87
6.2.3	Gel content.....	89
6.2.4	Analysis of swelling behavior .....	90
6.2.5	Mechanical properties described by rheology .....	91
6.3	Diffusion of FITC dextran and determination of functional mesh size .....	94
6.4	Bulk hydrogels for release of bioactive molecules.....	99
6.4.1	Quantification of mTyr released from crosslinked hydrogels .....	99
6.4.2	Release of model bioactive compounds.....	100
6.5	Summary.....	102
7	Conclusions and outlook.....	105
8	Material and methods.....	111
8.1	Materials .....	111
8.2	Instrumental analysis of precursors, model reactions and hydrogels.....	111
8.3	Precursor synthesis.....	113
8.3.1	Synthesis of monofunctionalized DAT-IOEG <sub>OMe</sub> .....	113
8.3.2	Synthesis of DAT- and DATT-sOEG .....	114
8.4	Purification of monofunctional oligomers by RP-HPLC.....	114
8.5	Preparation of solutions .....	115
8.6	Kinetic studies with mTyr .....	116
8.6.1	Dopachrome Assay.....	116
8.6.2	MBTH Assay .....	117
8.7	Model reaction solution for structural analyses.....	118
8.7.1	UV spectroscopic analysis.....	118
8.7.2	NMR .....	118
8.7.3	MALDI-ToF.....	119
8.7.4	HPLC and LC-MS analysis.....	119
8.8	Hydrogel synthesis .....	119
8.9	Hydrogel characterization methods .....	120
8.9.1	Gelation kinetics.....	120
8.9.2	Gel content.....	120
8.9.3	Swelling.....	120
8.9.4	Rheology .....	121
8.9.5	FITC Dextran release .....	121
8.9.6	Tyrosinase extraction .....	122
8.9.7	Heparin release studies.....	122
8.10	Statistics and error evaluation .....	123
9	Abstract/Zusammenfassung .....	125
9.1	Abstract.....	125

9.2 Zusammenfassung.....	129
Appendices .....	133
I. Peer reviewed publications .....	133
II. References .....	133
III. Abbreviations & Symbols .....	145
IV. List of Figures.....	147
V. List of Tables.....	149
VI. Curriculum Vitae .....	150



# 1 Introduction

## 1.1 Hydrogels

---

Hydrogels are water-swollen polymer networks, which are insoluble due to the presence of crosslinks between polymers [1], entailing a defined three-dimensional architecture. The capacity of hydrogels to absorb and retain high amounts of water [2] enables mechanical properties, resembling soft-tissues, and makes them very appealing for biomedical application [3].

### 1.1.1 Structural aspects of hydrogels

The water uptake depends on the hydrophilicity of polymer chains, the presence of polar functional groups and on the amount and type of crosslinks [1]. Hydrogels can be categorized based on the nature of their netpoints into chemical and physical hydrogels. Physical hydrogels can be formed by e.g., ionic interactions (e.g. hydrogelation in polyampholites [4] or complexation of the  $\alpha$ -L-guluronic acid (G) blocks in alginate with  $\text{Ca}^{2+}$  [5, 6], or by guest-host interactions. [7, 8] The inherently weak hydrophobic interactions [9] can form stable structured domains in physical gels in case many residues interact with each other, e.g. leading to crystallization in poly(vinyl alcohol) (PVA), [10, 11] or aggregation of isopropyl groups in poly(*N*-isopropylacrylamide) (PNIPAAm). [12, 13] In biopolymers on the other side, chain aggregation by cooperative interactions lead to stable secondary structures, e.g. helices in gelatin [14] or fibrils in collagen. [15, 16] For synthetic polymers, network formation is realized by polymerization of active monomers, such as 2-hydroxyethyl methacrylate (HEMA) [17] or NVP, [18] or from macromolecular precursors. In the latter case, precursors with tailorable architectures can be synthesized, while the crosslinkable groups can be integrated throughout the polymer backbone or be present as macromer terminal crosslinkable groups. Networks from linear bifunctional precursors could be formed only if netpoint functionality  $f \geq 3$ , i.e. one crosslink connects at least 3 polymer chains.

Polymer networks consist of polymer segments and a certain volume of netpoints (Fig. 1A), defined as crosslinking density,  $v_c$ . Synthetic networks are usually not homogeneous and contain clusters of high  $v_c$ , which are randomly distributed within regions of low  $v_c$  with respective high swelling.[3, 19] Discrepancies from idealized network architecture include chain junctions with  $f < 4$ , chain loops, resulting e.g. from intramolecular crosslinking, dangling chains ( $f = 1$ ) which do not contribute to the permanent elasticity of the network, [20, 21] as well as molecular entanglements as effective physical netpoints.[20, 22] Due to the random nature of the crosslinking process, only average values for the segment molecular weight between crosslinks,  $M_c$  (Fig. 1A), can be determined by theoretical approaches (see Ch. 1.1.2). The average mesh size  $\xi$ , i.e. the average linear distance between two adjacent crosslinks (Fig. 1A), is another important structural parameter of interest, which governs the diffusion of macromolecules in- and outwards of the network.[23]

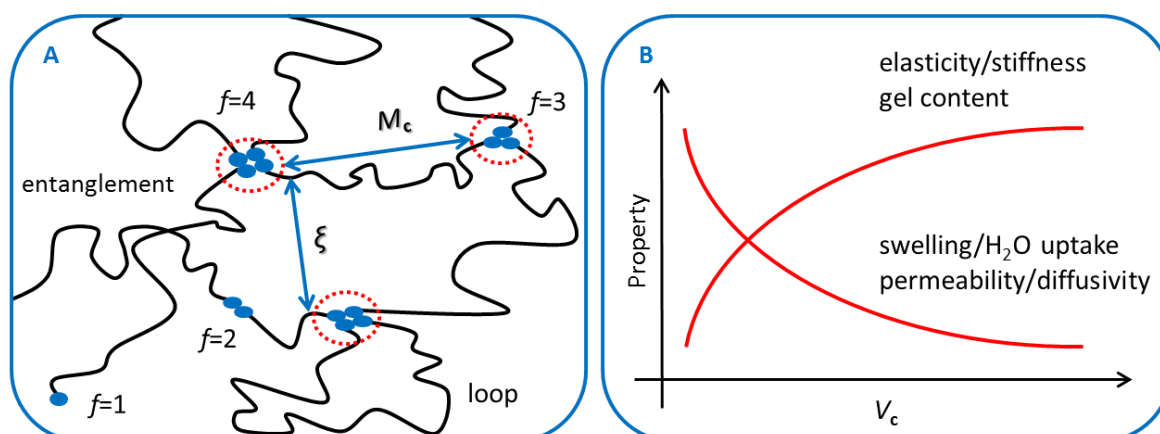


**Figure 1: A scheme of network structure and network structure-property relationship**

(A): visualization of a hydrogel network with flexible polymer segments (black), bearing crosslinkable end groups (blue circles) and netpoints (dashed red circles); average segment molecular weight between netpoints  $M_c$ ; average mesh size  $\xi$ ; netpoint functionality  $f$ : netpoints ( $f \geq 3$ ) and network defects: dangling chains ( $f = 1$ ), intramolecular loops and physical entanglements; (C): a schematic of the dependence of hydrogel properties on crosslinking density  $v_c$ , modified from [24].

As illustrated in Fig. 1B, the properties of hydrogels can be adjusted by tailoring of network molecular structure. Some hydrogel characteristics of interest, which may give insight into the network structure are described in the following chapter.

### 1.1.2 Characterization of structure-property relationship

The incorporation of precursor reactive groups into a network is essential parameter to adjust the formation of hydrogels with desirable properties. The gel content  $G$  shows

the effectivity of the covalent crosslinking reaction and can be determined by the dry masses of hydrogels before ( $m_0$ ) and after extraction of unreacted precursors ( $m_{ex}$ ):

$$G \text{ (wt\%)} = \frac{m_{ex}}{m_0} \cdot 100 \quad (\text{Eq. 1})$$

Another important property of networks is volumetric degree of swelling ( $Q$ ). Experimentally,  $Q$  is determined by the volume ratio between swollen and dry sample and can be calculated considering the mass of the dry sample  $m_d$ , the mass of the equilibrium swollen sample  $m_{sw}$ , the specific density of the solvent  $\rho_s$  and the density of the polymer network  $\rho_p$  according to eq. 2.

$$Q \text{ (vol\%)} = 1 + \rho_p \left( \frac{m_{sw}}{m_d \cdot \rho_s} - \frac{1}{\rho_s} \right) \cdot 100 \quad (\text{Eq. 2})$$

On the molecular level, swelling is a thermodynamically driven process, governed by the heat of mixing and an entropy increase by stretching of the polymer molecules towards dissolution. The retractive elastic force of the network arising from the netpoints limits the swelling and determines the swelling equilibrium, where the osmotic pressure and the elastic force are balanced. [22] Therefore, the swelling capacity is related to the amount of netpoints, which is estimated by the average molecular weight between crosslinks,  $M_c$ . The swelling  $Q$  and  $M_c$  were correlated by the theory of Flory-Rehner (Eq. 3) for networks, obeying the affine network model. [25] Here, the number-average molecular weight of the polymer chains  $M_n$ , the polymer volume fraction in the swollen state  $v_{sw} = Q^{-1}$ , the molar volume of water  $V_1$  and the polymer-solvent interaction parameter  $\chi$  are taken into consideration.

$$\frac{1}{M_c} = \frac{2}{M_n} - \frac{\bar{v}}{V_1} \frac{(\ln(1-v_{sw}) + v_{sw} + \chi \cdot v_{sw}^2)}{\sqrt[3]{v_{sw}} - v_{sw}/2} \quad (\text{Eq. 3})$$

The crosslinking density,  $\nu_c$  refers to the number of netpoints in a specified volume and can be determined by the equation  $\nu_c = \rho_p/M_c$ . Accordingly, the average mesh size can be predicted by  $M_c$  according to Eq. 4, where  $C_n$  is a constant (the Flory characteristic ratio),  $M_r$  is the molecular weight of the repeating unit and  $l$  is the bond length along the polymer backbone. [26]

$$\xi = \sqrt{\frac{2 \cdot C_n \cdot M_c}{M_r}} \cdot v_{sw}^{-1/3} \cdot l \quad (\text{Eq. 4}),$$

When interpreting the network structure, it should be taken into account that  $M_c$  and the parameters derived thereof, i.e.  $\nu_c$  and  $\xi$  are accessible by a theoretical model, which is applicable to idealized networks. Therefore,  $M_c$  does not regard network defects and

inhomogeneities, being discussed in Ch. 1.1.1. For networks, which are derived from telechels, the architecture of the precursors should also be taken into consideration.[27]

Alternatively, hydrogel mechanical properties may give information on the network molecular structure. The hydrogels mechanics in the swollen state can be investigated by rheology, whereby applying small amplitude oscillatory shear to networks to study their viscoelastic response.[28] Herein, the storage modulus  $G'$  measures the deformation energy, being elastically stored in the material, while the loss modulus  $G''$  shows the portion dissipated energy by viscous flow during shearing.[29] According to the rubber elasticity theory, a sample deformation, e.g. across a shear gap, as applied in rheology, leads to displacement of the netpoints and conformational change of the segments, followed by complete recovery of the hydrogel dimensions, being based on the entropy-elasticity of crosslinked networks according to the affine network model.[30, 31] Thus, the average mesh size  $\xi$  can be determined from rheological analysis using  $G'$  according to Eq. 5, when taking into account the universal gas constant  $R$  ( $8.31 \text{ J}\cdot\text{mol}^{-1}\cdot\text{K}^{-1}$ ), the absolute temperature  $T$  and the Avogadro constant  $N_A$  ( $6.022\cdot 10^{23} \text{ mol}^{-1}$ ). [32, 33]

$$\xi = \left( \frac{G' \cdot N_A}{R \cdot T} \right)^{-1/3} \quad (\text{Eq. 5})$$

The hydrogel mesh size as effective area for solute diffusion is essential in view of potential biomedical applications of the hydrogels. Precise control on properties by modifying hydrogel molecular architecture is desired towards broad applicability of hydrogels systems in different areas. [34]

### 1.1.3 Applications for controlled release

Hydrogels found various applications in everyday life, e.g. as superabsorbers, [35, 36] or wound dressings, [37] but also hold a great promise towards biomedical applications owing to their hydrophilic character and the potential biocompatibility, e.g. in tissue engineering [38, 39] and as matrices for cell delivery. [40] Beside the typical compatibility to soft tissues, water-swollen networks may be a suitable environment for sensitive bioactive molecules. Thereby, hydrogels were already widely used for pharmaceutical applications as matrices to release drugs, [41-43] peptides and proteins. [38, 44, 45]

While the liberation of bioactive compounds in polymeric systems with low affinity to water is predominantly governed by the degradation and/or swelling of the matrix

material, the release of molecules from water-swollen hydrogels is mainly controlled by their diffusion. General approaches to modify the release function of hydrogels include design of polymeric systems with functionalities to enhance physical interactions between polymer and loaded compound (Fig. 2.2A-E), or covalent immobilization of the loaded molecules (Fig. 2.2F). Commonly used physical interactions of the payload with polymer molecules include hydrophobic or ionic interactions, hydrogen bonds, molecular recognition by aptamers or antibodies, as reviewed by Neffe, Wischke, Racheva and Lendlein. [46] Nevertheless, these concepts may require complex modification of the macromolecules and strong physical interactions with the polymeric matrix may lead to too slow release or in case of proteins, even irreversible change of the payload structure.

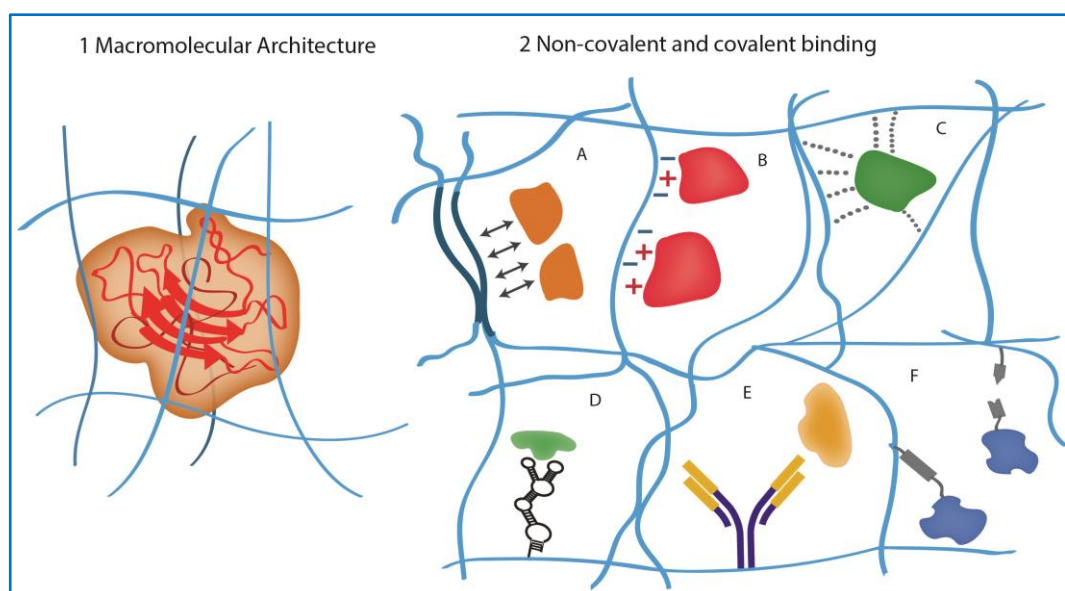


**Figure 2: Concepts for controlled release from hydrogels:**

*Design of hydrogel macromolecular architecture (1), binding of drug to polymer matrix (2): non-covalent polymer-drug interactions: hydrophobic (A), ionic (B) interactions, hydrogen bonding (C) and molecular recognition by aptamers (D) or antibodies (E); covalent binding of drugs. Reprinted with permission from [46] © 2013 Taylor & Francis Group*

Changing the molecular architecture of hydrogels, on the other side, is a universally applicable strategy. Control on the hydrogel mesh size is a desirable but particularly challenging approach, which was investigated in this work.

The payload encapsulation may be realized after gel formation by diffusion into the network, [38] which however often leads to poor encapsulation efficiencies. Loading of the hydrogel matrix prior to network formation allows quantitative incorporation of the solute and homogenous distribution. [45] The latter superior loading strategy requires a mild and selective crosslinking chemistry to preserve the structure of the payload.

Hydrogel synthesis by enzymatic crosslinking, being currently intensively investigated, [47] may fulfil these requirements, and may be applicable to in situ forming hydrogels, enabling minimally invasive administration and site-specific treatment. The enzymatically mediated hydrogel formation is further described in Ch. 1.3.

## 1.2 Enzymes as biocatalysts in chemical syntheses

---

Enzymes can increase the rate of chemical reactions by lowering the activation energy and stabilizing a transition state with respect to the reference reactions. [48] Similarly to conventional catalysts, being not modified during the catalyzed reactions, enzymes are typically regenerated by the formation of products and thus available to initiate a new catalytic cycle. Compared to metal or organic catalysts, which require high energy input, e.g. extreme temperature or pressure, enzymes function already in mild conditions [49] and can be easily deactivated by denaturation. Moreover, enzymes raise less toxicity concerns in contrast to conventional catalysts, where elaborate crude product purification from the catalysts [49, 50] as well as from toxic by-products [51] is required. Employing conventional catalysts in the large-scale industrial production of chemicals leads to a massive production of toxic waste and byproducts, as well as consumption of resources. [52, 53] Enzymes as biopolymers, on the other hand, are biodegradable and thus environmentally friendly.

Replacing conventional catalysis in industrial production processes was facilitated in the early 90s by the advances in gene engineering, which enabled the production of enzymes in large scales instead of their isolation from different sources [54] and initiated the development of white biotechnology. For the production of recombinant enzymes, the target enzyme-encoding gene should be first identified, then sequenced and cloned and the DNA is recombinantly overexpressed in host organisms, usually bacteria or yeast cell strains.[55] The final enzyme purification leads to high quality of the isolated biocatalyst. Furthermore, by a process termed directed evolution (combination of directed mutagenesis and screening of libraries), [56] it is possible to modify enzyme characteristics, such as stability, substrate specificity and turnover [57] to match the specific needs.

Due to the various advantages of enzymes as biocatalysts, they have long been used in food and cosmetic industry, [58] in production of pharmaceutical products, [59] e.g. antibiotics [53, 59] or chiral compounds owing to enzyme enantioselectivity.[57] Enzymes were also applied for catalysis of polymerization reactions, [60-63] as well as polymer functionalization.[64, 65] Due to the capacity of enzymes to convert polymeric substrates, they were also investigated for the synthesis of hydrogels.

### 1.3 Enzymatically crosslinked hydrogels

---

In contrast to conventional crosslinking reactions, the enzyme-mediated crosslinking approach is inspired by physiologically occurring processes, where the molecular recognition of sterically complementary molecules is the basis for the selective conversion of specific substrates.

Enzymatic catalysis was first applied for the stabilization of unmodified biopolymers by crosslinking with transglutaminases.[66] This approach resulted in high gelation times and too soft materials.[67, 68] Chemical modification of polymers with substrate-derived molecules significantly improved the performance of transglutaminase catalyzed crosslinking.[69-71]

Horseradish peroxidase (HRP) is an alternative biocatalyst being the most widely used enzyme for hydrogel synthesis. HRP enables fast crosslinking (within seconds) of phenol functionalized precursors by coupling of aromatic radicals in presence of  $H_2O_2$ . Different hydrogel systems were reported using synthetic precursors as well as biopolymers to form *in situ* hydrogels, [72] where the fast hydrogel formation could be tuned by varying the amount of enzyme and cofactor, or as recently reported, by dispersing liposomes within the hydrogels matrix as second system, releasing biocatalyst on demand.[73] These hydrogels were already applied for the delivery of proteins, [74, 75] or as cell matrices, [76] being also suitable as stem cell niches.[77, 78] Recently, hydrogels were synthesized from hyaluronic acid with tyramine and furan pendent groups by integrating a HRP mediated tyramine conjunction within a Diels Alder cyclo-addition reaction to couple furan residues with bifunctional maleimide-OEG crosslinkers, which improved cell compatibility of the hydrogels and enhanced their mechanical performance, enabling repeated recovery after loading.[79]

However, the application of cytotoxic  $H_2O_2$  is a serious concern associated with potential applications *in vivo* or involving cells. Thus, hydrogel systems were developed, in which the cosubstrate  $H_2O_2$  is exogenously supplied at a low rate, being immediately consumed [80] or generated during the crosslinking process by a second multi-enzyme cascade reaction.[81]

Mushroom tyrosinase, mTyr is an alternative enzyme, enabling hydrogel formation by oxidative phenol coupling. The crosslinking process is superior to HPR/ $H_2O_2$  in terms of cytocompatibility [76, 82] and the enzyme was not so intensively studied with regard to hydrogel formation, therefore mTyr will be investigated further here.

## 1.4 Overview on tyrosinase catalyzed hydrogel synthesis

The potential of mTyr to crosslink polymeric substrates was first described with synthetic peptides [83] and proteinous biopolymers, the latter being coupled to polysaccharides aiming mechanical stabilization for food industry applications.[84] Furthermore, mTyr was applied to synthesize hydrogels from macromolecular precursors, functionalized with artificial tyrosine-derived substrates. For example, terminally tyramine-functionalized poloxamer could be crosslinked by mTyr, while the limited chain immobilization allowed crowding of the hydrophobic domains into micellar structures on heating above 37 °C.[85] The gelation time and in some cases, the crosslinking density of hydrogels were shown to depend on the amount of bio-catalyst.[76, 86]

Further studied artificial polymeric substrates were gallate as natural polyphenol derivatives, which could initiate hydrogel formation by mTyr catalysis, when applied as terminal groups of branched 4-arm poly(ethylene glycol).[87] The crosslinking by mTyr catalysis was repeatedly reported to be compatible with different cell types, including stem cells,[76, 88, 89] underlining the potential of mTyr crosslinking for preparation of hydrogel matrices to encapsulate and release functional cells. Hydrogels were also formed when chitosan, containing nucleophilic primary amines, coupled with gelatin, bearing tyrosine moieties, which were activated by mTyr catalysis,[90, 91] showing that mTyr mediated phenol coupling is not the only possible crosslinking mechanism enabling hydrogel formation. Interestingly, mTyr was also demonstrated to disrupt peptide physical hydrogels, formed by  $\pi$ - $\pi$  interactions of tyrosine tetra-peptide building blocks,

which lost the ability for further physical interactions after mTyr catalyzed oxidation to non-aromatic amino acids in the peptides.[92] This study demonstrated the complex interactions of polymers, involving phenolic groups.

A big portion of the reported hydrogels basing on mTyr catalyzed crosslinking focused on precursors functionalized with catechol moieties being alternative mTyr substrates. Catechols belong to the main constituents in mussel byssus, which enable their unique properties, [93] and are relevant for the mechanical stability and enhanced adherence to various surfaces of catechol-bearing materials.[94] Moreover, polypeptide hydrogels could be formed by a combination of mTyr mediated covalent coupling of catechol moieties and their additional complexation of  $\text{Fe}^{3+}$ .[95] The same approach combining covalent and physical netpoints was reported for gelatin hydrogels, in which the  $\text{Fe}^{3+}$  complexing catechol groups were formed as intermediates in the mTyr mediated crosslinking pathway.[96] In another example combining different types of hydrogel netpoints, it was shown that mTyr could diffuse into covalent hydrogels when introduced after network formation, and mediate a further enhancement of the mechanical stability of hydrogels, applied for cell encapsulation.[97] This approach was also successful in self-assembled tyrosine-bearing peptide-based gels, which became stiffer after applying mTyr as biocatalyst, and the network stabilization was further increased by interactions of unreacted catecholic moieties with silica nanospheres.[98]

Recently, hydrogels from 4-arm OEGs functionalized with catechol or cyclooctyne terminal groups were synthesized by integrating mTyr catalysis for the formation of reactive quinone intermediates from catechols, within crosslinking of quinone and cyclooctyne according to a newly reported cyclooctyne-1,2-quinone cycloaddition (SPOCQ).[99] Combining the two approaches led to fast gelation and mechanics tailorable by varying the catechol to cyclooctyne ratio.[100] However, the possibility to click an azide-functionalized fluorescent probe in one pot into those hydrogels, having a balanced catechol:cyclooctyne ratio (by a competing strain promoted azide-alkyne cycloaddition, SPAAC) demonstrated that dangling chains remained by the SPOCQ crosslinking. Moreover, quinone-quinone coupling is expected to compete with the other introduced crosslinking reaction, SPOCQ, both taking place simultaneously and contributing to the hydrogel properties.

Furthermore, mTyr catalysis was successfully combined with a second enzymatic crosslinking process, e.g. with HRP [101] and transglutaminase, [89, 102, 103] where the researches made use of the tissue adhesion capacity of dopa intermediates, formed by mTyr catalysis.

In conclusion, the literature demonstrated the applicability of mTyr for hydrogel formation involving tyrosine, catechol and polyphenol groups in various oligomeric precursors. Many of the reported hydrogels focused on the hydrogel applications rather than control of the properties of the formed systems. The recent development of the topic showed that mTyr catalysis is predominantly employed in combination with other crosslinking approaches for hydrogel formation, increasing further the complexity of the systems. The examples of hydrogels synthesized by combining different crosslinking approaches demonstrated that mTyr catalyzed substrates conversion and the further spontaneous crosslinking may potentially not be quantitative. However, the contribution of the different crosslinking reactions in these rather complex systems was not addressed and remains unclear. Therefore, many mechanistic questions involving mTyr catalysis for hydrogel formation were not satisfactorily addressed previously. Understanding the catalysis process, as well as the following non-enzymatic reactions, being relevant for crosslinking, may give a deeper insight into the structure of hydrogels, formed by mTyr catalysis. This may allow to control the formation of hydrogels in order to achieve networks with desirable properties. Furthermore, the effect of systematic variation of precursor characteristics on the hydrogel properties was not yet comprehensively investigated, and will be further studied within this work.

## 1.5 Biocatalysis by mushroom tyrosinase

---

Tyrosinases (Tyr) are ubiquitously distributed in a wide range of organisms and differ in their tertiary structure and location within cells and tissues, [104] but are similar in function, arising from similarities in the binuclear copper active sites (classified as type 3 copper complexes). Physiologically, Tyr catalyze tyrosine oxidation as the rate-determining step towards the formation of the macromolecular biological pigments, melanins. Melanins are inherently heterogeneous in structure and their composition is defined by the availability of different substrates and depend on the type of organism. In

mammals, the tyrosine-derived reactive intermediates are subjected to spiro cyclization with the amino group in the side chain. The activated indole moieties form adducts with other indole derivatives or present nucleophilic functional groups. Conjugation of the indole derivatives predominantly with  $\text{NH}_2$  of basic amino acids leads to the formation of brown to black eumelanins, while the involvement of SH groups from cysteine residues during the spontaneous oligomerization result in the biosynthesis of reddish pheomelanins. In contrast, the biological pigments in other organisms, such as various plants, are free of sulphur and mostly nitrogen (allomelanins). Melanins are subscribed manifold protective functions, related to sclerotization of exoskeleton in mature insects, [105, 106] stabilization of cell walls or membranes related to wound healing [107] photoprotection through absorption of excessive UV irradiation, [108] antioxidation by free radical scavenging, as proven for synthetic melanins. [109]

Tyr from the common edible mushroom (*Agaricus bisporus*) is by far the most intensively studied model tyrosinase to investigate the chemistry of melanin formation due to its high homology with the human tyrosinase, stability and commercial availability. Mushroom tyrosinase (mTyr) is located in the cytoplasm and typically present in the latent form. The activation of mTyr takes place after cell injury as a part of their chemical defense mechanisms, protecting these organisms from pathogen invasion through an impermeable layer. [110] On the molecular level, the zymogen activation process of mTyr is realized by a proteolytic cleavage of a protein from the C-terminal domain. For the mTyr isoform PPO<sub>3</sub> (polyphenol oxidase 3), the protein fragment with size ~ 20 kDa was ascribed an active-site shielding function, achieved by interaction of a bulky phenylalanine residue with the active site, thereby preventing substrate binding. [111, 112]

MTyr has a molecular weight of approximately 120 kDa. Six different mTyr isoforms (PPO<sub>1</sub> to PPO<sub>6</sub>) [113, 114] were characterized in the mushroom extract. Analysis of the crystal structures of isoforms PPO<sub>3</sub> and PPO<sub>4</sub> verified the previously postulated heterotetrameric structure of the enzymes, being comprised of two heavy (H) chains of 43 kDa and two light (L) chains of 14-16 kDa. [115] The L chains are assumed to have a structure-stabilizing property, but their function is still not clarified [116, 117]. The H units, on the other hand, are defined as the catalytically relevant proteins. Six histidine residues coordinate the two copper ions (CuA and CuB) in the active site with their  $\text{N}_\epsilon$  atoms. The region is conserved by hydrogen bonds with the  $\text{N}_\delta$  atoms of these histidine residues, and

one of the CuB histidines is covalently fixed by a thioether bond to a neighboring cysteine.[113, 115]

Mature mTyr catalyzes two sequential reactions, using molecular oxygen as a cosubstrate: monophenol hydroxylation to *o*-diphenols (monophenolase activity), and the oxidation of the latter to the corresponding *o*-quinones (diphenolase activity). The active site can adopt four different oxidation states, as depicted in Fig. 3A.[118] The inactive enzyme (E) in the *deoxy* state is activated by binding O<sub>2</sub>, which is complexed Cu<sup>2+</sup> in the peroxy configuration in E<sub>oxy</sub> of mTyr. The E<sub>oxy</sub> form is competent in oxidation of phenols and catechols to *o*-quinones.[119] On the basis of crystal structures of bacterial Tyr from *Streptomyces castaneoglobisporus*, [120] it is hypothesized that monophenols approach the pocket of the active site in the *oxy* state, and change their orientation by a π-π interaction with one of the histidines on CuB, so that the phenolic C-O binds to the proximally lying CuA. The peroxy complex between the two Cu<sup>2+</sup> atoms rotates to a side-on conformation pointing towards the phenolic ring (Fig. 3B), enabling an electrophilic attack of the Cu<sub>2</sub>O<sub>2</sub> moiety at the *ortho*-position of the phenol to take place, leading to phenol hydroxylation with simultaneous O-O bond scission. Finally, two electrons are transferred to catechol, leading to a *o*-quinone molecule, and deactivation of mTyr to the E<sub>deoxy</sub> state. When *o*-diphenols bind to E<sub>oxy</sub>, the substrate oxidation to *o*-quinone leads to reduction of the active center to E<sub>met</sub>. In this state, both Cu<sup>2+</sup> ligate a hydroxyl ion and mTyr cannot bind monophenolic substrates and oxygen. E<sub>met</sub> can catalyze a second *o*-diphenol oxidation, leading to mTyr inactivation. The E<sub>deoxy</sub> state is regenerated to E<sub>oxy</sub>-mTyr by coordination of a O<sub>2</sub> molecule. If catechol is oxidized by E<sub>oxy</sub> following the oxidative mechanism for a phenolic substrates, the catechols can be hydroxylated to 3-hydroxybenzene derivatives (Fig.3A). The concomitant proton release results in reduction of Cu<sup>1+</sup> to Cu<sup>0</sup>, leading to irreversibly deactivated mTyr (suicide inactivation).

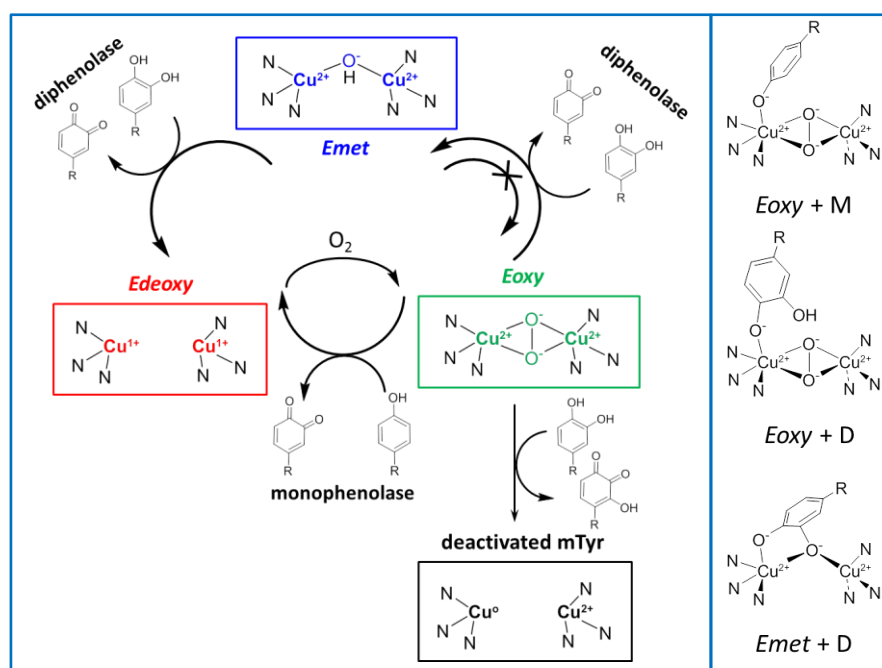


Figure 3: Scheme of the catalytic cycle of mTyr (A) and enzyme-substrate complexes (B).

The catalytic cycle in A) comprises four states of the mTyr active site: inactive mTyr Edeoxy state (red), active Eoxy (green) and Emet (blue) states and the dead-end pathway as a result of reductive Cu elimination (black), modified according to [118]; B) proposed structures of enzyme-substrate complexes with monophenols (M) and *o*-diphenols (D).

An initial lag phase is characteristic for the monophenolase activity of tyrosinases. During this phase of slow turnover of monophenolic substrates, a mTyr autoactivation process takes place. 85% of native mTyr is present in the *Emet* state, [121] which is not capable to catalyze phenol oxidation. The mTyr activation is initiated by a reaction with *o*-diphenol, which leads to the Edeoxy state of the active center. Subsequently, the enzyme can be transferred to the active Eoxy state after O<sub>2</sub> binding. The duration of lag phase ( $\tau$ ) depends on the concentration of enzyme, particularly in the Eoxy state [122] and monophenolic substrate.[123] Catalytic amounts of *o*-diphenol can minimize the length of the lag phase.[124, 125]

In conclusion, the catalytic oxidation of monophenol substrates is a complicated two-step process. The formed reactive intermediates further involve in non-enzymatic coupling reactions, which were not yet fully understood. Understanding occurring chemical processes finally leading to crosslinking of polymeric substrates, which will be attempted in this work, would allow to control them, in order to achieve materials with desired and tunable properties.



## 2 Motivation, aims and hypotheses

### 2.1 Motivation

---

Based on the capacity of enzymes to convert non-natural substrates sharing a specific structural moiety, polymeric substrates have recently gained substantial interest. Accordingly, enzyme mediated hydrogel formation has been considered as an alternative approach to form covalent networks in mild conditions for biomedical applications. A full understanding of the underlying mechanisms of hydrogel synthesis and the characteristics of enzymatically synthesized materials is of fundamental interest. A comprehensive knowledge on the processes of enzymatic and non-enzymatic pathways in crosslinking may allow to control the crosslinking process and to form hydrogels with well-defined and controllable architectures.

### 2.2 Aims and hypotheses

---

Within this thesis, the principles of hydrogel synthesis with tyrosinase as a ubiquitously distributed and physiologically relevant enzyme should be explored in depth including the selection of an artificial substrate, the analysis of the products of the crosslinking reactions, and the demonstration of applicability for the synthesis of hydrogels with structure-property relationships e.g. in terms of diffusion-controlled compound release.

The work bases on following hypotheses: (1) Desaminotyrosine (DAT) and desaminotyrosyl tyrosine (DATT) as amino-acid derivatives are suitable alternative substrates of mushroom tyrosinase (mTyr); (2) the use of DAT alone or in combination with suitable oligomers allows to explore the reaction principles and products formed by mTyr-initiated crosslinking reactions, (3) these substrates, employed as end groups of hydrophilic star-shaped oligomers enable mTyr mediated hydrogel synthesis; (4) hydrogel properties and diffusive characteristics can be controlled by application of precursors with different properties, amount of substrate and enzyme.



### 3 Concept and strategies

The following chapter describes the experimental approach towards investigation of the previously stated hypotheses. The selected enzyme oxidizes phenols in a two-step reaction. The following non-enzymatic cascade reactions of the reactive intermediates determine the complex heterogeneous structure of resulting oligomers and enable the final crosslinking, which should be explored.

Catechol polymer functionalities, which often build the basis for oxidation mediated covalent crosslinking, are prone to autooxidation. In contrast, phenol oligomerization is controlled only by enzyme mediated conversion to reactive intermediates. Therefore, the phenols desaminotyrosine (DAT) and desaminotyrosyl tyrosine (DATT) were studied for their potential to serve as substrates for mushroom tyrosinase (mTyr). DAT should enable oligomerization based on couplings at the aromatic ring rather than cyclization with side-chain amino groups, as common for *L*-tyrosine, e.g. during tyrosinase catalyzed melanin biosynthesis. DATT, which was not previously reported and comprises two phenol moieties per molecule, was investigated in terms of its potential to form more crosslinks in hydrogels as a result of the higher amount of potential active sites for adduct formation.

Oligo(ethylene glycol) was selected to be applied as oligomer backbone in the further investigations, since it is a stable uncharged hydrophilic precursor. The availability of OEGs with different properties and architectures, bearing various functional end groups is important in view of the planned mechanistic investigations. The limited protein adsorption of OEG is particularly appealing in the context of the planned work, since no interactions with mTyr are expected to influence the process of enzymatic catalysis.

One-step functionalization of linear and branched precursors with DAT and DATT was previously established [126] and the pharmaceutical relevance of the compounds was underlined by their cell compatibility [127] and the potential to stabilize colloidal particles.[128] The aromatic end groups of these amphiphilic compounds engage in physical interactions, which lead to surfactant-like properties [127, 128] rather than the formation of physical hydrogels. Therefore, the potential of branched DAT(T)-sOEGs as

macromolecular precursors for covalent hydrogels, formed by mTyr catalysis, should be investigated.

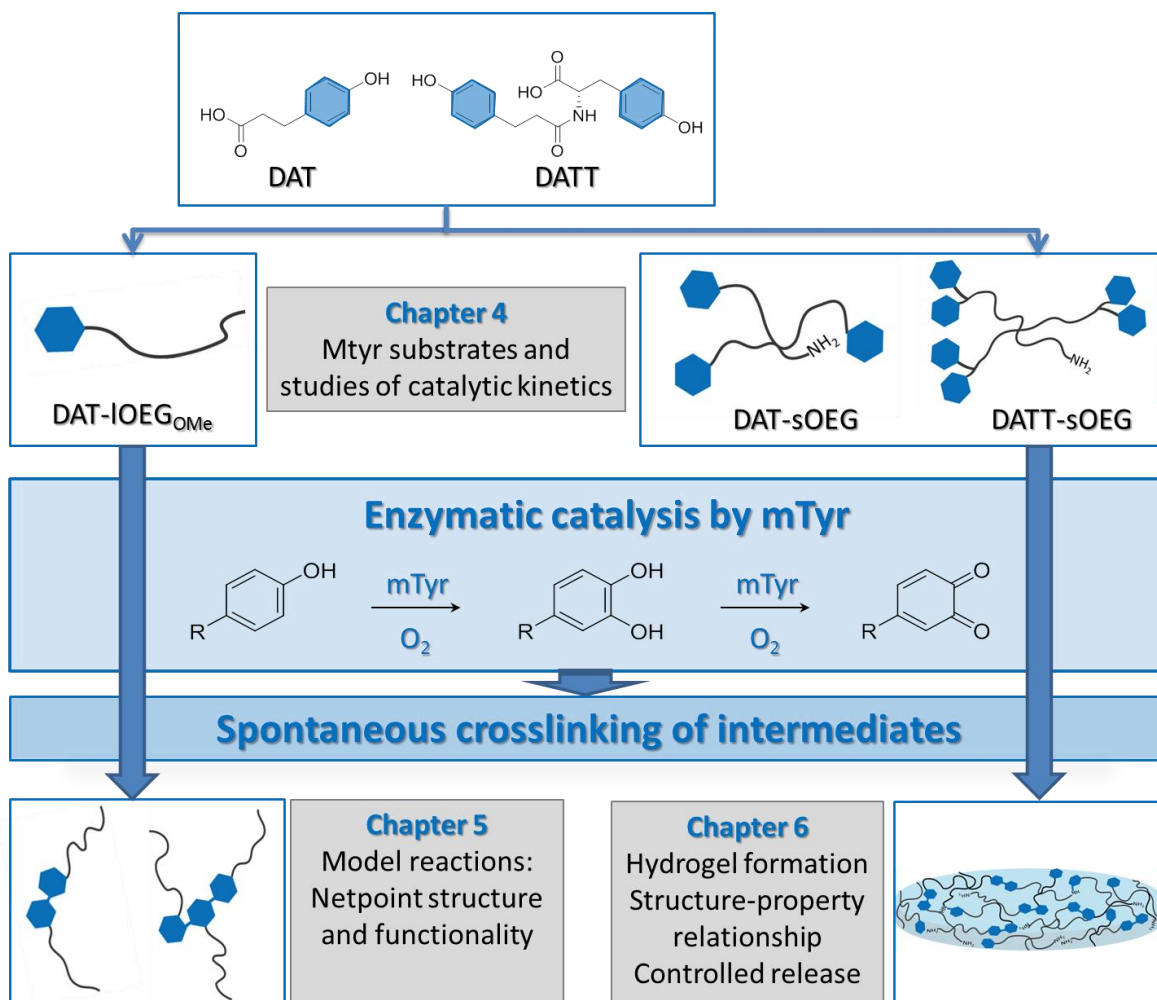


Figure 4: Concept of the planned experimental work.

The thesis is divided into three chapters addressing: the mTyr catalysis of free substrates (Ch.4), the investigation of enzymatic and non-enzymatic reactions of model monofunctional oligomeric substrates (Ch. 5) and the application of the crosslinking reactions for the synthesis of hydrogels, where a systematic variation of macroscopic and diffusive properties should be realized (Ch. 6).

In the first step, the applicability of free DAT and DATT as mTyr substrates should be investigated. DAT(T) functionalized model polymeric substrates with an OEG backbone should be synthesized. For this purpose, the principal conversion of free DAT and DATT by mTyr in buffered aqueous solutions should be explored in comparison to the natural substrates *L*-tyrosine and *L*-dihydroxyphenyl alanine (*L*-dopa) in kinetic studies. Furthermore, the optimal reaction conditions for mTyr should be determined and serve as a basis for establishing standardized conditions in order to have comparable mTyr activity in all further studies. Model substrates of single DAT(T) coupled to linear OEG with a second non-reactive end group, as well as four-arm star shaped precursors should be

synthesized enabling on the one hand mechanistic investigations of the crosslinking mechanisms, and hydrogel synthesis on the other hand.

In the second step, DAT-monofunctionalized linear OEG with a second unreactive methoxy end group (DAT-IOEG<sub>OMe</sub>) is selected as substrate for studying the types of reactions occurring in presence of mTyr. The precursor is expected to be converted to soluble oligomeric reactions products by mTyr catalysis, which should be further analyzed by different spectroscopic methodologies. UV-Vis, FT-IR and NMR spectroscopy should give insight on the reactive intermediates, formed by enzymatic catalysis, as well as on the following spontaneous reaction pathways. Further important aspects to be explored are the kinetics of enzymatic oxidation by applying free and oligomer-bound DAT. The structure and functionality of adducts, formed in model reactions with DAT-IOEG<sub>OMe</sub>, should be further investigated by MALDI-ToF and LC-ESI-MS analyses. An important aspect was the number of repeating units per netpoint being formed, for which both DAT with and without bulky oligomeric tail should be explored. The potential side reactions of the reactive intermediates with nucleophiles, in this case primary amino groups, should be included in the analysis of potential reaction products. Therefore, a narrowly distributed DAT-ImOEG<sub>OMe</sub> should be prepared, whereby the purity of the compound excluding non-functionalized NH<sub>2</sub>-ImOEG<sub>OMe</sub> was particularly important in order to distinguish on the favored mechanisms for crosslinking.

In the last step, the knowledge gained in the fundamental studies should be applied to synthesize hydrogels. For this, tetrafunctional star-shape sOEGs functionalized with DAT and DATT end groups should be employed. An in-depth knowledge on the hydrogel structure should be gained by a systematic variation of precursor properties and a comprehensive analysis of the physicochemical properties of the formed networks. Precursor differing in their end groups (DAT or DATT), segment length, i.e.  $M_n$  (5, 10 and 20 kDa), and degree of end group functionalization *d.f.* comprising different relative contents of DAT(T) substrate will be explored for their potential to form hydrogels. The network properties, as well as the gelation kinetics should be varied by applying different mTyr concentrations. Moreover, the hydrogel average mesh size should be investigated by subjecting rheological data to analysis by the rubbery elasticity theory, as well as by studying the diffusivity of FITC dextrans with varying molecular weights as model solutes.

Finally, the potential of selected hydrogels for controlled release of therapeutically relevant macromolecules should be investigated.

## 4 Biocatalysis by mTyr: synthesis of polymeric substrates and studies of enzyme activity

Within this chapter, the synthesis and characterization of artificial oligomeric mTyr substrates (precursors) for mechanistic studies (Ch. 4.1) and hydrogel synthesis (Ch. 4.2) are described. Furthermore, the mTyr catalytic activity towards natural and artificial substrates should be explored. This includes the analysis of experimental parameters on enzymatic activity and the selection of standardized conditions for further experiments (Ch. 4.3). The selected artificial substrates DAT and DATT were investigated in terms of mTyr activity and substrate-specific catalytic constants were calculated (Chapter 4.3).

### 4.1 Synthesis of monofunctional DAT-IOEG<sub>OMe</sub> as model polymeric substrate

---

For fundamental studies on the mTyr catalysis with artificial polymeric substrates, desaminotyrosine (DAT) functionalized OEG should be investigated. DAT instead of tyrosine was chosen since a one-step functionalization procedure without the need of protective groups can be applied. A linear oligo(ethylene glycol) (IOEG) oligomer with one unreactive methylated telechel ( $\text{OCH}_3$  end group, later referred to as OMe) and one functionalizable  $\text{NH}_2$  end group was selected for modification with DAT (Fig. 5). Due to the OEG monofunctionalization with DAT (DAT-IOEG<sub>OMe</sub>), the products of the after mTyr catalyzed DAT oxidation were expected to be soluble analytes instead of a crosslinked network.

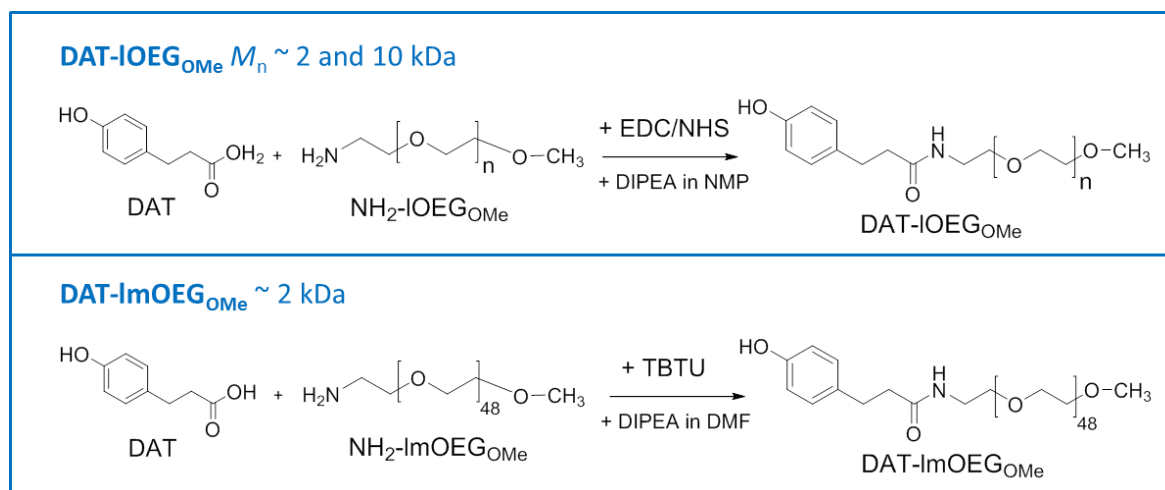


Figure 5: Applied approaches towards the synthesis of DAT-IOEG<sub>OMe</sub> and DAT-ImOEG<sub>OMe</sub> as model oligomeric mTyr substrates.

First, DAT-IOEG<sub>OMe</sub> 10 kDa was prepared according to an already established functionalization procedure, i.e. EDC/NHS activation of DAT carboxylic groups and subsequent amide coupling (Fig. 5). The protocol was adapted to achieve a high degree of end group functionalization (*d.f.*) (Ch. 8.3.1). Purification by precipitation and subsequent dialysis led to a *d.f.* of 87 mol% for DAT-IOEG<sub>OMe</sub> 10 kDa, as found by <sup>1</sup>H-NMR (Table 1). This oligomer was later applied to study mTyr catalyzed DAT oxidation by UV-Vis spectroscopy (Ch. 5.2).

Table 1: Summary of characteristics of different synthesized DAT-IOEG<sub>OMe</sub> oligomers

Oligomer	$M_n$ (kDa)	<i>d.f.</i> <sup>b</sup> (mol%)
DAT-ImOEG <sub>OMe</sub> 2 kDa	2.29 <sup>a</sup>	95 <sup>c</sup>
DAT-IOEG <sub>OMe</sub> 2 kDa	2.15 <sup>b</sup>	78 <sup>d</sup>
DAT-IOEG <sub>OMe</sub> 10 kDa	10.5 <sup>b</sup>	87 <sup>d</sup>

<sup>a</sup> mass of discrete derivative, as determined by MALDI-ToF; <sup>b</sup>  $M_n$  measured by MALDI-ToF, <sup>c</sup> *d.f.* estimated according to the MALDI analysis of DAT functionalized oligomers <sup>d</sup> degree of DAT functionalization, *d.f.* was calculated by <sup>1</sup>H-NMR.

Furthermore, an oligomer with lower  $M_n$  was desired in order to increase the DAT amount in solution at the standard polymer concentration of 5% (w/v). The resulting increase of the end group to oligomer signal ratio was desired for FT-IR and NMR spectroscopic studies as reported later (Ch. 5.3 and 5.4). An oligomer with  $M_n$  of 2 kDa (DAT-IOEG<sub>OMe</sub> 2 kDa) was synthesized according to a similar protocol as the bigger model substrate (Fig. 5). Due to the short OEG segment length, a quantitative purification by dialysis was challenging. Furthermore, DAT-IOEG<sub>OMe</sub> 2 kDa could not be purified by precipitation, because of the high solubility of OEG at this molecular weight and the

amphiphilic character of the precursor due to the relatively hydrophobic aromatic end groups. Therefore, a chromatographic purification procedure by semi-preparative RP-HPLC was established (Ch. 8.4). By this method, the purified product could be enriched with the desired DAT-IOEG<sub>OMe</sub> derivative and the *d.f.* was increased from 53 mol% to 78 mol% (Table 1). The identity and purity of the compound were verified by <sup>1</sup>H-NMR and FT-IR spectroscopy. A detailed interpretation of the spectra can be found in Ch. 5.4 (<sup>1</sup>H-NMR) and Ch. 4.4 and 5.3 (FT-IR). However, unfunctionalized NH<sub>2</sub>-IOEG<sub>OMe</sub>, as well as other oligomeric impurities from the commercial precursors could not be quantitatively removed. Linear OEG with OH instead of OMe and NH<sub>2</sub> end groups, as well as dimers with unknown structure were identified as minor impurities by MALDI-ToF and LC-MS (see Fig. 6).

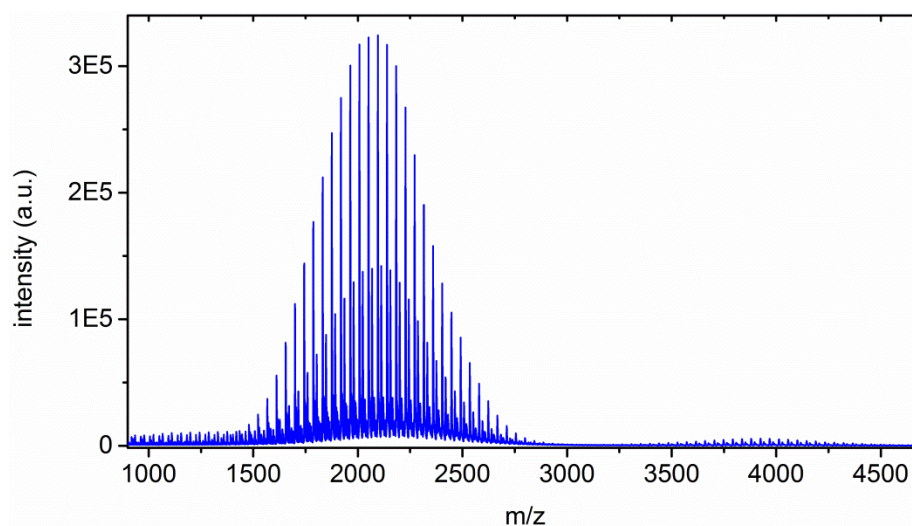
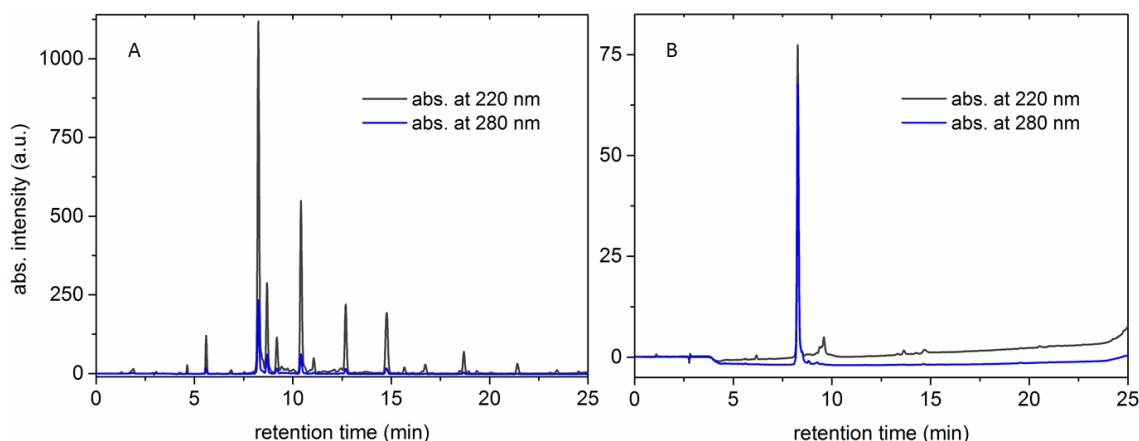


Figure 6: MALDI-ToF spectrum of DAT-IOEG<sub>OMe</sub> 2 kDa after purification by RP-HPLC (stationary phase based on polystyrene and divinylbenzene polymeric beads).

Based on the relatively broad size distribution of IOEG<sub>OMe</sub> 2 kDa, narrowly distributed, quasi monodisperse (further on abbreviated as m) NH<sub>2</sub>-ImOEG<sub>OMe</sub> with *M<sub>w</sub>* 145 Da was selected as additional model precursor for DAT functionalization (DAT-ImOEG<sub>OMe</sub>). This material should later be used in the analysis of netpoint structure by MS methodologies (Ch. 5.5 and 5.6). In order to achieve sufficiently high *d.f.*, here another synthesis procedure based on 2-(1H-Benzotriazole-1-yl)-1,1,3,3-tetramethyluronium tetrafluoroborate (TBTU) as a more potent DAT activator was selected (Fig. 5). For the final product DAT-ImOEG<sub>OMe</sub>, a *d.f.* of 75 mol% was demonstrated by <sup>1</sup>H-NMR (by relating the peak integrals of end group protons, i.e. the average areas of the aromatic and side chain protons of DAT and the area of the OMe protons, see Ch. 8.3.1), considering a *d.f.* relative error of up to 5%, as typical for peak integration in NMR

spectra. A chromatographic purification procedure of the product by RP-HPLC was chosen to remove unreacted chemicals and synthetic side products, as well as other oligomers to yield the desired DAT-ImOEG<sub>OMe</sub> in high purity.

Since purification of DAT-IOEG<sub>OMe</sub> 2 kDa from the educt, NH<sub>2</sub>-IOEG<sub>OMe</sub> 2 kDa by conventional RP-HPLC on C18 columns was not satisfactory, a method with a mixed stationary phase with balanced ratio of C18 and phenylpropyl groups was developed for DAT-ImOEG<sub>OMe</sub> purification here (Ch. 8.4). The aim was to attain stronger retention of aromatic compounds and achieve the desired product in high purity as should be used in subsequent investigation of netpoint structures (Ch. 5.5 and 5.6). The HPLC analysis of DAT-ImOEG<sub>OMe</sub> after synthesis (Fig. 7A) revealed the presence of side products. All peaks with retention times > 4.6 min were relatively sharp, as expected for narrowly distributed oligomers. By monitoring the chromatographic separation at 220 and 280 nm, the presence of DAT groups in the detected compounds could be verified by the absorption of phenols at 280 nm. Although DAT functionalization of NH<sub>2</sub>-ImOEG<sub>OMe</sub> was not quantitative (*d.f.* 75 mol% by NMR) in the crude product, the educt (main peak was eluted after 4.4 min, chromatogram not shown) was not detected by HPLC. The crude reaction product DAT-ImOEG<sub>OMe</sub> was purified by semi-preparative RP-HPLC, aiming to separate the desired compound (retention time 8.3 min) from the residual impurities. By this process, DAT-ImOEG<sub>OMe</sub> was almost quantitatively separated from other impurities (Fig. 7B). A slight tailing of the main peak indicated the presence of other oligomers, probably having higher molecular weights. A purity of 94% was calculated for DAT-ImOEG<sub>OMe</sub> by relating the areas of integrated peaks detected by HPLC at 280 and 220 nm (Table 1). It was assumed that the residual minor compounds could not be separated from DAT-ImOEG<sub>OMe</sub> due to the similar polarity of oligomers, differing only by one end group.



**Figure 8: Chromatograms of DAT-ImOEGOMe before (A) and after (B) semi-preparative purification**

The analysis was performed by RR-HPLC (column with C18/phenyl mixed phase, as used also for the purification) by a gradient elution (H<sub>2</sub>O and ACN as eluents with increasing ACN amount in the mobile phase) and monitored by UV detector ( $\lambda$  220 and 280 nm).

The narrow distribution and high purity of DAT-ImOEGOMe after chromatographic purification was confirmed by MALDI-ToF analysis. Mostly DAT-functionalized IOEGOMe species (abbreviated as P) were detected, as demonstrated in Fig. 8.

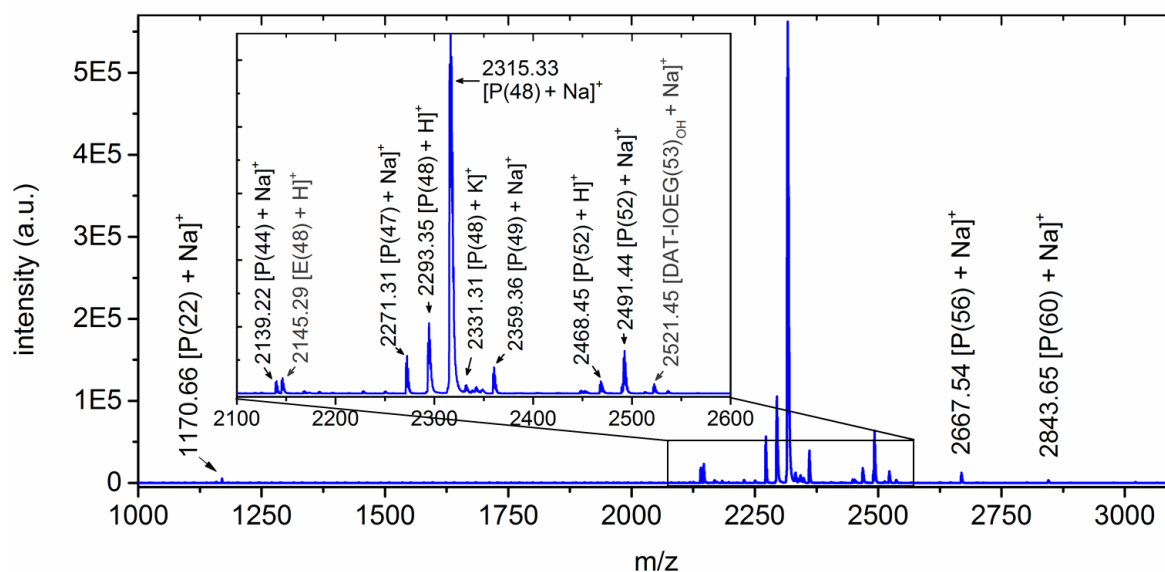


**Figure 7: MALDI-ToF spectrum of purified DAT-ImOEGOMe 2 kDa.**

*P* stands for product, i.e. DAT-ImOEGOMe, *E* for educt, i.e. NH<sub>2</sub>-IOEGOMe. The number of OEG repeating units, *n* is in parenthesis.

The main oligomer fraction in Fig. 8 consisted of DAT-ImOEGOMe derivatives with 47 to 49 ethylene glycol repeating units. Almost 80% of the detected oligomers in MALDI-ToF spectra belonged to the desired compound DAT-ImOEG(48)OMe, as calculated by relating the areas of all detected peaks to the areas of the peaks corresponding to the respective compound (most abundant DAT-ImOEG(48)OMe isotopes with theoretical  $m/z$  2293.36, 2315.33 and 2331.31 for P with counter ions H<sup>+</sup>, Na<sup>+</sup> and K<sup>+</sup>, respectively, see

Fig. 8). Only minor amounts of the detected oligomers were not functionalized with DAT. E.g., the educt  $\text{NH}_2\text{-IOEG}_{\text{OMe}}$  (abbreviated as E in Fig. 8) was detected in the product  $\text{DAT-ImOEG}_{\text{OMe}}$  by MALDI-ToF at a relative amount of only 1.4 mol% (calculated by integration of peak areas in MALDI-ToF). Therefore, this compound was expected to be suitable to investigate the crosslinking reactions mediated by mTyr in the subsequent model studies (Ch. 5.5 and 5.6).

## 4.2 Synthesis and characterization of DAT and DATT functionalized four-arm sOEG

Branched tetrafunctional, i.e. star-shaped oligo(ethylene glycol)s (sOEG) with terminal amino groups were selected as additional oligomers for functionalization with DAT and DATT. Based on their 4-arm structure, those precursors were expected to form hydrogels by mTyr catalysis. For a systematic study of the gelation ability and hydrogel properties, precursors with three different molecular weights, i.e. 5, 10 and 20 kDa were investigated.  $\text{NH}_2\text{-sOEGs}$  were functionalized with DAT and DATT by amide coupling with EDC/NHS, as previously established [126, 127] (structures shown in Fig. 9).

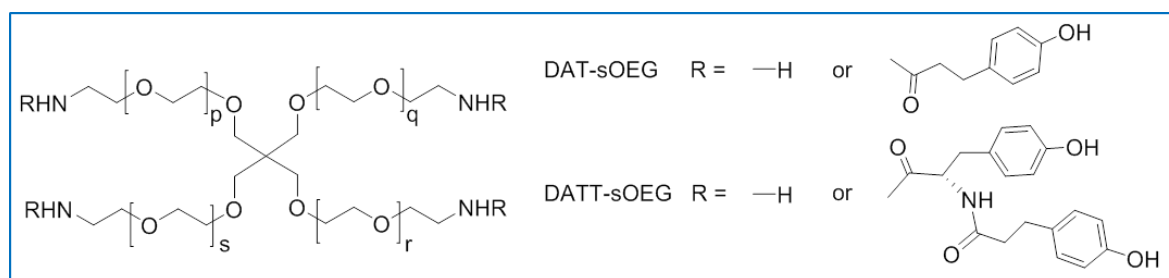


Figure 9: Chemical structures of DAT- and DATT-sOEG.

*R* indicates DAT(T) or H dependent on the d.f., i.e. statistical amount of functionalized end groups.

The presence of specific functional groups before and after DAT functionalization of  $\text{NH}_2\text{-sOEG}$  was studied by FT-IR spectroscopy. The spectra, shown in Fig. 10, displayed very intensive bands due to the absorption by the OEG segments: peaks at  $1095\text{ cm}^{-1}$  and  $2900\text{ cm}^{-1}$  corresponded to the stretching vibrations of C-O (s) and  $\text{sp}^3\text{-C-H}$  (m) of OEG respectively, and the peak at  $1465\text{ cm}^{-1}$  was assigned to the C-H bending vibration of the OEG repeating units. [129, 130] The unfunctionalized precursors exhibited a broad peak with a maximum at  $3440\text{ cm}^{-1}$  assigned to the N-H stretching vibration of aliphatic primary

amines. After DAT functionalization, a broad band with maximum at  $3340\text{ cm}^{-1}$  was detected, where N-H stretch of secondary amides, phenol O-H stretching and hydrogen bonds could be seen (residual  $\text{NH}_2$  groups of unfunctionalized DAT-sOEG arms were not detectable). Phenolic groups exhibited a further band at  $1180\text{ cm}^{-1}$  (associated to C-O stretching vibration or O-H in plane bending). [130, 131] The most conclusive region is depicted in the inset of Fig. 10. The band at  $1640\text{ cm}^{-1}$ , representing the N-H bend of primary amines in  $\text{NH}_2$ -sOEG, disappeared after functionalization.[87] Instead, the amide formation in DAT-sOEG was indicated by the broad bands at  $1660$  and  $1550\text{ cm}^{-1}$ , assigned to amide I (C=O stretch) and amide II (N-H bend), respectively. [129, 131] The successful incorporation of DAT in DAT-sOEG was further demonstrated by the bands at  $1616$  and  $1515\text{ cm}^{-1}$ , diagnostic of aromatic C=C stretch vibrations, as well as three bands of low intensity in the region  $1780$ - $1710\text{ cm}^{-1}$  representing characteristic aromatic combination vibrations of DAT aromatic groups.

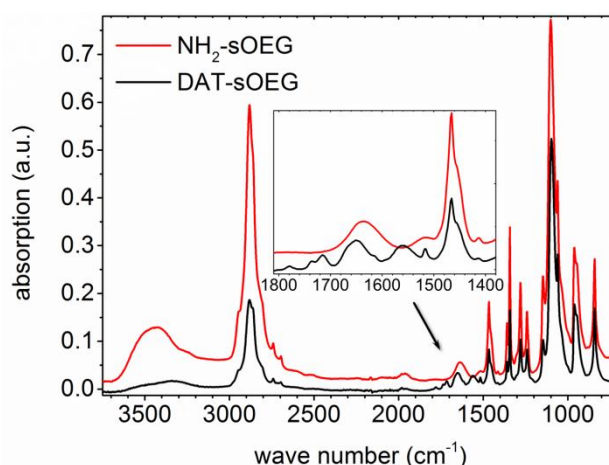


Figure 10: FT-IR spectra of DAT-sOEG 5 kDa (black) compared to the unfunctionalized precursor (red).

FT-IR, as well as  $^1\text{H-NMR}$  spectroscopic analyses revealed successful synthesis of the desired compounds in high purity. The properties of the synthesized compounds are summarized in Table 2. The degrees of DAT(T) functionalization (*d.f.*) of modified polymers were calculated by  $^1\text{H-NMR}$  by relating the integrals of peaks corresponding to protons of the aromatic DAT groups ( $\delta = 6.6$  and  $6.9\text{ ppm}$ ) or the  $\alpha$ -CH group of DATT ( $\delta = 4.4\text{ ppm}$ ), and the  $\text{CH}_2$  of the OEG repeating unit ( $\delta = 3.5\text{ ppm}$ ). Statistically, in average two to three out of four arms could be functionalized in repeated experiments. One possible explanations of the observed incomplete DAT(T) functionalization of all sOEG arms could be the incomplete amine functionalization of the commercial sOEGs, which was already observed in  $\text{NH}_2$ -IOEG<sub>OMe</sub> (Ch. 4.1). Furthermore, the architecture of the employed sOEG

may differ from an ideal scenario with all arms being of identical length, which may often not be true in synthesized materials. In this likely case, shorter OEG arms may not be available for further DAT(T) functionalization due to the steric hindrance by the other well solubilized or already functionalized neighbouring OEG chains.

Table 2: Summary of sOEG characteristics after DAT and DATT functionalization:  $M_n$  measured by MALDI-ToF, given in parenthesis, degrees of DAT(T) functionalization.

DAT-sOEG		DATT-sOEG	
$M_n^a$ (kDa)	<i>d.f.</i> <sup>b</sup> (mol%)	$M_n^a$ (kDa)	<i>d.f.</i> <sup>b</sup> (mol%)
5 (5.8)	62	5 (6.0)	64
10 (10.8)	61	10 (11.2)	66
20 (20.9)	52	20 (21.6)	51

<sup>a</sup>  $M_n$  values of sOEG precursors given by supplier were used further on for simplification reasons, since they were in good agreement with the values calculated by MALDI-TOF analysis, which are given in parenthesis. <sup>b</sup> *d.f.* were calculated by <sup>1</sup>H-NMR.

While network precursors with comparable *d.f.* of 51 to 66 mol% were selected as starting materials for hydrogel synthesis (Ch. 6.2 to 6.5), almost quantitative conversion of NH<sub>2</sub> end groups (90 mol%) could be achieved for DATT-sOEG 10 kDa selected to explore the influence of *d.f.* on the properties of DATT-sOEG networks as described in Ch. 6.1.2.

### 4.3 Selection of conditions for mTyr biocatalytic studies

In order to properly design the subsequent experiments, the principles of the mTyr catalyzed reactions and its activation process need to be considered. mTyr catalyzes a two-step oxidation of monophenols. Oxygen as a mTyr cosubstrate is consumed during the reaction as it is needed to regenerate mTyr from the inactive *Edeoxy* state to active *Eoxy* by complexation with Cu at the active site (Ch. 1.5). As visualized in Fig. 11, in the first step of biocatalysis,  $\frac{1}{2}O_2$  is used for *ortho* hydroxylation of monophenols to *o*-diphenol. The latter is subsequently oxidized to *o*-quinone with simultaneous oxygen reduction to H<sub>2</sub>O.

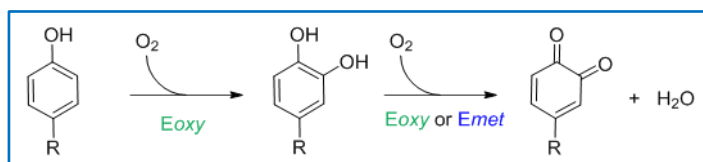


**Figure 11:** Scheme of the enzymatic conversion of monophenols to *o*-quinones (monophenolase mTyr cycle)

which takes place under the consumption of 1 mol  $O_2$ .<sup>[122]</sup> Phenols are substrates only to mTyr in the Eoxy state, while *o*-diphenols can be oxidized to *o*-quinones by the Eoxy and Emet mTyr states (diphenolase activity).

An initial lag phase of slow conversion of monophenolic substrates is characteristic for tyrosinases, until all of mTyr, being present in the native Emet state, <sup>[121]</sup> which is capable to oxidize *o*-diphenols, but not monophenols (Fig. 11), is transformed into Eoxy. Although catalytic amounts of *o*-diphenol can minimize the length of the lag phase, <sup>[124, 125]</sup> no *o*-diphenol derivative was added in the following kinetic studies with monophenols as substrates, since it may affect the subsequent non-enzymatic reactions, which should be investigated for pure DAT- and DATT-functionalized oligomers (Ch. 5 and 6). As the lag phase is characterized by low enzymatic activity, as described above, the mTyr activity towards monophenols in Ch. 4.3 and 4.4 had to be determined in the subsequent linear phase, in which kinetics were representative for the mTyr overall catalysis rate within the experiments.

Initially, the properties of commercial mTyr, extracted from the common mushroom *Agaricus bisporus*, were investigated with natural enzyme substrates. As solution medium, an isotonic PBS buffering to a physiological pH (7.4) was selected. The buffer was saturated with the cosubstrate  $O_2$ . Using this system, the effect of different factors such as pH, temperature and storage conditions on mTyr stability and activity towards *L*-tyrosine and *L*-dihydroxyphenyl alanine (*L*-dopa) as Tyr natural substrates should be explored.

A prerequisite to determine the substrate-specific enzyme activity is the saturation of mTyr active centers with the substrate. In this way, the observed initial rate of enzymatic conversion of the substrate is maximal (0. order kinetics). Due to the limited solubility of the studied phenolic substrates in aqueous buffers (1 mM used here), a low mTyr concentration in the nM range (calculated basing on mTyr  $M_r$  of 120 kDa) was applied (see Ch. 8.6).

The dopachrome assay <sup>[132]</sup> was chosen for mTyr activity analysis. By this method, the rate of *o*-quinone formation from monophenols can be indirectly determined by

spectroscopic measurement of the appearance of reddish dopachrome at 475 nm (see Fig. 52, Ch. 8.6.1). For an exact description of the kinetics, a quantitative conversion of *o*-quinone as a product of enzymatic oxidation, to dopachrome is needed. Since dopachrome autocatalytically polymerizes to melanin, the reaction was followed only within a limited time range (< 3 min) in which the amount of formed dopachrome is very low. Therefore, the rate and extent of the secondary spontaneous reactions can be neglected with respect to the dominating biocatalytic pathway.

The enzyme activity, given in U, is defined as the amount of product ( $\mu\text{mol}$ ) produced by an enzyme molecule per min. The specific activity in  $\text{U} \cdot \text{mg}^{-1}$ , visualized in Fig. 12 and 13, was calculated from the initial velocity of the enzymatic oxidation of the respective substrate, i.e. the slope  $\Delta A/\Delta t$  of absorbance at 475 nm per min according to Eq. 6. Here, the volumes of the substrate and enzyme solution,  $V_S$  and  $V_E$  respectively, the concentration of the mTyr solution  $c_E$ , the molar absorption coefficient ( $\epsilon_{475 \text{ nm}}=3600 \text{ M}^{-1} \cdot \text{cm}^{-1}$ ) and the path length ( $d=1 \text{ cm}$ ) are considered.

$$\text{specific activity (U} \cdot \text{mg}^{-1}\text{)} = \frac{\Delta A \cdot V_S}{\Delta t \cdot d \cdot V_E \cdot c_E \cdot \epsilon} \quad (\text{Eq. 6})$$

First, the pH optimum of mTyr in the selected buffer was studied at r.t. For this, the pH of PBS/ $\text{O}_2$  was adjusted to values between 5.5 and 7 by addition of HCl. The catalysis of substrate oxidation was not performed at  $\text{pH} > 7.4$ , because dopa autooxidation occurring at basic conditions would interfere with the assay. A lower activity of mTyr was observed at acidic conditions (pH 5.5 and 6.5) compared to neutral pH (Fig. 12A). This result is in accordance with the reported optimum of mTyr at pH 6.8-7.[133] As a high mTyr activity at the preferred physiological pH 7.4 comparable to pH 7 was confirmed, the further investigations were conducted at pH 7.4.

Furthermore, the effect of temperature on the substrate oxidation rate was studied. As apparent from Fig. 12B, the mTyr specific activity towards *L*-tyrosine and *L*-dopa was relatively low at 5 °C. The activity could be increased substantially by increasing the temperature to 25 °C and 37 °C (approximately 3.5 and 10-fold increase, respectively). It was reported that Tyr from other sources may show a temperature optimum at 40-45 °C. [134, 135] The further investigations were performed at r.t. for practical reasons, but a significantly faster oxidation rate can be expected if the reactions are performed at elevated temperature.

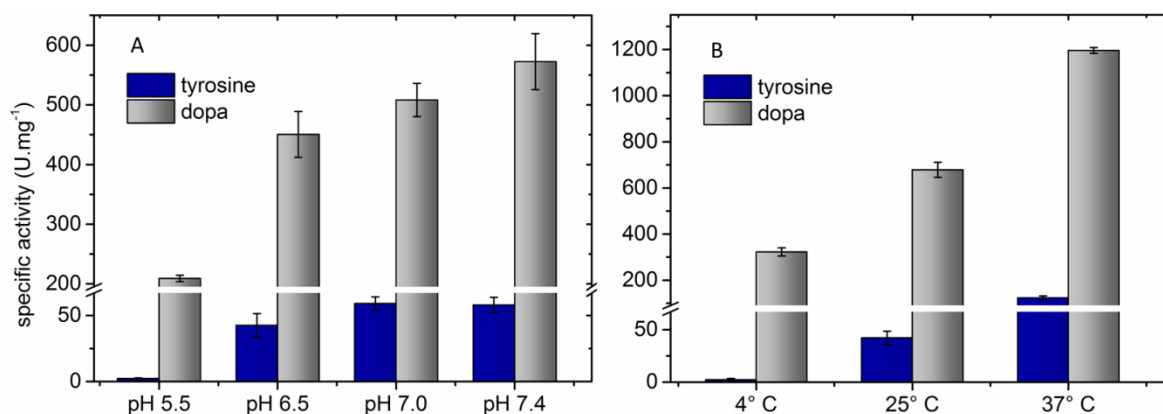


**Figure 12:** Specific activity of mTyr towards L-tyrosine (blue bars) and L-dopa (grey bars), which was tested in PBS/O<sub>2</sub> at different pH values at 25 °C (A) and at different temperatures at pH 7.4 (B). The activity was calculated by determining the linear slope of the enzymatic conversion of the substrates to dopachrome, measured at 475 nm ( $n=6$ ,  $\bar{x} \pm SD$ ). The experiments were conducted within a student internship.

Another important aspect when studying mTyr as a biocatalyst is its integrity and thus the preservation of its activity. Considering the specific activity of the employed mTyr (1715 U·mg<sup>-1</sup>), enzyme amounts in the  $\mu\text{g}$  range would be involved in most of the further studies. Thus, the application of stock solutions is necessary. The activity of enzymes typically decreases during storage in aqueous solutions. Therefore, the effect of mTyr stock solution storage at different conditions was investigated in comparison with freshly dissolved mTyr. As visualized in Fig. 13, all calculated specific activities with both substrates were in the same range independent on the time and conditions of storage. Therefore, the mTyr activity did not significantly change on storage for 6h at r.t. and for up to 48h at 4 °C. The average values of activity towards dopa even seemed slightly increased after 6h at r.t. and 48h at 4 °C, which may be due to the higher SD in these cases. However, mTyr activity with tyrosine as a monophenolic substrate seemed slightly reduced on storage of the enzyme solution > 6h. Therefore, a consumption of already dissolved mTyr within few hours (<< 6h) seemed necessary for reproducible mTyr activity in future investigations. Therefore, storing of frozen aliquots of mTyr stock solution, and thawing directly before use was selected as a practicable approach for standardized reactants with preserved high activity for each study.

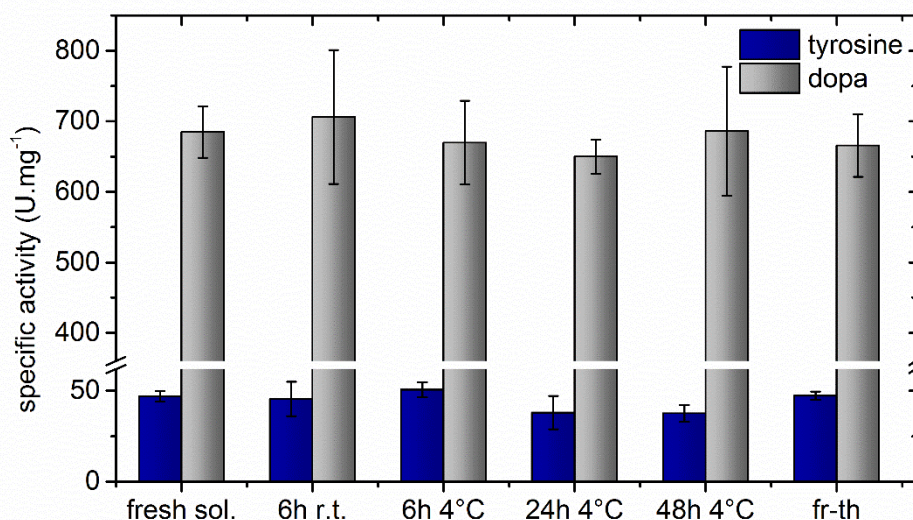


**Figure 13: Tyrosinase activity towards *L*-dopa (blue bars) and *L*-tyrosine (grey bars)**

*under different storage conditions: fresh solution, 6h at room temperature (RT), storage at 4 °C (in fridge) for 6h, 24h and 2 days (d) and after freezing and thawing. The activity was calculated by determining the linear slope of the enzymatic conversion of the substrates to dopachrome, measured at 475 nm at 25 °C in PBS/O<sub>2</sub>, pH 7.4 (n=6,  $\bar{x} \pm SD$ ). The experiments were conducted within a student internship.*

In all of the experiments reported above, the specific activity of mTyr to the catecholic substrate *L*-dopa (*o*-diphenol) was higher compared to *L*-tyrosine (monophenol). Since activity is a kinetic parameter, the monophenol hydroxylation being a slow, rate-determining step in the enzymatic catalysis [136, 137] may explain the slower product formation from monophenols by the two-step enzymatic conversion. Furthermore, *o*-diphenol oxidation to *o*-quinone requires only 0.5 mol O<sub>2</sub> per oxidation cycle, thus higher substrate amounts can be converted with the same concentration of dissolved O<sub>2</sub> compared to monophenols. Another aspect is that mTyr in the Eoxy as well as Emet states possess diphenolase activity (Fig. 11), which increases the amount of mTyr in solution that is able to catalyze the oxidation of the *o*-diphenolic substrate.

In conclusion, it was observed that the selected physiological pH value of 7.4 was suitable for further studies. The catalysis rate could be substantially accelerated by increasing temperature from 25 to 37 °C. Furthermore, mTyr activity towards the investigated natural substrates was relatively stable during storage of mTyr stock solution aliquots in the selected conditions. A standard handling of mTyr solutions by storing of frozen aliquots and thawing directly before usage was defined to be best suited for further investigations.

## 4.4 Analysis of mTyr activity with DAT and DATT as substrates

Here, the catalytic activity of mTyr towards the selected artificial substrates, i.e. DAT and DATT, will be investigated in comparison to the natural substrates *L*-tyrosine and *L*-dopa (Fig. 14), studied in Ch. 4.3. Here, a precise characterization of mTyr activity with DAT and DATT is crucial. The kinetics, determined by the dopachrome method, might be biased by downstream non-enzymatic reactions of *o*-quinone instead of being quantitatively converted to dopachrome. In the alternative MBTH assay, used here, *o*-quinone self-polymerization pathways are less probable, since MBTH was applied in 6-fold excess to initial substrate concentration. Moreover, the MBTH assay provides stability and high molar absorption coefficient of the MBTH-quinone adducts, resulting in high sensitivity of the method.[138]

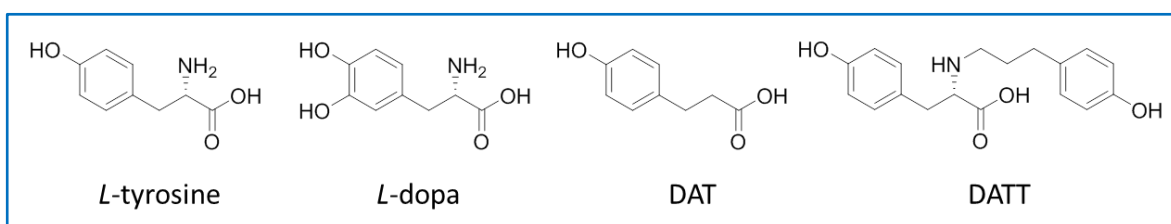
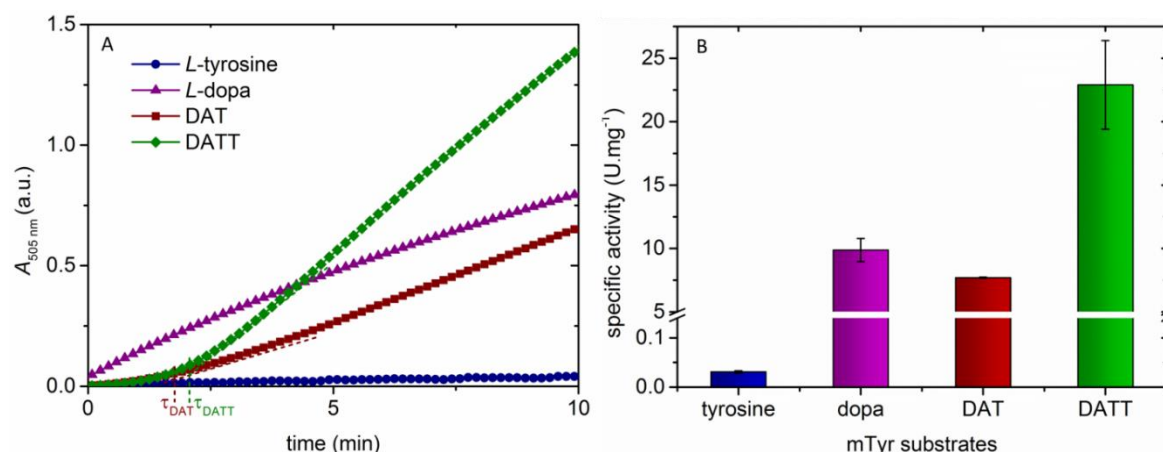


Figure 14: Structures of mTyr substrates: natural, i.e. *L*-tyrosine and *L*-dopa; and artificial, DAT and DATT.

In a first step, the selected substrates (1 mM) were mixed with mTyr (5 nM) and MBTH. Then, the absorption of the pigments formed from enzymatically produced *o*-quinones and their reaction with MBTH (reaction scheme shown in Fig. 52, Ch. 8.6.2) was measured at 505 nm [139] (Fig. 15A). The characteristic lag phase  $\tau$  for the monophenolic substrates DAT/DATT and *L*-tyrosine was approximately 2 min and 3 min, respectively, under the selected conditions.  $\tau$  was not considered for determination of the initial reaction velocity  $v_0$  ( $\Delta A/\Delta t$ ). The specific activity of mTyr for the investigated substrates, which was calculated according to eq. 1, is demonstrated in Fig. 15B. The monophenols DAT and DATT were found to be better mTyr substrates than the natural substrate *L*-tyrosine. While DAT was comparable to the *o*-diphenol *L*-dopa in terms of catalytic oxidation rate, DATT was by far the best of the analyzed substrates. This suggests that DAT and DATT are very interesting substrates to explore in this thesis.



**Figure 15: Kinetics of mTyr catalysis and specific activity with L-tyrosine, L-dopa, DAT and DATT**

(A) Kinetics measured by the absorbance of the respective MBTH-quinone adducts and (B) mTyr specific activity to the natural and artificial substrates at the selected conditions (1 mM substrate, 5 nM mTyr, PBS (50 mM)/O<sub>2</sub>/2% DMF at pH 7 and 25 °C) ( $n=3$ ,  $\bar{x} \pm SD$ ).  $\tau$  indicates the lag phase for DAT and DATT as substrates, respectively, which was not taken into account for calculation of mTyr specific activity in (B).

In the studies reported above,  $v_0$  of mTyr catalyzed oxidation was analyzed in saturated conditions, where  $v_0$  did not increase on further increase of substrate concentration. In the following experiment, however, the concentration the selected artificial substrates was varied to study substrate-specific catalytic parameter for relevant concentrations of DAT and DATT in more detail. Reducing the concentration of DAT and DATT resulted in a decrease of product formation, as measured by the absorbance of the respective MBTH-quinone adducts (Fig. 16, left). Furthermore, it was evaluated if the mTyr catalyzed oxidation of DAT and DATT obeys the Michaelis-Menten (MM) theoretical model.[140, 141] The law of MM postulates that the rate of enzymatic reactions is proportional to the concentration of the enzyme–substrate complex  $ES$ , as described by the equation  $E + S \leftrightarrow ES \rightarrow E + P$  ( $E, S, P$  denote the concentration of enzyme  $E$ , substrate  $S$  and product  $P$ , respectively). The dependence of the measured  $v_0$  from the substrate concentration  $[S]$  is predicted by the MM parameter  $K_M$  and  $v_{max}$  according to Eq. 7:

$$v_0 = \frac{v_{max} \cdot [S]}{[S] + K_M} \quad (\text{Eq. 7})$$

The non-linear fit was computed by the software Origin 9.0.0 according to the Marquard-Levenberg algorithm. Fig. 16 (right) illustrates the plots of the measured  $v_0$  against the substrate concentration, fitted to Eq. 7. Hyperbolic saturation kinetic curves were observed for both investigated substrates, i.e. DAT and DATT. While the DATT curve saturation leveled off above 1.6 mM, higher DAT concentration may lead to faster catalytic

rates. However, this state could not be reached due to solubility limitation of the latter substrates.

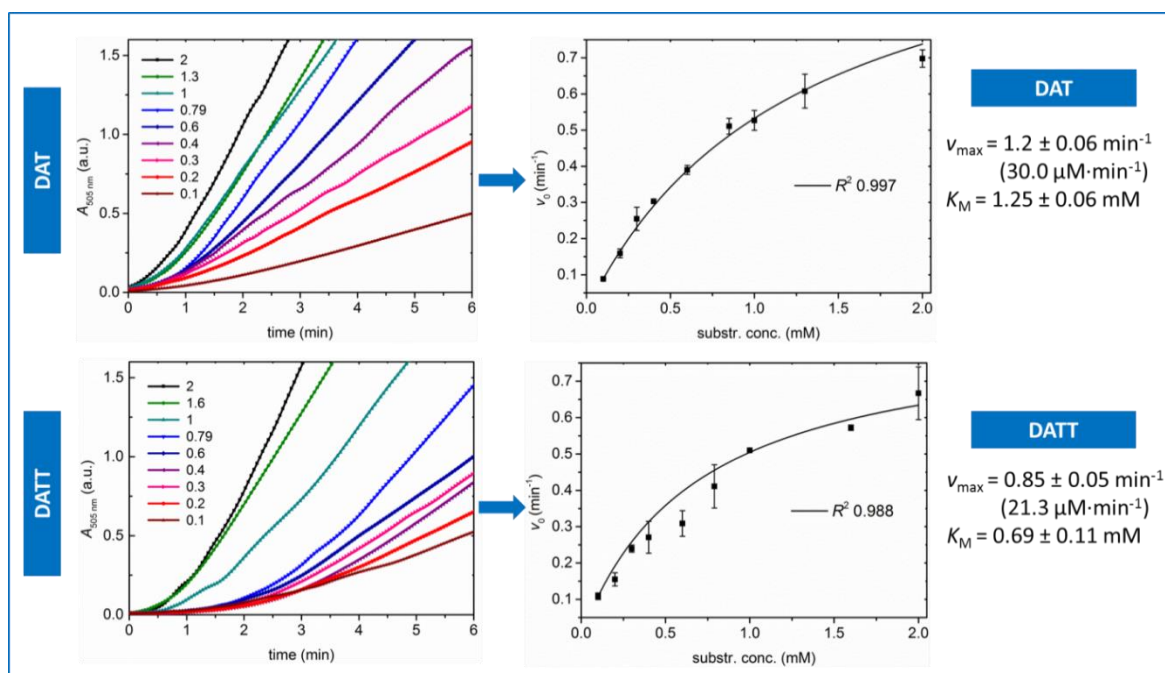


**Figure 16: Dependence of mTyr kinetics on substrate concentration and MM plots for DAT and DATT and determined kinetic constants:**

*mTyr kinetics with DAT and DATT (0.1–2 mM) as substrates, measured by MBTH assay ( $\Delta A_{505\text{nm}}$ ) (left). Plots of the measured initial velocity  $v_o$  vs substrate concentration ( $n=3$ ,  $\bar{x} \pm \text{SD}$ ), fitted to the MM model (right) and determined kinetic parameters  $K_m$  and  $v_{\text{max}}$  (the first  $v_{\text{max}}$  value considers the increase of absorption a.u. at  $\lambda_{505\text{nm}}$  per min).*

If the rate of product formation, i.e. the dissociation rate of the ES complex to E + P is higher than the rate constant for  $\text{ES} \rightarrow \text{E} + \text{S}$ ,  $K_M$  may give an indication of the affinity of the different substrates to the active site of mTyr. In this case, the lower  $K_M$  found for DATT, may indicate that the affinity of DATT to mTyr ( $K_M = 0.69 \pm 0.11 \text{ mM}$ ) was 1.8 times lower compared to DAT ( $K_M = 1.25 \pm 0.06 \text{ mM}$ ), which may be a result of the limited interactions of the sterically demanding substrate bearing two phenol residues with amino acids in the proximity of the mTyr active center. However, this could not be verified for the analyzed enzyme kinetics due to the complex catalytic mechanism, involving two subsequent oxidation steps. The potency of mTyr in oxidizing substrates was increased for DAT, compared to DATT, as demonstrated by the higher maximal catalysis rate  $v_{\text{max}}$ , i.e. maximal amount of converted substrate per min for DAT ( $v_{\text{max}} = 30 \pm 1.5 \mu\text{M}\cdot\text{min}^{-1}$ ) compared to DATT ( $v_{\text{max}} = 21.3 \pm 1.3 \mu\text{M}\cdot\text{min}^{-1}$ ). Since  $v_{\text{max}}$  is proportional to the turnover number  $k_{\text{cat}}$  ( $k_{\text{cat}} = v_{\text{max}} \cdot c_E$ , where  $c_E$  represents mTyr concentration), [142] the oxidation of DAT was more efficient compared to DATT. This finding was surprising considering the higher specific mTyr activity in the initial DATT oxidation, discussed above. However, a

limited dissolution of DATT at concentrations above 2 mM may have prevented the identification of higher  $v_0$  values on further increase of DATT concentration. Thus,  $v_{\max}$  of DATT may potentially be higher than the here determined value.

For mTyr catalyzed DAT oxidation, a reference value of  $v_{\max} = 15.2 \pm 1.1 \mu\text{M}\cdot\text{min}^{-1}$  exists, [143] which is lower than the determined value ( $v_{\max} = 30 \pm 1.5 \mu\text{M}\cdot\text{min}^{-1}$ ). This means that the catalysis is approximately two times more efficient at the selected conditions than previously found. The deviation may be ascribed to the fact that the applied industrially produced mTyr was not purified in contrast to the cited authors. Therefore, other active mTyr species except the tetrameric form, e.g. monomeric H units of mTyr may be present in the commercial extract. Moreover, the chemical and mechanical stress during purification and the separation of other active isoenzymes is usually accompanied by a decrease of catalytic activity, which may lead to slower turnover rate. A further investigated question was the influence of substrate functionalization with SOEG on the kinetics of mTyr catalysis. To study this, free DAT and DATT were compared to DAT- and DATT-SOEG 10 kDa. All analytes were incubated with 5 nM mTyr at a substrate concentration of 2 mM. The low polymer concentration ( $8.77$  and  $8.47 \text{ g}\cdot\text{L}^{-1}$  for DAT- and DATT-SOEG 10 kDa, respectively) allowed avoiding a crosslinking of the oligomeric precursors. While the initial rate of enzymatic oxidation of DAT-SOEG was not clearly reduced compared to DAT, a lower mTyr catalysis rate was observed for DATT-SOEG with respect to DATT (Fig. 17). The initial catalysis velocity after the lag phase seemed comparable for both oligomeric substrates, i.e. DAT- and DATT-SOEG. However, the lag phase during enzymatic oxidation of DATT-SOEG was dramatically increased compared to all other tested artificial substrates. Thus, additional dynamic interactions between DATT residues in DATT-SOEG, e.g. a clustering, may compete with the enzymatic oxidation process. The higher viscosity of the oligomer solutions, i.e. DAT- and DATT-SOEG 10 kDa, possibly leading to hindered biocatalyst diffusion and lower catalysis rate, should also be taken in consideration on a longer timescale. It should further be noted that in these systematic mechanistic studies, a fixed low enzyme concentration was used. Therefore, the values of kinetic parameters determined here may not be identical when higher enzyme concentrations are applied.

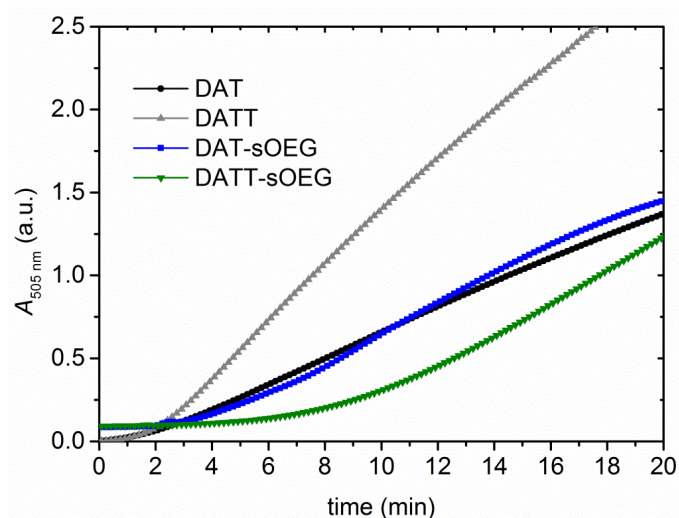


**Figure 17:** Kinetics of mTyr catalyzed oxidation of DAT(T) and DAT(T)-functionalized sOEG:

*the kinetics were measured by the MBTH assay at pH 7 and 25 °C. All solutions contained 2 mM of DAT(T) substrate and 5 nM mTyr in PBS/O<sub>2</sub>/2% DMF.*

All experiments were conducted at standardized conditions in O<sub>2</sub> saturated solutions. O<sub>2</sub> solubility in saline-containing aqueous media is known to be relatively low. For the selected PBS (50 mM), a solubility of 187.4 μM O<sub>2</sub> was predicted (calculation according to the algorithm found here [144]). This means that O<sub>2</sub> depletion may occur in the course of mTyr catalysis, when high enzyme and substrate concentrations were used. Indeed, a darker color at the surface of solutions, placed in cuvettes was observed in some experiments (incubation times > 1h), indicating that the catalysis rate was faster at the solution/air interphase, where fast O<sub>2</sub> diffusion from air is allowed. Thus, the rate of enzymatic catalysis may be limited by cosubstrate depletion in long-term mTyr catalytic studies, since each monophenolase catalytic cycle (from DAT to respective *o*-quinone) necessitates 1 mol O<sub>2</sub>. [122] When molecular O<sub>2</sub> was directly and continuously supplied to the reaction mixture by bubbling with pure oxygen, a detrimental effect on catalysis rate was observed, possibly as a result of mTyr deactivation by partial denaturation at the liquid-air interphase. Therefore, for long reaction times, provision of oxygen from the air environment by diffusion into the open reaction vessels was used.

In summary, the artificial mTyr substrate DAT was found to be a better substrate in terms of mTyr catalytic efficiency than natural monophenolic substrates like tyrosine. With DATT, which have not yet been investigated as mTyr substrate, the observed initial oxidation kinetics were faster than with *L*-dopa and DAT as substrates. No substantial decrease in catalysis rate for DAT-sOEG 10 kDa compared to free DAT was observed. However, a dramatic decrease in the mTyr oxidation rate in DATT-sOEG 10 kDa compared

to unbound DATT was demonstrated. More detailed studies on the kinetics of mTyr catalysis of oligomeric substrates, i.e. DAT(T) functionalized OEGs, with a particular focus on the subsequent non-enzymatic crosslinking reactions will be reported subsequently (Ch. 5.2, 5.4 and 6.1.1).

## 4.5 Summary

---

Within this chapter, the synthesis of polymeric substrates for further studies was described. Linear DAT monofunctionalized oligomers with high *d.f.*, DAT-IOEG<sub>OMe</sub>, were selected for further mechanistic investigation of mTyr potential to crosslink the artificial polymeric substrates of interest. A successful synthesis and purification of quasi monodisperse DAT-ImOEG<sub>OMe</sub> 2 kDa (purity > 94 %) could be achieved by RP-HPLC. Branched four-arms sOEG derivatives functionalized with DAT(T) with varying  $M_n$  and *d.f.* were synthesized as precursors for hydrogel synthesis. Furthermore, the conditions for the further studies on mTyr catalyzed substrate oxidation were chosen by investigating mTyr activity at different temperatures and pH values. The salinity of isotonic PBS, medium saturation with O<sub>2</sub> as cosubstrate and pH 7.4 and r.t. were identified as standard experimental conditions to attain high mTyr activity. The storage of frozen mTyr aliquots and thawing on demand was found to be a practicable approach to handle biocatalyst stock solutions without activity loss. The selected artificial substrates DAT and DATT were superior to *L*-tyrosine as natural substrate in terms of mTyr activity. While mTyr activity with DAT was comparable to the *o*-diphenol *L*-dopa, there was evidence that DATT was a much better mTyr substrate than the latter. Within Ch. 5, the effect of mTyr catalysis and the subsequent non-enzymatic processes for the formation of adducts from DAT and DAT functionalized oligomers will be investigated in model studies.

## 5 Mechanistic analysis of mTyr catalyzed crosslinking of DAT and DAT-functionalized polymers

The suitability of DAT and DATT to act as mTyr substrates was demonstrated in Chapter 4. To realize mTyr catalyzed formation of covalent networks, a functionalization of the precursors with Tyr substrates is necessary. Within this chapter, the crosslinking mechanism is investigated on the basis of model reactions with DAT derivatives as mTyr substrates. Monofunctional telechels (here DAT functionalized linear OEG, DAT-IOEGOMe) were investigated in addition to small molecules, i.e. DAT and DAT methyl ester (DAT ester), which were expected to yield soluble analytes instead of hydrogel networks after mTyr catalyzed oxidative oligomerization.

### 5.1 Overview on proposed crosslinking mechanisms and relevance for the selected system

---

The mechanism of network formation from DAT-functionalized oligomers by mTyr catalysis can be divided into two distinct pathways, i.e. an enzymatic and subsequent non-enzymatic pathway, being proposed as summarized in Fig. 18. Those pathways and their application to DAT as substrate have been studied in more detail, as discussed below.

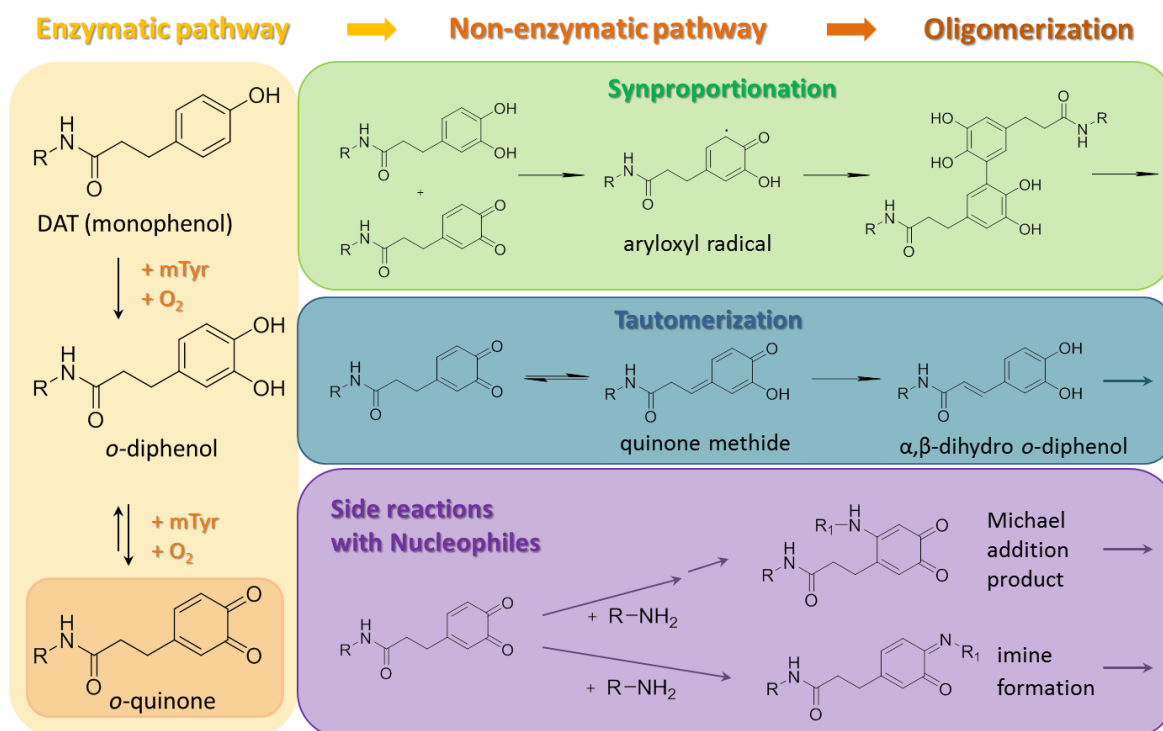


**Figure 18:** Proposed reaction scheme for network formation from DAT-functionalized OEG by tyrosinase (TYR) catalysis, involving enzymatic and non-enzymatic pathway.

The non-enzymatic reactions are summarized in accordance with the reactions discussed in literature, as recently reviewed [145]. R denotes the OEG chain in the proposed structures.

### 5.1.1 Factors affecting mTyr catalysis

The enzymatic pathway is well studied for other types of substrates and involves initial catalysis of hydroxylation of phenol to a catechol derivative. This process is accompanied with O<sub>2</sub> consumption and is followed by catechol oxidation in two sequential one-electron abstraction steps to an *o*-quinone through an *o*-semiquinone intermediate.

Most of the published studies focus on mTyr-catalyzed hydrogel formation from *o*-diphenol functionalized precursors. Applying phenols as substrates for crosslinking reactions poses an additional level of complexity. The monophenol hydroxylation is the rate-determining step, which explains the relatively slow kinetics of mTyr mediated oxidation, demonstrated in some of the studies further on (Ch. 5.2 to 5.7 and 6.1.1).

Within this chapter, it was investigated if the DAT turnover to oxidized intermediates and netpoints is quantitative for the selected model substrates. The effect of DAT substrate type on the crosslinking reactions is enlightened by investigating small molecules and oligomeric substrates, i.e. DAT, DAT ester and DAT-IOEGOMe. A further

aspect affecting the crosslinking kinetics is the presence of catechol intermediates, which are required to reduce met-Tyr to the active oxy-Tyr state (see Ch. 1.5 and 4.3).

While the initial enzyme activation process was completed within < 5 min in the kinetic studies discussed in Ch. 4, the quantitative mTyr activation may take longer if much higher biocatalyst amounts were applied (as in Ch. 5 and 6). A retardation of the catalysis rate in may be rationalized since much higher amounts of mTyr (>10 orders of magnitude) were applied, while the substrate concentrations are comparable. One further aspect to consider may be a suicide-inactivation of mTyr by *o*-diphenols (Ch. 1.5). However, this is expected to play a minor role due to the high mTyr concentration used here.

### 5.1.2 Factors affecting non-enzymatic crosslinking

While the enzymatic reaction is very specific to phenol residues, the exact crosslinking mechanism and role of the different spontaneous reactions between the formed reactive intermediates is still a matter of debate. [145] The different non- resulting adducts are referred to as netpoints further on.

Since catechols enzymatic crosslinking routes, demonstrated in literature for other substrates, are summarized in Fig. 18. The and quinones are prone to redox reactions, aryloxy coupling by synproportionation is anticipated to be the major pathway towards network formation. The rate of *o*-diphenol dimerization in this pathway depends on the availability of *o*-diphenol and semiquinone radicals. The amount of radical intermediates thus should correlate with the amount of formed netpoints, as illustrated by reaction equilibrium 2 in Fig. 19. Thereby, slower catechol oxidation leads to longer availability of catechols as reaction partners (reaction 1, Fig. 19) and may favor higher degree of polymerization. [146] The formed catechol dimers condense with further aromatic moieties or other available intermediates. These reaction pathways compete with the formation of quinones being the final oxidation stage of DAT. *O*-quinones can form adducts with phenols, other quinones or nucleophiles.

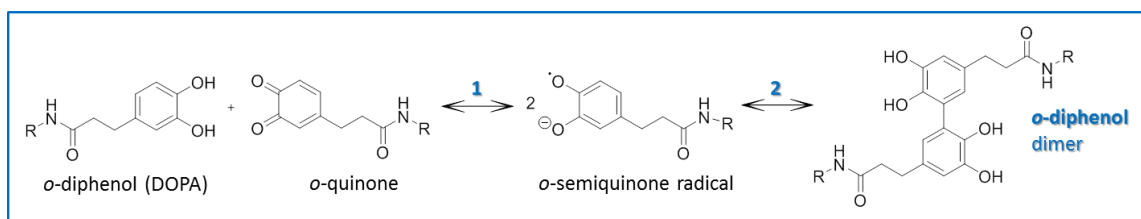


**Figure 19:** Formation of *o*-semiquinone radicals during mTyr catalysis.

The radicals are formed by abstraction of one electron from catechol, or through a redox reaction between formed catechols and *o*-quinones, illustrated here. Two radicals disproportionate immediately to a catechol and a quinone molecule (1), or give rise to a di-catechol dimer (2).

Primary amines as strong nucleophiles are other potential reaction partners for quinone intermediates. The amine reaction with *o*-quinone can lead to two different products, depending if the nucleophile attacks the ring (Michael addition mechanism), or the ketone group of *o*-quinone (imine formation). Adducts between quinones and amines were found to play an important role in biological systems, including the amino acids lysine,[147] histidine,[148, 149] or proline. [150] However, the exact reaction pathway is not yet fully understood. Also the MBTH assay, which is used to study the mTyr activity in Ch. 4.4, bases on a reaction of quinones with the primary amino group of the hydrazine moiety to a chromophoric Michael addition product (Fig. 52, Ch. 8.6.2). Therefore, the formation of quinone-amine adducts was of interest, i.e. investigating the relevance of these reactions for mTyr mediated DAT-IOEG<sub>OMe</sub> oligomerization and the followed reaction mechanism.

Furthermore, quinone can possibly tautomerize and form quinone methide intermediates. Although this pathway is usually demonstrated in laccase- and not Tyr-mediated oxidation reactions, [151] Waite and Rzepecki found mechanistic explanation for the occurrence of  $\alpha,\beta$ -unsaturated diphenol derivatives in Tyr-catalyzed crosslinking of a DOPA ester derivative. The non-enzymatic abstraction of two protons from the side chain at C $_{\alpha}$  [152] was attributed to the presence of phosphate ions as Lewis bases (also present in the PBS medium for dissolving mTyr and substrates). The tautomerization is favored at acidic pH, [153] as demonstrated by the relative high conversion efficiency (70-80% at pH 6, but only up to 19% at pH 8). The non-quantitative tautomerization is ascribed to aryl couplings and other competing reactions. [154] The  $\alpha,\beta$ -unsaturated N-acetyl dopamine was demonstrated to oligomerize forming up to tetramers with heterogeneous structure by Tyr oxidation. [153]

The abundance of the products formed by the non-enzymatic reactions, shown in Fig. 18, depend on the availability of reaction partners, but also on external factors, such as pH or rate of oxidation, i.e. concentration of enzyme and substrate. The relevance of the discussed reaction pathways to the selected systems, DAT functionalized oligomers, was investigated focusing on mechanistic, as well as kinetic aspects. Model reactions with DAT and derivatives thereof were studied by spectroscopic and MS techniques (Ch. 5.2 to 5.6). The side reactions between DAT-IOEG<sub>OMe</sub> and amines were investigated in Ch. 5.7. Furthermore, the netpoints formed in enzymatically crosslinked hydrogels from DAT-sOEG were subjected to direct spectroscopic analysis after hydrolysis of the network (Ch. 5.8).

## 5.2 Investigation of mTyr catalyzed crosslinking by UV-Vis spectroscopy

---

In order to study the enzymatic oxidation of DAT-functionalized macromolecules by mTyr and particularly understand the formation of intermediates, UV-Vis spectroscopy was applied. Model reactions with aqueous solutions of monofunctionalized DAT-IOEG<sub>OMe</sub> 10 kDa were incubated with mTyr at different concentrations and characterized at different time points in comparison to DAT-sOEG. It should be noted that the exposure of DAT-functionalized macromolecules to mTyr resulted in a brown coloration of the sample, which started within few minutes after addition of the enzyme. While the solutions and gels absorb light in the whole near visible range, corresponding to brown color, the intermediates can be investigated based on the occurrence of characteristic absorption peaks in the UV range.

First, a highly diluted DAT-IOEG<sub>OMe</sub> solution (0.63 wt%) was deliberately incubated with an excess mTyr concentration (500 U·mL<sup>-1</sup>) in order to achieve a high turnover of DAT groups (Fig. 20A). The UV-Vis spectra of this model reaction were compared to a highly diluted solution of DAT-sOEG 10 kDa, which did not form a hydrogel at the investigated concentration (0.1 wt%) (Fig. 20B). Both solutions had similar DAT concentration in the beginning of the experiments (absorbance  $A_{276\text{nm}}$  was 1.1 and 0.9 in Fig. 20A and B, respectively). However, the overall absorption of DAT-IOEG<sub>OMe</sub> at 505 nm ( $A_{505\text{nm}}$  selected, since products of couplings with DAT derivatives expected to absorb in this

range, as discussed above) was much higher compared to DAT-sOEG after 4 h (0.4 vs 0.1 in Fig. 8A and B, respectively). Therefore, the DAT oxidation kinetics can be concluded to be much slower in branched telechels compared to linear OEG precursor.

Importantly, the formed peaks are the same, which indicated that the same reaction occurred in both cases. For DAT-IOEG<sub>OMe</sub> (Fig. 20A), a bathochromic shift and broadening of the absorption maximum at 276 nm were observed within 15 min. A shoulder at 320 nm was distinguished, which increased further within 24 h. A further broad peak at 405 nm arose, which disappeared already after 1 h, giving rise to a broad plateau in the near visible range.

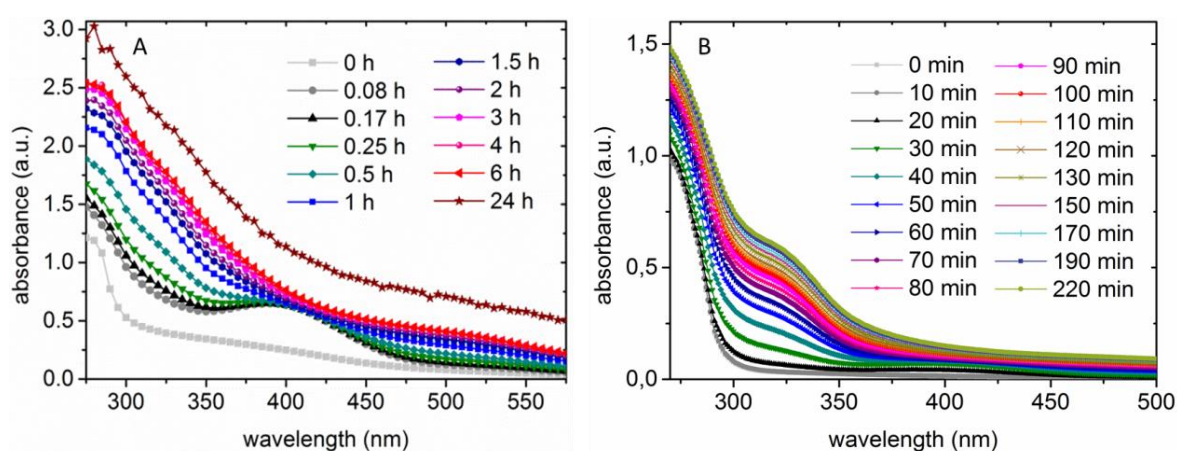
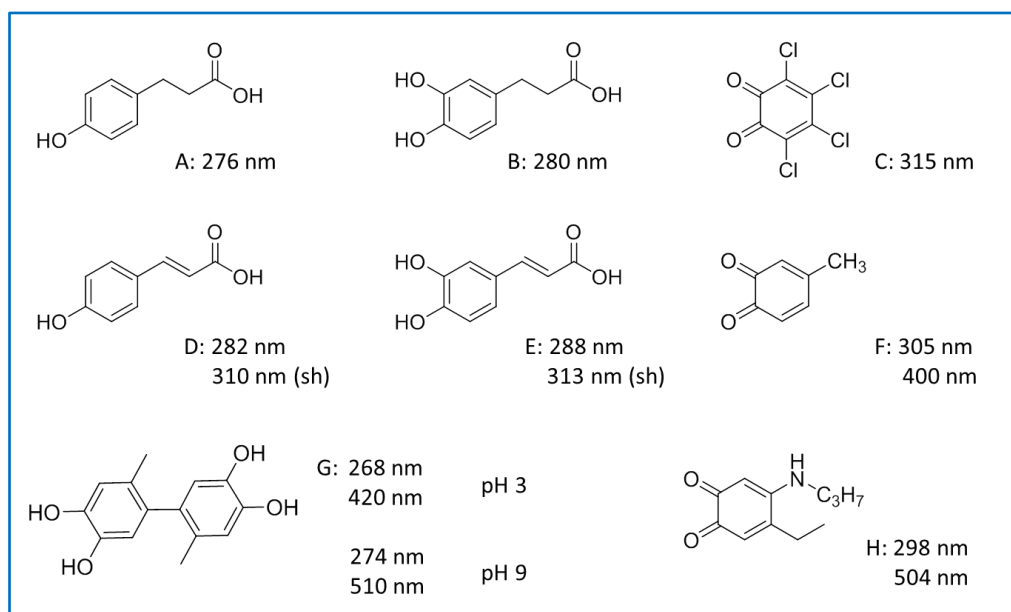


Figure 20: UV-Vis absorption spectra of linear and branched DAT-OEG, oxidized by mTyr vs time.

A) DAT-IOEG 10 kDa (6.25 mg·mL<sup>-1</sup>), B) DAT-sOEG 10 kDa (1 mg·mL<sup>-1</sup>) incubated with 500 U·mL<sup>-1</sup> mTyr and measured at different time points within 24 and 3.7 hours, respectively.

The absorption spectra gave some insights into the structure and kinetics of intermediates being formed by mTyr catalysis. The broadening of the peak at 276 nm ( $\lambda_{\max}$  of DAT, A in Fig. 20) and the  $\lambda_{\max}$  shift to 280 nm might be assigned to *o*-diphenol formation. The shoulder at 320 nm could be attributed to the formation of  $\alpha,\beta$ -unsaturated diphenol intermediates (reference substances D and E in Fig. 21). The presence of these derivatives was discussed above (quinone tautomerization pathway in Fig. 18) and already identified during oxidative crosslinking of chinone groups by other authors. [155, 156] Regarding the shoulder at 320 nm, an additional contribution from *o*-quinonoid species may be expected, since  $\lambda_{\max}$  of 315 nm was observed for the model stabilized *o*-quinone (C in Fig. 21) and an absorption at 310 nm was reported for unsubstituted 1,2-quinone. [157]



**Figure 21: Wavelength of maximum absorption  $\lambda_{\max}$  of model catechols, quinones and crosslinks.**

Measured reference substances: DAT (A), catechol derivative of DAT (B), tetrachloro-*o*-quinone (C), *p*-coumaric acid (D), and caffeic acid (E). Further data from literature: 4-methyl-*o*-quinone (F): [158], di-DOPA adducts (G): [159], quinone-lysine adduct (H): [160].

The peak with maximum at 405 nm could be assigned to *o*-quinone intermediates in accordance with literature: 1,2-quinone exhibits a  $\lambda_{\max}$  at 389 nm [157] and other publications state  $\lambda_{\max}$  at 390-400 nm for different *p*-substituted *o*-quinones (exemplary structure F, Fig. 20).[158] Furthermore, the presence of a peak at 410 nm was ascribed to the formation of an *o*-diphenol dimer by other authors, [83] which was detected by MALDI-ToF (see also G in Fig. 21). Therefore, the peak with a maximum at 405 nm cannot be clearly assigned to a specific structure, but contributions from quinone species as well as phenol coupling products were conceivable.

Quinone-amine adducts are repeatedly reported to exhibit red color, associated with absorption maxima in the near visible range, e.g. proline-DOPA adducts with  $\lambda_{\max}$  520 nm [150] or compound H in Fig. 21 with  $\lambda$  504 nm. Within this thesis, 87 mol% of IOEG-amine end groups were functionalized with DAT. Accordingly, side reactions with the residual unfunctionalized  $\text{NH}_2$  groups could possibly be responsible for the observed broad absorption band with maximum at 505 nm. However, no contribution of amines to the netpoints was found by MALDI-ToF in reaction mixtures of DAT-ImOEG<sub>OMe</sub> and  $\text{NH}_2$ -ImOEG<sub>OMe</sub> containing 10 mol%  $\text{NH}_2$  as reactive precursor end groups in solution, as will be detailed later (Ch. 5.7). Since the substrate amount in the here described

investigation, was low, the probability of reactive intermediates to meet is relatively low and thus a limited netpoint formation compared to intermediate species was assumed.

In a second investigation, the concentrations of DAT-IOEG<sub>OMe</sub> and mTyr were chosen to be comparable to the amounts in DAT(T)-sOEG that may later be used to synthesize bulk hydrogels (5 wt% polymer, 100 or 500 U·mL<sup>-1</sup> mTyr). At different time points of this reaction, aliquots were collected and diluted prior to UV/VIS measurement to allow analysis. The absorption spectra in Fig. 10 showed a characteristic development over time within 24 h.

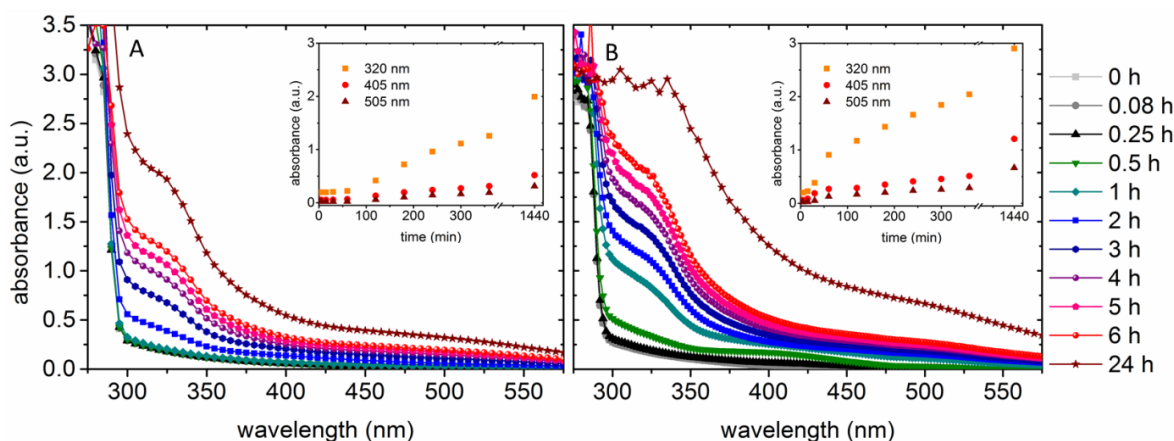


Figure 22: UV-Vis absorption spectra of DAT-IOEG<sub>OMe</sub> mixed with differing amounts mTyr vs time.

The model precursor (50 mg/mL) was incubated with 100 (A) and 500 U·mL<sup>-1</sup> (B) mTyr, diluted and measured at different time points within 24 hours. In the insets, absorption at three observed  $\lambda_{max}$  is plotted over time.

The comparison of the spectra shown in Fig. 20 and 22 should enlighten the reactions, which play a role during netpoint formation. The spectra of solutions containing higher DAT-IOEG<sub>OMe</sub> concentration showed distinct differences with respect to the highly diluted polymer solutions. The bathochromic shift of the peak at 276 nm corresponding to DAT  $\lambda_{max}$  was not so pronounced in both spectra in Fig. 22. Also, the peak with a maximum at 405 nm was detectable only in DAT-IOEG<sub>OMe</sub> incubated with higher mTyr concentration, but disappeared in the course of time giving rise to a broad absorption plateau in the near visible region (Fig. 22B). These findings indicated that intermediate species such as catechols as well as quinones are consumed during the subsequent non-enzymatic routes of reaction, suggesting their involvement in netpoint formation.

Three distinct  $\lambda$  were selected, at which absorption maxima were observed and plotted over time for better visualization of the reaction kinetics (insets Fig. 22). The addition of a higher enzyme amount resulted in faster kinetics, as demonstrated in the

inset of Fig. 22B. The lag period was approximately 1 hour for the lower mTyr concentration.

At 405 and 505 nm, which above were discussed as quinone intermediates and *o*-diphenol dimers/reaction products formed with primary amines, a parallel increase of absorption took place, thus indicating that both processes took place simultaneously. Therefore, it was confirmed that quinone intermediates are vital for the further non-enzymatic crosslinking reactions. At all selected wavelengths, a higher absorption after 24 hours was measured when DAT-IOEG<sub>OMe</sub> was incubated with the higher mTyr amount. This may suggest a higher amount of netpoints resulting from catalysis with higher mTyr concentration. However, the strong increase of absorption in the whole tested spectral region between 6 and 24 h suggested that the reactions would proceed further on.

This observation from model reactions may indicate for a network synthesis in bulk hydrogels by mTyr that the network formation may in principle be ongoing. The kinetics of mTyr catalyzed intermediate formation from DAT-sOEG are slow, as seen in Fig. 10B. Crosslinking of these precursors with a concomitant increase in viscosity has two-fold consequences for further enzymatic and non-enzymatic reactions: (1) further DAT oxidation by mTyr may be limited due to hindered enzyme diffusion before the catalytic process has reached steady-state; (2) the rate of formation of new netpoints is decreased by limited free movement of already activated sOEG end groups. Therefore, premature oligomerization end point may be reached where contacts between reactive end groups are no longer possible before complete conversion of telechelic groups in the hydrogels.

In conclusion, the mTyr-catalyzed oxidation of DAT groups was demonstrated in the model reactions of DAT-IOEG 10 kDa by UV-Vis spectroscopy. The crosslinking rate could be accelerated by application of linear DAT-IOEG<sub>OMe</sub> 10 kDa instead of four-armed DAT-sOEG 10 kDa, and by five-fold increase in the mTyr concentration. The broad absorption plateaus indicate the formation of various intermediates and netpoints with overlapping absorption maxima. Rather, an absorption increase in the whole near visible spectral region was exhibited, which is responsible for the brown color of the formed products of mTyr-catalyzed crosslinking. Furthermore, *o*-diphenols, *o*-quinones and of  $\alpha,\beta$ -unsaturated diphenols as reaction intermediates were deduced when highly diluted DAT-IOEG<sub>OMe</sub> solutions were applied. The consumption of *o*-diphenol and *o*-quinone

intermediates in solutions with higher polymer concentrations supported the assumed pathways of dismutation, which seemed to be a relevant crosslinking mechanism. In contrast, the occurring tautomerization was probably not the key mechanism for netpoint formation.

### 5.3 Study of netpoint chemical structure by FT-IR spectroscopy

---

Despite the expected high complexity of products being formed from DAT-functionalized macromolecules by mTyr biocatalysis, FT-IR may allow identifying changes in chemical structure upon conversion of aromatic DAT. For this set of experiments, DAT-IOEG<sub>OMe</sub> 2 kDa as a model oligomer with relatively low  $M_n$  was selected, as it provides a higher ratio of functional groups to repetitive units in the OEG segments. Therefore, the detected bands of telechelic groups and netpoints were more intensive compared to the hydrogels described in Ch. 6.2.2, and more elaborate interpretation of the FT-IR spectra was possible.

The FT-IR investigation of the model compound after incubation with mTyr (48 h) revealed a high conversion of the telechelic DAT groups, demonstrating predominantly quinoid character (Fig. 23). The oxidation of the DAT groups to *o*-quinone species was confirmed by the disappearance of the peaks at 1780 and 1515  $\text{cm}^{-1}$ , representing aromatic ring skeletal vibrations and aromatic C=C stretch in DAT respectively. Moreover, a decrease in intensities of the bands at 1180  $\text{cm}^{-1}$  was observed, which is the typical range for C-O stretching vibrations as well as deformation vibrations of phenolic O-H groups. Similarly, the signals at 705  $\text{cm}^{-1}$  decreased after mTyr addition, which are possibly related to phenolic O-H out-of-plane bending. Both observations can be related to a reduction of phenolic moieties in the oligomer after mTyr catalysis. In addition, the rise of the bands at 1660 (compare Ch. 6.2.2) and 1200  $\text{cm}^{-1}$  (C-C stretch adjacent to a ketone group) indicated quinone formation.

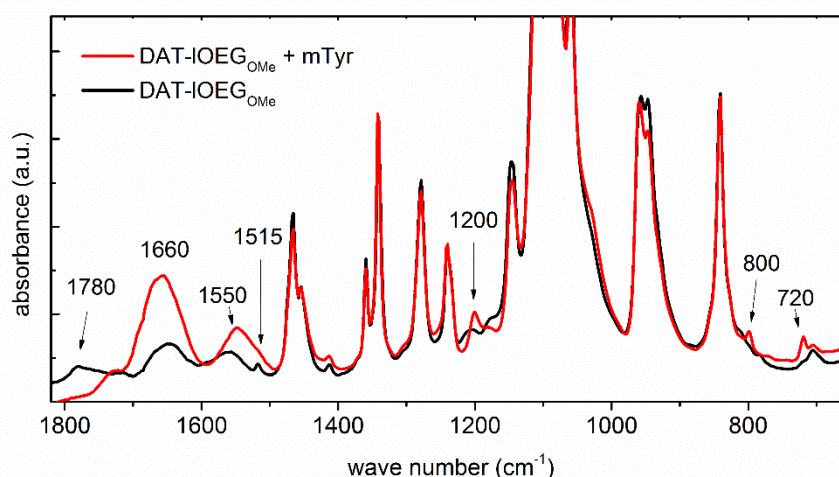


Figure 23: FT-IR spectra for monofunctional DAT-IOEGOMe 2 kDa incubated with mTyr vs the non-oxidized precursor

Within the region of  $900\text{--}650\text{ cm}^{-1}$ , the aromatic ring substitution pattern can be identified on the basis of characteristic bands from aromatic C-H out-of-plane bending vibrations and coupling of vicinal protons. In this region, the following changes of the FT-IR spectrum of DAT-IOEGOMe after oxidation by mTyr should be evaluated: A decrease in the peak representing the vibration of two vicinal aromatic H atoms, such as in 1,4 di-substituted aromatics (usually strong for symmetrical substitution as in DAT) [161] This signal may be expected at  $860\text{--}800\text{ cm}^{-1}$ ; however, no change within this region was found after incubation with mTyr, indicating that it may probably be overlapping with the strong OEG signals at  $840\text{ cm}^{-1}$ . Furthermore, one may expect the appearance of a peak at  $900\text{--}850\text{ cm}^{-1}$  corresponding to isolated aromatic protons due to *ortho* substitution and netpoint formation. In the spectrum, a new sharp peak at  $800\text{ cm}^{-1}$  was observed, which might correspond to isolated aromatic protons with a shift to lower wave numbers due to the crosslinking. However, this band is usually low in intensity and may not be detectable since aromatics are end groups. Conversely, the peak at  $800\text{ cm}^{-1}$  may also be attributed to a C-H out-of-plane deformation vibration in  $\text{R}_2\text{C}=\text{CHR}$  functionalities, which occur in crosslinked quinone derivatives. Nevertheless, the detection of the growing band at  $720\text{ cm}^{-1}$ , which could be attributed to C-H bend at unsaturated hydrocarbons, may indicate the presence of non-crosslinked quinones after mTyr-mediated DAT-IOEGOMe oxidation.

Conclusively, the presence of quinone groups and DAT oxidation under loss of its aromatic character was verified in DAT-IOEGOMe by numerous bands in the FT-IR spectra. Potentially, netpoints composed of quinones as well as free quinone species could be

expected. Still, the heterogeneous structure of the formed crosslinks and the presence of many functional groups leading to peak overlapping set limits for a peak assignment to specific chemical structures of netpoints. The presence of quinone groups as netpoints may need to be verified by other methods.

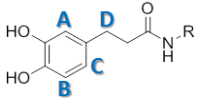
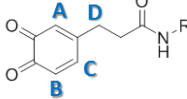
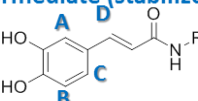
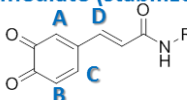
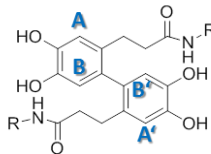
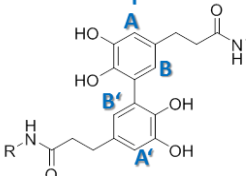
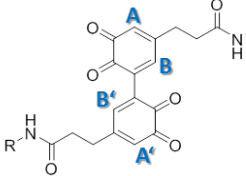
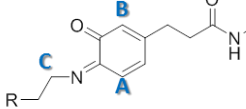
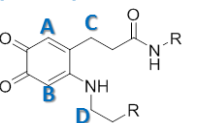
## 5.4 Study of netpoint chemical structure by NMR spectroscopy

---

The formation of soluble reaction intermediates originating from DAT as well as their further rearrangements to netpoints result in changes of the chemical structure, which can be studied by  $^1\text{H}$ -NMR spectroscopy.

Considering the structural complexity of possible products, a rational approach was followed in this investigation. First, the  $^1\text{H}$ -NMR spectra of expected intermediates and some exemplary netpoints were predicted via different computer programs (Table 3). From the chemical shifts predicted by three different programs, an average value  $\delta_{\text{av}}$  was calculated and adjusted considering the effect of  $\text{D}_2\text{O}$  as solvent. Subsequently, model reactions should be carried out by incubating DAT, DAT ester and DAT-IOEG<sub>OMe</sub> 2 kDa with mTyr. While an unequivocal assignment of the signals to individual structures cannot be expected due to the presence of a mixture of compounds, conclusions on categories of involved structure may be possible. The most pronounced changes in signals after mTyr-catalyzed crosslinking were expected in the range of aromatic protons of DAT (doublets at 6.75 and 7.1 ppm in  $\text{D}_2\text{O}$ ), since ring adducts are supposed to be the predominantly formed netpoints. In addition, the signals of protons of DAT side chain in  $\alpha$  position to the ring may also be substantially shifted. It should be noted that in some cases  $\text{MeOH-d}_4$  was used as solvent to allow for sample solubility. The peaks detected in  $\text{MeOH-d}_4$  are expected to be 0.05-0.1 ppm lower than  $\delta_{\text{av}}$  predicted in  $\text{D}_2\text{O}$ , as observed in various studies with DAT-derived substances.

Table 3: Structures of intermediates and netpoints, potentially formed after mTyr catalyzed crosslinking of DAT-IOEG<sub>OMe</sub>, and prediction of their <sup>1</sup>H-NMR signals in D<sub>2</sub>O

#	Expected compounds Chemical structure	Prot.	Signal mult. <sup>(1)</sup>	Predicted chemical shift $\delta$ (ppm)			
				CD <sup>(2)</sup>	Spinus <sup>(3)</sup>	ACD <sup>(4)</sup>	$\delta_{pred}$ <sup>(5)</sup>
1	<b>Intermediate</b> 	A	S	6.86	6.6	6.65	6.9
		B	D	6.73	6.65	6.66	7.1
		C	D	6.68	6.6	6.65	6.8
		D	T	2.37	2.75	2.56	2.8
2	<b>Intermediate (short-lived)</b> 	A	S	6.05	6.46	6.21	6.2
		B	D	5.89	7.25	6.38	6.5
		C	D	7.23	7.95	7.0	7.3
		D	T	2.24	2.67	2.42	2.5
3	<b>Intermediate (stabilized)</b> 	A	S	6.36	7.25	7.36	7.2
		B	D	6.42	6.76	6.29	6.6
		C	D	6.91	7.65	7.92	7.6
		D	D	7.22	7.5	6.28	7.2
4	<b>Intermediate (stabilized)</b> 	A	S	6.28	7.15	7.24	7.3
		B	D	6.89	7.23	6.87	6.8
		C	D	6.63	7.99	8.22	7.6
		D	D	7.41	7.7	6.46	7.3
5	<b>Netpoint</b> 	A/A'	D	7.12	6.9	6.94	7.1
		B/B'	D	6.95	7.05	7.1	7.2
6	<b>Netpoint</b> 	A/A'	D	6.54	6.83	6.65	6.8
		B/B'	D	6.74	7.54	7.21	7.3
7	<b>Netpoint</b> 	A/A'	S	7.25	8.27	8.16	7.5
		B/B'	S	6.05	7.0	6.21	6.5
8	<b>Netpoint (imine form.)</b> 	A	D	5.85	7.13	7.13	7.4
		B	S	6.28	7.15	7.24	7.3
		C	T	3.61	3.92	3.66	3.8
9	<b>Netpoint (Michael add.)</b> 	A	S	6.01	6.44	6.18	6.4
		B	S	5.25	5.87	5.46	5.7
		C	T	1.96	2.68	2.28	2.4
		D	T	2.36	3.64	2.82	3.1

signal multiplicity: expected signal splitting if no NMR spectra of higher order; S – singlet, D – doublet, T – triplet; <sup>(2)</sup>, <sup>(3)</sup>, <sup>(4)</sup>  $\delta$  prediction by different computer software: <sup>(2)</sup> ChemDraw; <sup>(3)</sup> Spinux on nmrdb.org; <sup>(4)</sup> <sup>1</sup>H NMR Predictor of ACD Labs on ilab.acdlabs.com/ iLab2; no specification of solvent in <sup>(2)</sup>, <sup>(3)</sup> and <sup>(4)</sup>; <sup>(5)</sup> estimated  $\delta$  values,  $\delta_{pred}$  based on the average  $\delta$  from the modeled <sup>1</sup>H-NMR spectra and the predicted values detected in D<sub>2</sub>O.

In the experimental studies, DAT was first incubated with mTyr in D<sub>2</sub>O saturated with O<sub>2</sub>. After 15 min of incubation, several new peaks of low intensity were detected in the range of 6 to 6.6 ppm (Fig. 24). After 28h, some of the peaks disappeared, indicating that these compounds are further oxidized or involve in oxidative couplings with other intermediates in the heterogeneous reaction mixture.

The singlet signal at 6.55 ppm and the multiplet at 6.6 ppm (protons A and B of compound 2, Table 3 respectively) indicated the appearance of intermediates with quinonoid structure. [162, 163] The peaks at 6.5-6.6 ppm may also represent quinone groups, being part of netpoints. This assumption is supported by the absence of a peak corresponding to protons C of compound 2, Tbl 3. The broadening of the peak at 6.75 ppm, assigned to the aromatic protons of DAT vicinal to the side chain, and the appearance of an additional singlet at 6.55 ppm may indicate catechol formation (also seen in DAT ester, see Fig. 26). The three aromatic protons of catechols usually appear as a multiplet rather than as separate well resolved peaks. The peaks assignable to derivatives *o*-diphenols and *o*-quinones were still detectable after 28 hours. The high signal intensity of residual DAT aromatic protons after 28h confirmed that most of DAT in solution was not oxidized by mTyr. This is in accordance with the observed reactions, which take place over > 24 h (Ch. 5.2). The slow reaction kinetics were demonstrated also by the slight difference of spectra between 0.25 and 28h. This may be explained by the use of D<sub>2</sub>O as solvent. Considering that the oxidation of monophenol to quinone requires the exchange of protons, the reaction rate in D<sub>2</sub>O may be decreased compared to H<sub>2</sub>O, as already observed by other authors. [164] Generally, the low intensity of new signals in Fig. 24 can be explained by the limited solubility of the resulting DAT intermediates, i.e. quinones and associated oligomers in aqueous media.

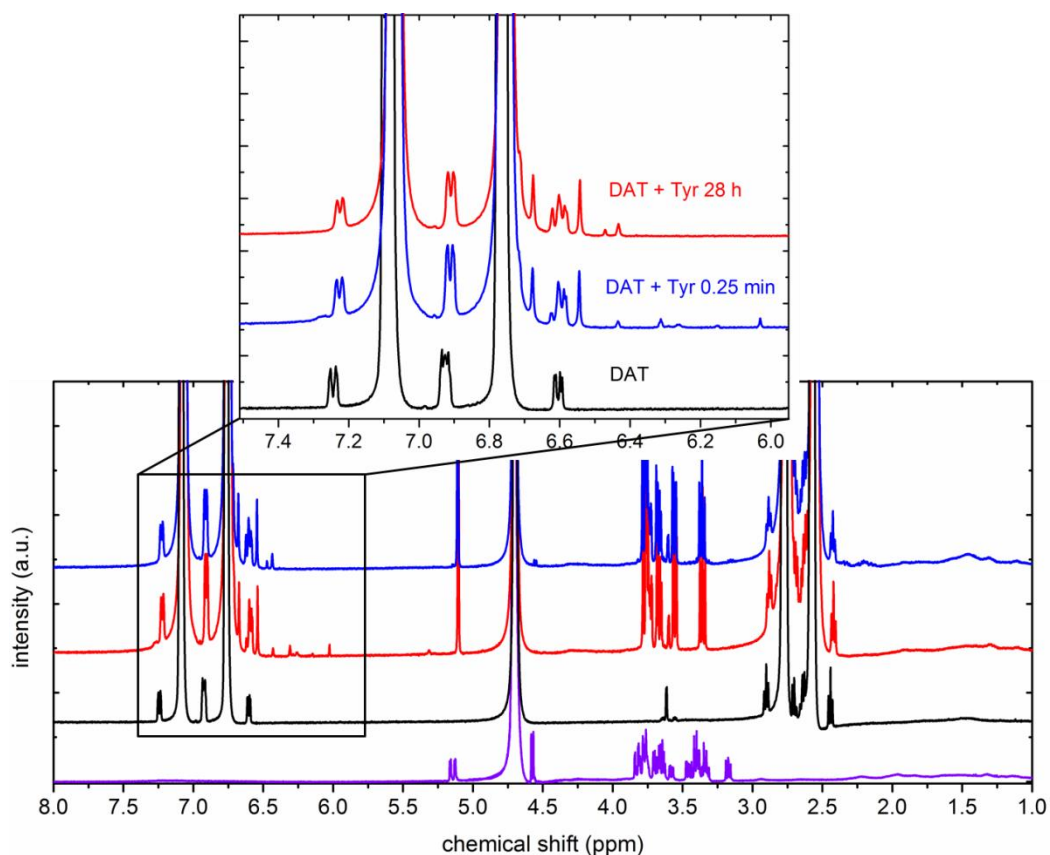


Figure 24:  $^1\text{H}$ -NMR spectra of mushroom tyrosinase (Tyr, purple), DAT (black) and a mixture thereof in  $\text{D}_2\text{O}$  incubated for 15 mins (red), as well as 28 hours (blue) in  $\text{D}_2\text{O}$ .

Indeed, a brown precipitate was observed in  $\text{D}_2\text{O}$  as a result mTyr-mediated crosslinking of DAT, indicating that larger structures with low solubility are formed. The precipitate was insoluble in  $\text{DMF-d}_7$ ,  $\text{DMSO-d}_6$  and  $\text{DCCl}_3$ , but could be partially solubilized in  $\text{D}_2\text{O}$  upon addition of deuterated  $\text{NaOH}$  (Fig. 25A) and in  $\text{MeOD-d}_4$  (Fig. 25B). The  $^1\text{H}$ -NMR spectra collected under these conditions will allow studying different types of compounds. The partial dissolution in basic solution may be due to the deprotonation of phenols available as adducts in the mixture. However, it should be noted that quinones and catechols are susceptible to oxidative changes such as decarboxylation in basic conditions [165] or self-oligomerization, being also dependent on the pH, as discussed in Ch. 5.1.2. Therefore, the spectrum in Fig. 25A might possibly contain artefacts derived from the initially formed DAT oligomer structure, which may explain the different structure of the soluble analytes in both solvents (Fig. 25). The abundance of peaks with  $\delta > 6.7$  ppm (Fig. 25B) may indicate that netpoints are predominantly composed of *o*-diphenol derivatives (see compounds 3, 5 and 6 in Table 3) rather than quinones. The peak at 7.8 ppm could be attributed to the protons of phenolic OH groups.

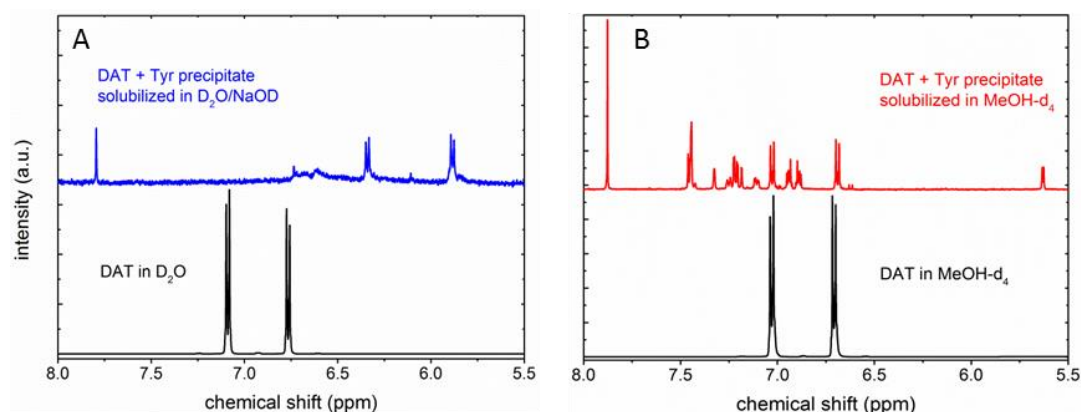


Figure 25:  $^1\text{H}$ -NMR spectra of DAT (black) and the water-insoluble fraction of the oligomers formed by incubation of DAT with mTyr (>28 h), dissolved in A)  $\text{D}_2\text{O}/\text{NaOD}$  (blue) and B)  $\text{MeOH-d}_4$ .

In another set of experiments, the reaction was conducted in  $\text{H}_2\text{O}/\text{O}_2$ , here using DAT-ester as substrate to be incubated with mTyr. The enzymatic oxidation reaction of DAT ester was stopped at different time points by removal of water (freeze-drying), and the products were subsequently dissolved in  $\text{MeOH-d}_4$  (dissolution incomplete). Fig. 26 showed the appearance of various peaks after incubation with mTyr for 15 min and 5h. The fast formation of o-diphenols (peaks at 6.6-6.7 ppm, partially overlapped by the protons of DAT ester at 6.7 ppm) and o-quinones after 5h of mTyr incubation (peaks ~ 6.55 ppm) can be assumed from the observed spectra, as already discussed for the enzymatic conversion of DAT. The formation of various peaks from DAT ester by mTyr catalysis suggested that many different reactions occurred simultaneously. After 48h, the aromatic protons of DAT ester at 6.7 and 7.0 ppm completely disappeared. The products exhibited a broad peak as an evidence for the formation of heterogeneous structures. The main changes observed during the first 5h of mTyr-catalyzed DAT ester crosslinking are in the high field of the aromatic region (~ 6.4-7.3 ppm). Since the protons in the vicinity of the phenolic OH groups are detected there, the newly formed peaks at 6.2 to 6.7 ppm indicated that the 5-position of DAT ester, adjacent to the phenolic OH is more prone to oxidative changes. This result was also reported for other substrates, stating that formation of catechol dimers coupled at the 5,5'-position is favored (see compound 6, Table 3).

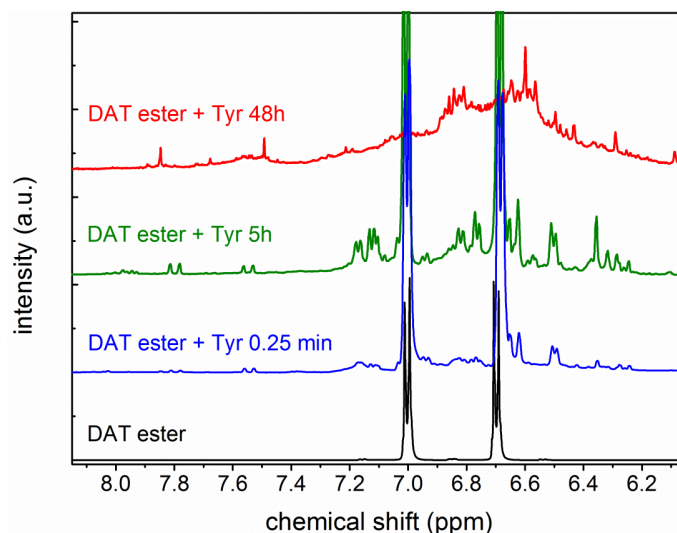


Figure 26:  $^1\text{H-NMR}$  spectra of DAT ester before (black) and after incubation with mushroom tyrosinase (Tyr) for 15 min (blue), 5 h (green) und 48h (red), recorded in  $\text{MeOH-d}_4$ .

Furthermore, model reactions with purified DAT-IOEG<sub>OMe</sub> 2 kDa, incubated with mTyr in  $\text{D}_2\text{O}/\text{O}_2$  were carried out to investigate the favored crosslinking pathway of DAT bearing an oligomer tail. The reaction mixture was measured at different timepoints.  $^1\text{H-NMR}$  spectroscopic analysis showed only minor changes after 24h (Fig. 26). After 7 days, the aromatic protons of DAT disappeared to give rise to a broad peak of oligomeric compounds, similar to the spectrum of DAT ester after 48h. Also, changes in the region between 2.2 and 3 ppm were demonstrated, indicating that the chemical environment of the protons of the aliphatic chain in DAT has changed, as predicted in Table 3. The modification of DAT-IOEG<sub>OMe</sub> 2 kDa by mTyr is slower compared to DAT, which may be due to the detrimental effect of OEG on Tyr catalysis rate. This finding is supported by literature stating that the oxidation rate of *o*-diphenol derivatives is reduced with increasing the length and decreasing the hydrophobicity of the substituent in *p*-position with respect to the phenolic OH groups.[166]

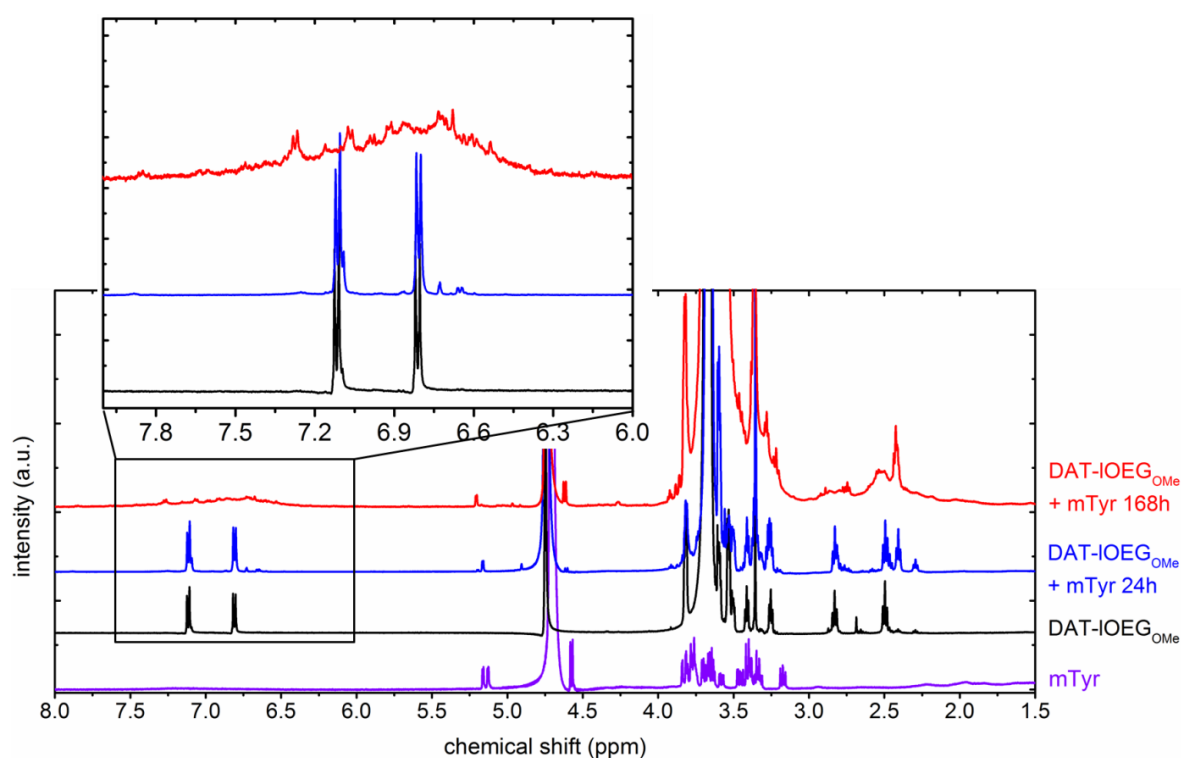


Figure 27:  $^1\text{H-NMR}$  spectra of DAT-IOEG<sub>OMe</sub> before (black) and after incubation with tyrosinase mTyr in  $\text{D}_2\text{O}/\text{O}_2$  for 24 h (blue) und 7 d (red).

In summary, DAT, DAT ester and DAT-IOEG<sub>OMe</sub> all showed to be successfully crosslinked by mTyr. The  $^1\text{H-NMR}$  spectra showed a difference in the composition of the three studied reaction mixtures, which may origin from a difference in the favored reaction pathways for the three substrates. *O*-diphenols as intermediates were assumed for both DAT and DAT ester, while *o*-quinones seemed to be present to a higher extent in DAT containing reaction mixtures, and these structures may be possibly found in the adducts, formed from the latter substrate by enzymatic oxidation. Importantly, the fact could also result from the difference in the mTyr catalysis rate among the different substrates. This is relevant to note as the coupling of DAT derivatives in the non-enzymatic pathways may be based on the kinetics of their generation in the preceding enzymatic step. The multitude of peaks for reaction intermediates, e.g. in DAT ester oxidation, demonstrated that many chemical processes took place in the same time. Some of the multimers formed from DAT and DAT ester by mTyr catalysis were inaccessible for spectroscopic analysis due to the occurrence of fractions that are both insoluble in non-polar and only partially soluble in polar solvents. The products of mTyr-catalyzed oligomerization of different substrates could be elucidated by  $^1\text{H-NMR}$  investigation due to the structural complexity.

Thus, the structure and functionality of netpoints, formed in model reactions, was further studied by mass spectrometry, MS.

## 5.5 Analysis of netpoint structure and functionality by MALDI-ToF

---

In order to gain further insights in the abundance of specific reaction products that may serve as netpoints in case of mTyr crosslinked hydrogels, mass spectrometry should be applied. Within this chapter, three different mTyr substrates were incubated with the enzyme and the formed products were analyzed by MALDI-ToF-MS, aiming to enlighten the number of molecules per netpoint. Furthermore, the detected peaks should be assigned to specific compounds, since MS is very sensitive in detecting exact masses. As substrates, DAT and DAT ester were employed in addition to DAT-IOEG<sub>OMe</sub> 10 kDa and purified monodisperse DAT-ImOEG<sub>OMe</sub> 2 kDa (see Ch. 4.1). By this comparison, not only the reaction products but also the effect of the highly hydrated, sterically demanding OEG molecule on the oligomerization should be investigated.

Model reactions were first carried out with DAT and DAT ester. When considering all the routes for the non-enzymatic pathways reported in literature so far (Fig. 18), 5 reactive compounds may act as monomeric reaction partners for subsequent multimer formation (1-5, Fig. 28). Out of the different possibilities for combination among them, 14 theoretical dimers with different structures are possible. Considering the fact that the adduct formation on the aromatic/quinonoid ring can take place on positions 3 and 5 (resulting in 5,5', 3,3' or 3,5' isomeric dimers), [167] over 40 theoretical dimers are possible. The situation gains in complexity for each further added repeating unit. The selected mass spectrometry method is reliable for detection of masses with  $m/z$  larger than 500, which corresponds to DAT/DAT ester trimers with an additional  $m/z$  of  $\sim 180$  Da for each additionally added DAT and  $m/z \sim 194$  for each DAT ester derivative, respectively. Since the error of the MALDI-ToF measurement typically does not exceed  $m/z$  of 0.5, it should be possible to distinguish between the different intermediates 2-5 in Fig. 28. However, structural isomers with identical masses (compare compounds 3 and 4, 7 and 8, and 9 and 10 in Fig. 28) could not be discriminated by this methodology.

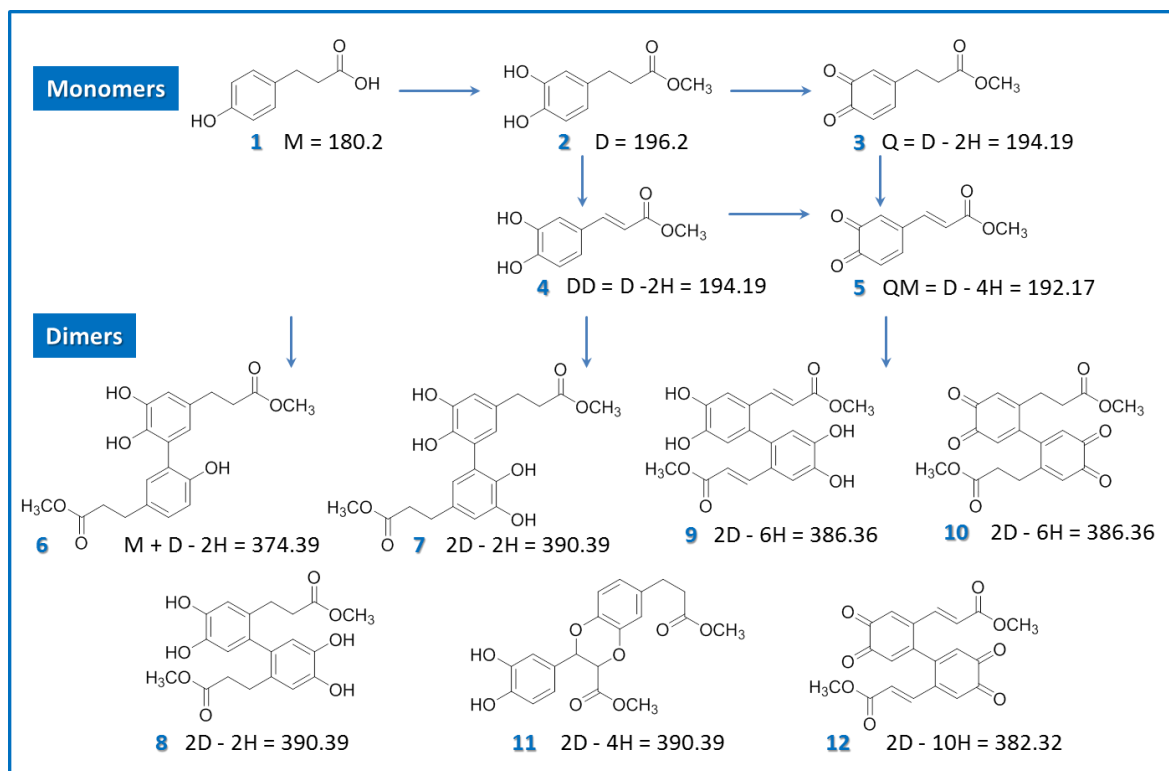


**Figure 28:** Prediction of possibly detected masses in model reactions with DAT ester.

Chemical structures of DAT ester (1) and monomeric intermediates (2-5), potentially resulting from mTyr catalyzed oxidation, as well as a selection of possibly formed dimers (6-12) with their theoretical calculated masses. The calculations considered the most abundant masses, formed with the main isotopes. *M* – monophenol, *D* – *o*-diphenol, *Q* – *o*-quinone, *QM* – quinone methide, *DD* –  $\alpha,\beta$ -dehydro *o*-diphenol

When DAT was incubated with mTyr for 48 h, MALDI-ToF detected peaks up to  $m/z$  1200 corresponding to multimers with two to six repeating units (Fig. 29A). The relative amount of oligomers decreased with increasing number of molecules per netpoint. A high background signal was observed, but some of the detected masses corresponding to tri- to pentamers could be assigned to expected compounds. Mostly quinone/ $\alpha,\beta$ -dehydro *o*-diphenol derivatives involved in oligomerization and they were connected to *o*-diphenol or DAT monomeric units, which is in accordance with NMR analysis in Ch. 5.4. Although MALDI-ToF is usually a non-destructive mass spectrometric method, the occurrence of peaks with unknown structure indicated that fragmentation of some DAT functional groups may have taken place.

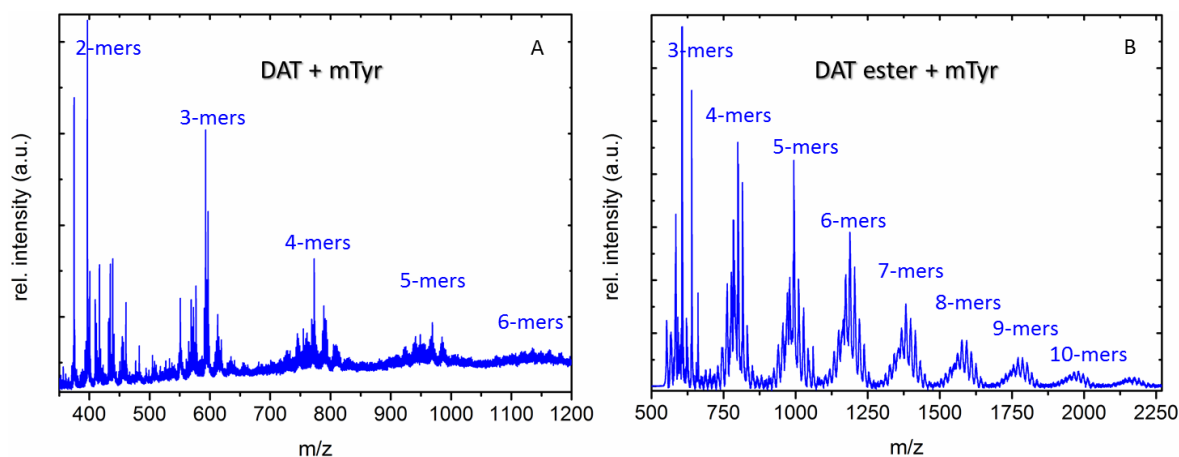


Figure 29: MALDI-ToF spectra of DAT (A) and DAT-ester (B) in presence of mTyr 48 hours after addition of the biocatalyst, The sets of peaks indicate the formation of oligomers with up to 6 (A) or 11 (B) repeating units.

For DAT ester, larger oligomers could be detected. Signals of compounds with  $m/z$  up to  $2250 \text{ g}\cdot\text{mol}^{-1}$  were detected, which corresponds to decamers (Fig. 29B). Almost all detected masses of tri- to pentamers could be assigned, see Table 2. The masses of the resulting intermediates vary by 2, and each coupling is associated with the loss of 2 protons, as demonstrated for the dimers shown in Fig. 28. The complexity of the formed structures increases with each further repeating unit. Therefore, an assignment of masses beyond pentamers was not attempted due to the various possible structural isomers that limit a precise assignment.

The detected oligomers were formed mostly by coupling of mono- and diphenolic species, and few quinone/ $\alpha,\beta$ -dehydro *o*-diphenol species. Remarkably, non-oxidized DAT seemed to take part in most of the detected netpoints (Table 4). This may be explained by the rate-limited character of the enzymatic phenol hydroxylation, meaning that DAT ester is present in a relatively high concentration in the crosslinking mixture. Other authors also found *o*-diphenol-phenol adducts when crosslinking short tyrosine-containing peptides with mTyr. [168]

Surprisingly, a trimer composed solely of DAT ester was identified after mTyr catalyzed oxidation. Monophenol adducts typically result from one-electron-oxidations described for other biocatalysts such as HRP or laccase. However, polymerization of unsubstituted phenols resulting from C-O couplings at positions 4 or 2 as well as from C-C couplings were reported to be catalyzed by model monooxygenase copper complexes.

[16g] Therefore, it is an interesting finding that mTyr catalysis apparently also produced phenoxy radicals.

Table 4: Proposed structures of multimers of DAT ester in H<sub>2</sub>O/O<sub>2</sub> in presence of mTyr after 48h based on assignment of calculated and detected masses by MALDI-ToF in two independent measurements (1 and 2).

Multimers	Proposed Structure	Calcul. mass (g·mol <sup>-1</sup> )	Detected mass (g·mol <sup>-1</sup> )	Rel. intensity (a.u.)	Measur. #
<b>Trimers</b>	[D + 2M + H] <sup>+</sup>	552.576	552.548	0.18	1
	[D + 2M + K] <sup>+</sup>	591.565	591.397	0.28	2
	[D + 2M + K] <sup>+</sup>	607.673	607.400	1.00	2
	[3M + H] <sup>+</sup>	584.574	584.743	0.48	1
	[3M + Na] <sup>+</sup>	605.564	605.475	1.00	1
<b>Tetramers</b>	[3D + M + H] <sup>+</sup>	762.761	763.050	0.29	1
	[D + 2Q + M + H] <sup>+</sup> or [3D + Q + H] <sup>+</sup>	776.859 or 776.760	777.072	0.32	1
	[2D + 2M + K] <sup>+</sup>	785.860	785.416	0.54	2
	[3D + Q + Na] <sup>+</sup>	799.750	799.685	0.68	1
	[3D + Q + K] <sup>+</sup>	815.858	815.837	0.57	1
			815.443	0.64	2
	[2D + Q + M + H] <sup>+</sup>	783.751	783.736	0.46	1
	[4D + Na] <sup>+</sup>	801.75	801.437	0.69	2
<b>Pentamers</b>	[4D + Q + H] <sup>+</sup>	970.946	971.335	0.26	1
	[4D + Q + Na] <sup>+</sup>	993.936	993.863	0.63	1
			993.487	0.58	2
	[3D + Q + M + H] <sup>+</sup>	954.947	956.303	0.17	1
	[4D + M + Na] <sup>+</sup>	979.937	979.892	0.30	1
			979.483	0.36	2
	[4D + Q + K] <sup>+</sup>	1010.044	1010.072	0.30	1
		1009.518	0.31	2	

Abbr.: M = monophenol (DAT ester), D = respective o-diphenol derivative, Q = o-quinone. Q or DD as structural isomers may be present in resp. crosslinks interchangeably.

Furthermore, the analysis of netpoint functionality was carried out with DAT monofunctionalized oligomers. DAT-IOEG<sub>OMe</sub> 10 kDa was incubated with mTyr, and the reaction mixture was analyzed after 2 and 8h (Fig. 30). A small fraction of dimers (peak at m/z ~21,000) and a minor amount of trimers (m/z ~32,000) were detected in addition to the precursor after mTyr catalyzed oxidation. The relative amount of DAT-IOEG<sub>OMe</sub> 10 kDa was reduced after 8h, indicating that it further engaged in reaction. However, the oligomer coupled DAT was not quantitatively converted to higher molecular weight products despite the high amount of DAT-functionalized end groups (*d.f.* = 87 mol%). The low percentage of oligomers can also reflect the fact that masses are less prone to be ionized and transferred into gas phase after laser treatment with increasing m/z, and thus are less likely to be detected by MALDI-ToF.

This investigation suggested that steric hindrance by the OEG chain might change the probability of mTyr catalyzing end group oxidation or hinders the formation of bigger adducts. Moreover, radicals or reactive intermediates randomly attack available reactions partners in the solution. There is lower probability of encountering a dimer than a monomeric species, since a higher fraction of the latter reaction partners was present in the reaction mixture as a result from the slow reaction kinetics and the observed incomplete precursor oligomerization. Another relevant aspect may be the lower mobility of macromolecules, i.e. DAT-IOEG<sub>OMe</sub> compared to DAT ester, which were more prone to form oligomers with higher number of repeating units. However, it remained unclear if the reaction products from DAT-IOEG<sub>OMe</sub> 10 kDa by mTyr mediated polymerization were ionized and detected by MALDI-ToF.

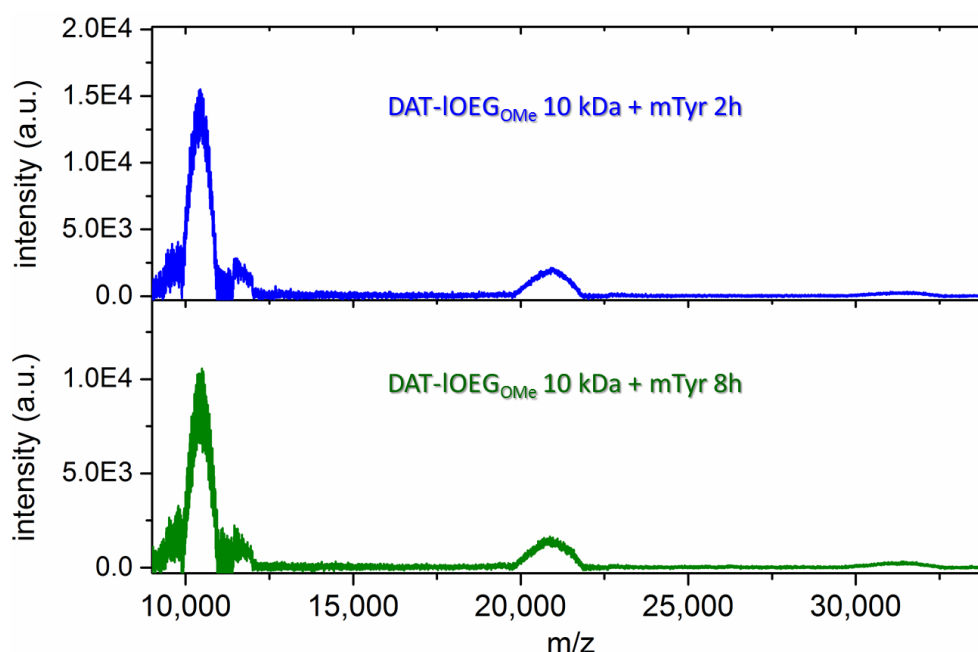


Figure 30: MALDI-ToF of DAT-IOEG<sub>OMe</sub> 10 kDa, incubated with mTyr for 2 h (top) and 8 h (bottom).

Since the number of polymer chains connected by mTyr- induced conversion of DAT could not be fully elucidated based on the spectra in Fig. 30, DAT-ImOEG<sub>OMe</sub> with a discrete and lower molecular weight of 2 kDa (highly purified by RP-HPLC, as reported in Ch. 4.1) was investigated in another set of experiments. Fig. 31 illustrates that the peaks corresponding to DAT-ImOEG(48)<sub>OMe</sub> ( $m/z$  2293.26, 2315.13 and 2331.18, representing the oligomer with H, Na and K as counter ions, respectively) disappeared almost quantitatively already 1h after addition of the biocatalyst. Oligomers with intensities comparable to the background noise due to the low amount in the purified oligomer precursor (overall impurities < 5%) considerably increased in intensity, as suggested exemplarily by the

peaks in the low  $m/z$  range below 1750. Some compounds in this range seemed to be incorporated into oligomer couplings much slower. For example, the amount of oligomers with masses detected at  $m/z$  800 to 1800, corresponding to DAT- or  $\text{NH}_2$ -ImOEG<sub>OMe</sub> of varying OEG chain length (unequivocal assignment due to very similar theoretical  $m/z$  values of the different ionized oligomers) decreased significantly in the course of incubation with mTyr (compare the peaks in the selected range after 1, 8 and 24 h of mTyr incubation, Fig. 31). Therefore, these compounds were also converted to chain junctions by enzymatic catalysis. Peaks indicating the conversion of DAT end groups to *o*-diphenol (D) and quinone (Q) residues, i.e.  $[\text{Q-ImOEG}(48)_{\text{OMe}}+\text{Na}]^+$  at  $m/z$  2330.474,  $[\text{Q-ImOEG}(48)_{\text{OMe}}+\text{K}]^+$  at  $m/z$  2345.512,  $[\text{Q-ImOEG}(51)_{\text{OMe}}+\text{K}]^+$  at  $m/z$  2481.458, and  $[\text{D-ImOEG}(49)_{\text{OMe}}+\text{K}]^+$  at  $m/z$  2391.489, were detected after 1h of incubation (see arrows in Fig. 31). Their relative intensity decreased within the next 24h of mTyr catalyzed oxidation, suggesting that the intermediates further formed junctions by non-enzymatic processes. A small fraction of precursor was apparently not reacting, as seen from the oligomer peaks, detectable after 24h of mTyr incubation. This includes MeO-ImOEG<sub>OMe</sub>, which bears not reactive end group (e.g.  $[\text{Me-ImOEG}(48)_{\text{OMe}}+\text{Na}^+]^+$ : 2181.561), and apparently also a fraction of  $\text{NH}_2$ -ImOEG<sub>OMe</sub> (compare Ch. 5.7). A detailed interpretation of the spectra by the disappearance of distinct oligomer peaks as a result from mTyr catalysis was possible, and DAT-ImOEG<sub>OMe</sub> seemed to be completely converted in the selected conditions, but the products seemed to be difficult to detect by MALDI-ToF.

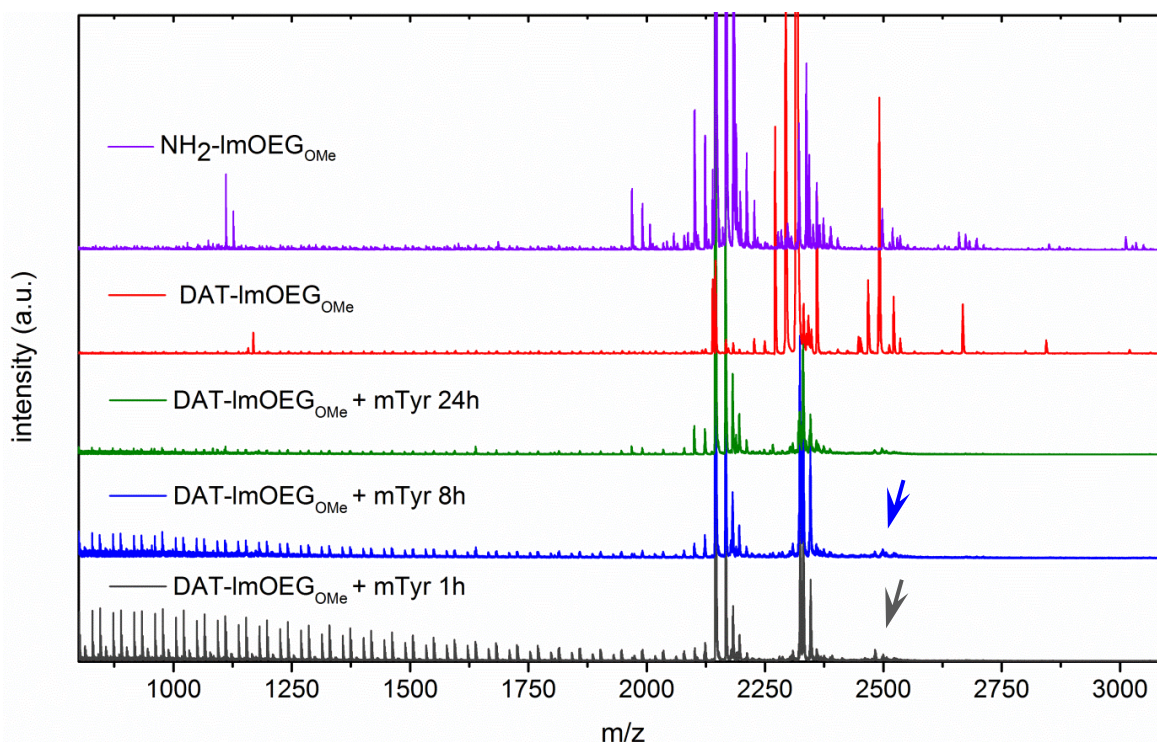


Figure 31: MALDI-ToF spectra of purified DAT-ImOEG<sub>OME</sub> 2 kDa, incubated with mTyr for 1h (grey), 8h (blue) and 24h (green) in comparison to the unmodified precursor DAT-ImOEG<sub>OME</sub> 2 kDa (red) and unfunctionalized NH<sub>2</sub>-ImOEG<sub>OME</sub> 2 kDa (purple).

A further aim of this analysis was to study the chemical structure of chain junctions formed from DAT-ImOEG<sub>OME</sub> by mTyr catalysis. However, marginal amounts of dimers and no trimers were found. Two peaks might be assigned to dimers from two molecules of Q-ImOEG(48)<sub>OME</sub> with Na<sup>+</sup> and K<sup>+</sup> counter ions ( $m/z$  4635.480 and 4650.992 respectively), but the interpretation is not very reliable due to the low relative intensity < 0.01. It is assumed that the di- and multimers from DAT-ImOEG<sub>OME</sub> 2 kDa did not crystallize with the applied matrix DHB despite the conducted variation of sample to matrix ratio (1:1 up to 1:50 tested). The better detection of di- and trimers from DAT-IOEG<sub>OME</sub> 10 kDa (Fig. 30) may be due to the higher tendency of OEG to crystallize with increasing OEG chain length.

In conclusion, the MALDI-ToF allowed gaining further insights in the chemical motives formed by enzyme induced reaction. This particularly applies for the model reactions with small molecular substrates, which formed multimers with up to 6 or 11 repeating units for for DAT and DAT ester, respectively. The products formed from DAT were mostly composed from Q/DD intermediates, combined with D and M residues (see Fig. 28), while the structures derived from DAT ester were predominantly D and M-like motives. In contrast, the detected range of products from DAT with a long oligomeric

chain, DAT-IOEG<sub>OMe</sub> 10 kDa, was limited to dimers and few trimers. The low detection of products with more than 3 repeating units was anticipated to rely on steric reasons. However, it could not be excluded that the formed oligomer junction products were not ionized and therefore undetectable by MALDI-ToF. The investigation of DAT-ImOEG<sub>OMe</sub> 2 kDa by MALDI-ToF revealed the quantitative conversion of DAT bearing oligomers by mTyr catalysis for the selected conditions. Since only marginal peaks resulting from chain couplings from DAT-ImOEG<sub>OMe</sub> 2 kDa could be detected by MALDI-ToF, the model reaction was investigated by LC-ESI-MS, as reported in the following Ch. 5.6. The study of side reactions of DAT with NH<sub>2</sub> groups mediated by mTyr is described in Ch. 5.7.

## 5.6 Analysis of netpoint structure and functionality by LC-ESI-MS

---

Liquid chromatography coupled electrospray ionization mass spectrometry (LC-ESI-MS) is an alternative approach to analyze the structure and functionality of netpoints formed by mTyr catalysis from DAT-ImOEG<sub>OMe</sub> derivatives. The higher accuracy of mass determination by ESI-MS (deviation between theoretical and detected masses usually below  $m/z$  0.05) compared to MALDI-ToF can be advantageous for the unambiguous assignment of detected compounds. The chromatographic separation of products prior to MS analysis would be particularly important to clarify the structures of the heterogeneous products of mTyr catalyzed DAT-IOEG<sub>OMe</sub> crosslinking, as indicated by NMR spectroscopy (Ch. 5.4).

First, the purified monodisperse DAT-ImOEG<sub>OMe</sub> (5 mg·mL<sup>-1</sup> (w/v)) was incubated with mTyr (1000 U·mL<sup>-1</sup>) for 24h and analyzed by standard RP-HPLC with UV detection. The chromatogram of the reaction mixture demonstrated several new peaks (Fig. 32, bottom) compared to the precursor in Fig. 32 (top). Beside the peak of mTyr, eluted after 1.9 min, a series of potential product peaks were detected. Among them, some minor sharp peaks (retention times 4.63, 13.63, 14.81, 16.75, 21.41, 23.44 min and several low-intensity peaks in the range 18.5-20.1 min) were detected aside from the main product peak (retention time 7.72 min). The most intensive peak was quite broad (eluting over more than 5 min), which indicated that these compounds could not be separated on a RP stationary phase

capped with C-18 and phenyl functional groups at the selected eluent composition (see Ch. 8.4).

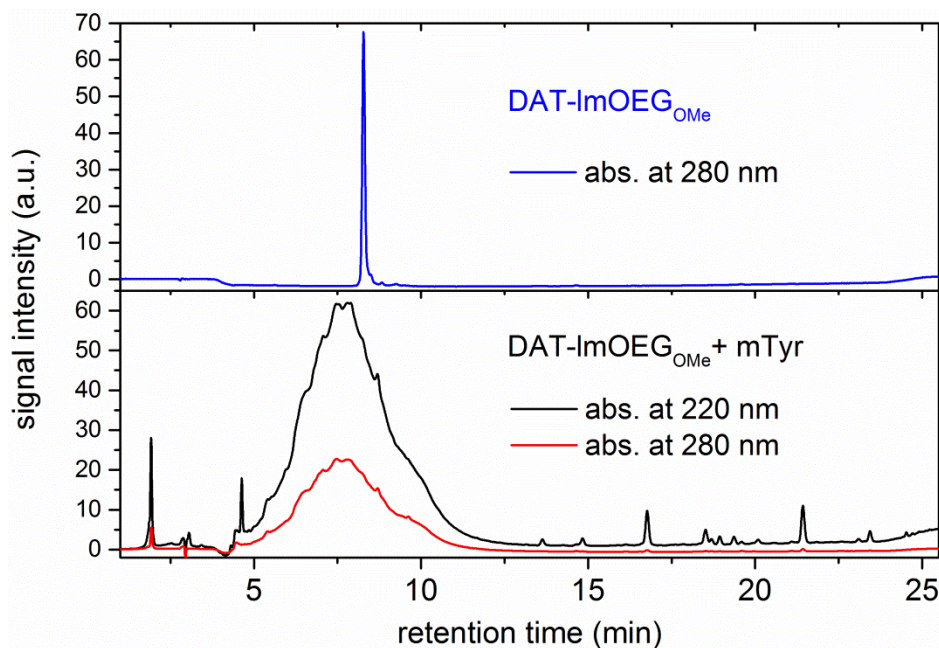
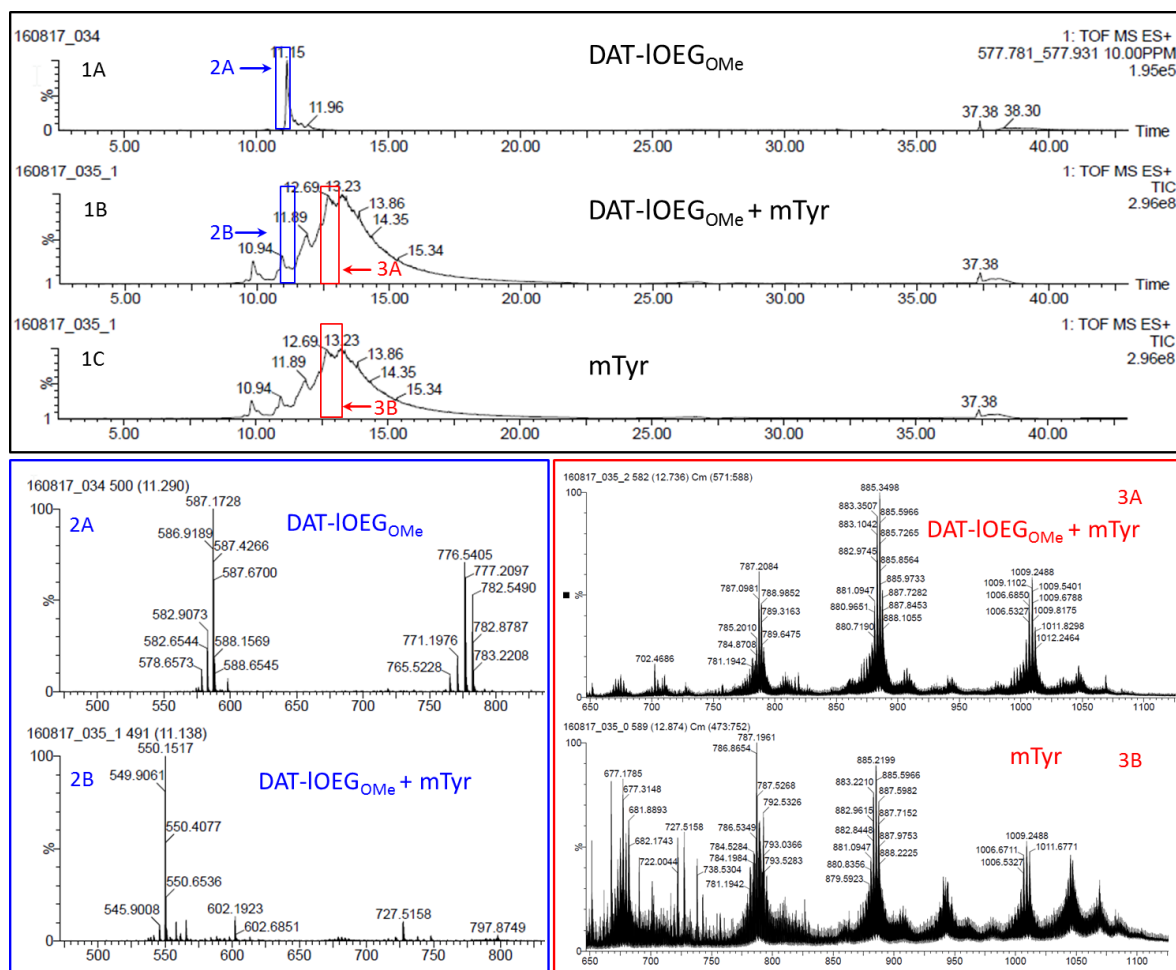


Figure 32: HPLC chromatogram of DAT-ImOEG<sub>OMe</sub> before (top) and after 24h of incubation with mTyr (bottom).

The products were separated on a RP column (C18/phenyl mixed phase) by a gradient elution (H<sub>2</sub>O and ACN as eluents with increasing ACN amount in the mobile phase), monitoring by UV detector ( $\lambda$  220 and 280 nm).

Furthermore, DAT-ImOEG<sub>OMe</sub> 2 kDa, incubated with mTyr for 24h was investigated by LC-ESI-MS. When comparing the total ion chromatograms (TIC) of the precursor before (Fig. 33-1A) and after mTyr catalysis (Fig. 33-1B), the main precursor peak (retention time 11.15 min) seemed to disappear as a result of complete enzymatic conversion. The MS spectra of product (Fig. 33-2B) compared to the precursor (Fig. 33-2A) confirmed that the peaks, corresponding to DAT-ImOEG<sub>OMe</sub> (DAT-ImOEG(48)<sub>OMe</sub>, P: [P+(NH<sub>4</sub>)<sub>3</sub>+H]<sup>4+</sup>: m/z theor. 587.1163, det. 587.173; [P+(NH<sub>4</sub>)<sub>2</sub>+H]<sup>3+</sup>: m/z theor. 776.81, det. 776.809) were not present in the reaction mixture after incubation with the biocatalyst.



**Figure 33: LC-MS analysis of model reactions of DAT-IOEG<sub>OMe</sub> 2 kDa and mTyr:**

Mass chromatograms (TIC) of DAT-IOEG<sub>OMe</sub> (1A), reaction mixture DAT-IOEG<sub>OMe</sub>+mTyr after 24h (1B) and mTyr (1C); ESI-MS spectra (*m/z* vs intensity, i.e. ion counts, as detected by ToF) of DAT-IOEG<sub>OMe</sub> before (2A) and after incubation with mTyr (2B) at retention times of 11.1 and 11.3 min, respectively; ESI-MS spectra of reaction mixture (3A) and mTyr (3B) at retention time 12.9 and 12.7 respectively. For accurate mass assignment, the MS spectrum 2A was recalculated by reference to an external standard and showed *m/z* values showing minor deviation to the theoretical *m/z* of DAT-ImOEG(4<sub>8</sub>)<sub>OMe</sub> adducts, given above.

The TIC of the reaction mixture DAT-ImOEG<sub>OMe</sub> + mTyr (Fig. 33-1B) and mTyr (Fig. 33-1C) differed negligibly. The ESI-MS spectra of those samples at a selected visually different TIC region, where products of oxidative oligomer coupling may be expected, demonstrated identical peaks, present in the reaction mixture (Fig. 33-3A) as well as mTyr solution (Fig. 33-3B). A detailed analysis of the ESI-MS spectra of the DAT-ImOEG<sub>OMe</sub> + mTyr solution showed some impurities originating from commercial mTyr while all peaks, which were not found in DAT-ImOEG<sub>OMe</sub>, resulted from mTyr. Therefore, the undetectable products formed from DAT-ImOEG<sub>OMe</sub> by mTyr catalysis were possibly not ionized.

To conclude, LC-MS analysis of DAT-ImOEG<sub>OMe</sub>, incubated with mTyr demonstrated that the purified model oligomer was quantitatively oxidized by the biocatalyst within 24h.

The products formed by mTyr catalysis were detected by absorption at 220 and 280 nm (HPLC with UV detection) but possibly not ionized and therefore not found in the ESI-MS spectra.

## 5.7 Evaluation of the influence of primary amines on the netpoint structure by model reactions and MS

---

It was hypothesized that amine moieties from unfunctionalized OEG may contribute to mTyr-catalyzed netpoint formation as introduced in Ch. 5.1.2. Therefore, a potential reaction of purified DAT-ImOEG<sub>OMe</sub> 2 kDa mixed with varying amount of nucleophiles, i.e. NH<sub>2</sub>-ImOEG<sub>OMe</sub> (further regarded as DAT+NH<sub>2</sub>-ImOEG<sub>OMe</sub>), was studied. The molar ratio of NH<sub>2</sub> and DAT as end groups in ImOEG<sub>OMe</sub> was systematically increased (simulating varying *d.f.* of OEG with DAT groups) in order to investigate if the amounts of NH<sub>2</sub> and DAT-derived reaction partners affect the netpoint types.

The model solutions (oligomer concentration 5 mg·mL<sup>-1</sup> (*w/v*)) were incubated with mTyr (500 U·mL<sup>-1</sup>) for 24 h in PBS/O<sub>2</sub>. As seen in MALDI-ToF spectra of all DAT-ImOEG<sub>OMe</sub> + NH<sub>2</sub>-ImOEG<sub>OMe</sub> model solutions, the main peaks corresponding to NH<sub>2</sub>-ImOEG(48)<sub>OMe</sub>, E ([E(48)+H]<sup>+</sup> *m/z*: theor. 2145.3, det. 2145.56; [E(48)+Na]<sup>+</sup> *m/z*: theor. 2167.28, det. 2167.48; [E(48)+K]<sup>+</sup> *m/z*: theor. 2183.25, det. 2183.47) were detected also after incubation with mTyr. However, the relative intensities of other NH<sub>2</sub>-ImOEG<sub>OMe</sub> (E) peaks (e.g. *m/z* 1969.194/1991.18 and 2321.5/2343.39 representing H<sup>+</sup> and Na<sup>+</sup> adducts of E(44) and E(52), respectively) decreased in the selected conditions. This suggested that amino groups partially reacted to netpoints with DAT-ImOEG<sub>OMe</sub>, activated by mTyr.

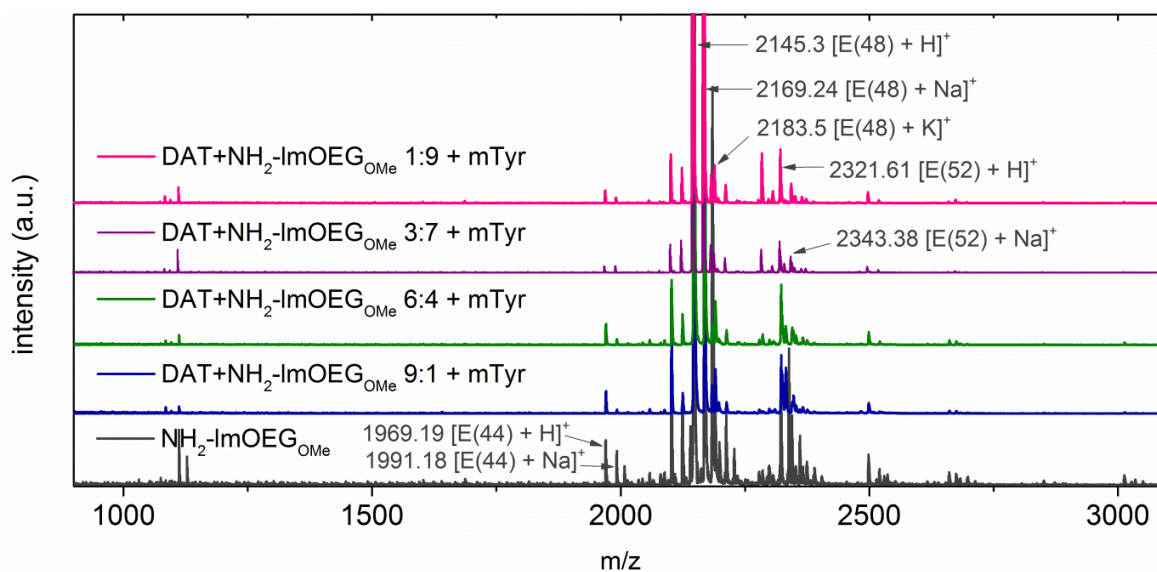


Figure 34: MALDI-ToF spectra of mTyr catalyzed reaction of DAT-ImOEG<sub>OME</sub> with NH<sub>2</sub>-ImOEG<sub>OME</sub> after 24 h.

The molar concentration of the unfunctionalized precursor was increased gradually from 10% (blue) to 40% (green), 70% (purple) and 90% (pink), while the overall oligomer concentration in the reaction mixtures remained constant (5 mg·mL<sup>-1</sup>). A decrease of the relative intensity of some oligomer peaks is obvious when compared to a standard solution of NH<sub>2</sub>-ImOEG<sub>OME</sub> (grey).

Another interesting aspect was to estimate the relative amount of NH<sub>2</sub> groups participating in netpoints depending on the sample composition. Exemplarily, the signals of NH<sub>2</sub>-ImOEG(24)<sub>OME</sub> were selected (Table 5). The areas of peaks, detected by MALDI-ToF, cannot be used for quantitative determination of the analyte composition, but the observed relative intensity may give a hint on the relative amount of the selected oligomer in condensed phase. At a 1:9 molar ratio of NH<sub>2</sub> and DAT, the relative intensity of the respective peaks did not decrease, indicating that NH<sub>2</sub>-bearing oligomers probably did not form any netpoints with DAT-ImOEG<sub>OME</sub>. The relative intensity of NH<sub>2</sub>-ImOEG(24)<sub>OME</sub> decreased considerably when increasing the relative amount of NH<sub>2</sub>-capped oligomer, peaking at a 1:1 molar ratio of NH<sub>2</sub>:DA. This might imply that 40 and 50 mol% amine functional end groups were optimal for incorporating NH<sub>2</sub>-bearing polymer chains into netpoints. Accordingly, multivalent precursors may be reactive when displaying DAT and NH<sub>2</sub> end groups in the given range.

The relevance of amine functionalities is also supported by literature. Catechol as well as amine groups need to be present to stabilize polymer networks, formed by catechol oxidation, as reviewed. [170] Other authors stated that individual catechols as end groups of polyglycerol dendrites fail to induce stable coatings by oxidative

polymerization, while amines telechels further stabilized these materials by interactions between different coating layers.[171] For other polymers functionalized with catechol groups, low density of surface aromatic groups (30 mol%) was used and the importance of side reactions with amines is proposed.[172]

**Table 5: Semi-quantitative estimation of NH<sub>2</sub>-ImOEG(24)<sub>OMe</sub> incorporation in netpoints after 24 h of mTyr incubation.**

	<b>NH<sub>2</sub>:DAT molar ratio</b>					
	10:0	9:1	7:3	5:5	4:6	1:9
det. rel. int. (a.u.) <sup>(1)</sup>	0.257	0.029	0.056	0.013	0.008	0.031
theor. rel. int. (a.u.) <sup>(2)</sup>	0.257	0.231	0.180	0.128	0.103	0.026
NH <sub>2</sub> residual. rel. amount	1.00	0.13	0.31	0.09	0.08	1.21

*The relative intensities of the peaks, as detected by MALDI-ToF, were used for this calculation comparing the theoretically expected peaks of NH<sub>2</sub>-ImOEG(24)<sub>OMe</sub> in the mixtures of NH<sub>2</sub>-ImOEG<sub>OMe</sub> + DAT-ImOEG<sub>OMe</sub> based on the spectra of pure NH<sub>2</sub>-ImOEG<sub>OMe</sub> precursors (10:0) with those after enzyme addition. <sup>(1)</sup>The values given are a sum of the relative intensities of the peaks with m/z 1087.67, 1111.68 and 1127.69, representing the mass of NH<sub>2</sub>-ImOEG(24)<sub>OMe</sub> with H<sup>+</sup>, Na<sup>+</sup> and K<sup>+</sup> as counter ions, respectively. <sup>(2)</sup>Calculated by relating the rel. int. of the respective peaks in the pure NH<sub>2</sub>-ImOEG<sub>OMe</sub> sample to the molar ratio of NH<sub>2</sub> functional groups in the reaction mixtures.*

It should be noted that DAT-ImOEG<sub>OMe</sub> reacted quantitatively in all studied oligomer compositions, indicating that the favored crosslinking mechanism is based on DAT-derived adducts. This may result from DAT self-polymerization being a kinetically favored process. This assumption is in accordance with literature, reporting that the aryloxy radical dismutation (synproportionation mechanism in Fig. 18) takes place faster than the condensation of amines and quinones. [173] Another aspect explaining the non-quantitative incorporation of unfunctionalized oligomer into netpoints is the relative low nucleophilic reactivity of the NH<sub>2</sub> groups at the selected pH. Deprotonated amines are stronger nucleophiles, therefore the optimal nucleophilic reactivity would be given at pH>10, since the pK<sub>a</sub> of NH<sub>2</sub>-ImOEG<sub>OMe</sub> is expected to be > 9 (pK<sub>a</sub> of 2-aminoethanol is 9.5).[174] However, mTyr is not expected to catalyze substrate oxidation at such high pH values due to denaturation.[175] It should also be considered that the reactivity of the quinone component may also exhibit pH dependency.

Data analysis included a more detailed examination of MALDI-ToF signals to eventually collect structural information on the formed reactions products formed from DAT ImOEG<sub>OMe</sub> + NH<sub>2</sub>-ImOEG<sub>OMe</sub> by mTyr catalysis. Peaks of minor intensity were detected in the m/z range expected for dimers (m/z > 4400). As summarized in Table 6,

some peaks could be assigned to dimers purely based on mTyr-oxidized DAT-ImOEG<sub>OMe</sub> derivatives. A few products also appear to result from Michael addition rather than Schiff base formation between DAT and NH<sub>2</sub> end groups. The latter finding is corroborated by a recent literature study of model catechols being polymerized by oxidation with NaIO<sub>4</sub> in presence of a model propylamine derivative at pH 11. In this study, the formation of adducts from catechol self-polymerization as well as Michael addition of amines were proven by different methods. [173]

Table 6: Proposed structures of dimers formed from DAT-ImOEG<sub>OMe</sub> + NH<sub>2</sub>-ImOEG<sub>OMe</sub> solutions by mTyr catalysis based on assignment of theoretically expected masses and detected m/z by MALDI-ToF. M = monophenol (DAT), D = *o*-diphenol, Q = *o*-quinone, MA = Michael addition.

NH <sub>2</sub> :DAT molar ratio	Detected m/z	Theor. m/z	Proposed structure
1:9	4495.804	4495.643	[Q-IOEG(48) <sub>OMe</sub> +NH <sub>2</sub> -IOEG(48) <sub>OMe</sub> +Na] <sup>+</sup> (MA)
	4546.986	4547.554	[2xQ-IOEG(47) <sub>OMe</sub> +Na] <sup>+</sup>
	4567.271	4568.590	[Q-IOEG(48) <sub>OMe</sub> +Q-IOEG(47) <sub>OMe</sub> +Na] <sup>+</sup>
	4624.424	4623.643	[M-IOEG(48) <sub>OMe</sub> +D-IOEG(48) <sub>OMe</sub> +Na] <sup>+</sup>
	4666.734	4667.669	[M-IOEG(48) <sub>OMe</sub> +D-IOEG(49) <sub>OMe</sub> +Na] <sup>+</sup>
4:6	4408.704	4407.590	[Q-IOEG(47) <sub>OMe</sub> +NH <sub>2</sub> -IOEG(47) <sub>OMe</sub> +Na] <sup>+</sup> (MA)
	4449.107	4449.601	[Q-IOEG(48) <sub>OMe</sub> +NH <sub>2</sub> -IOEG(47) <sub>OMe</sub> +Na] <sup>+</sup> (MA)
	4529.868	4528.596	[2xD-IOEG(47) <sub>OMe</sub> +H] <sup>+</sup>
	4536.550	4535.591	[M-IOEG(47) <sub>OMe</sub> +D-IOEG(47) <sub>OMe</sub> +Na] <sup>+</sup>
	4547.963	4547.554	[2xQ-IOEG(47) <sub>OMe</sub> +Na] <sup>+</sup>
	4562.827	4563.528	[2xQ-IOEG(47) <sub>OMe</sub> +K] <sup>+</sup>
	4622.343	4621.627	[M-IOEG(48) <sub>OMe</sub> +Q-IOEG(48) <sub>OMe</sub> +Na] <sup>+</sup>
	4644.708	4644.680	[M-IOEG(48) <sub>OMe</sub> +D-IOEG(49) <sub>OMe</sub> +H] <sup>+</sup>
4662.472	4660.675	[D-IOEG(48) <sub>OMe</sub> +D-IOEG(49) <sub>OMe</sub> +H] <sup>+</sup>	
5:5	4661.818	4660.675	[D-IOEG(48) <sub>OMe</sub> +D-IOEG(49) <sub>OMe</sub> +H] <sup>+</sup>
7:3	4563.912	4563.564	[2xQ-IOEG(47) <sub>OMe</sub> +K] <sup>+</sup>
	4621.048	4621.627	[M-IOEG(48) <sub>OMe</sub> +Q-IOEG(48) <sub>OMe</sub> +Na] <sup>+</sup>
9:1	4563.049	4563.564	[2xQ-IOEG(47) <sub>OMe</sub> +K] <sup>+</sup>

In summary, incorporation of nucleophilic NH<sub>2</sub> groups as ImOEG<sub>OMe</sub> end groups by mTyr catalysis was studied in DAT-ImOEG<sub>OMe</sub> + NH<sub>2</sub>-ImOEG<sub>OMe</sub> mixtures with decreasing DAT amount by MALDI-ToF. NH<sub>2</sub>-ImOEG<sub>OMe</sub> did not quantitatively react with mTyr-activated DAT end groups, while generally all DAT-ImOEG<sub>OMe</sub> appear to be converted suggesting the coupling of aromatic derivatives to be the kinetically preferred

crosslinking mechanism. Still, the contribution of amine groups to netpoints, presumably formed by Michael addition of  $\text{NH}_2$  to Q residue, has clearly been proven.

## 5.8 Investigation of netpoint structure after hydrogel hydrolysis

In contrast to the model reactions in mTyr containing solutions described in the previous chapters, here it was attempted to investigate the chemical structure of netpoints by isolation from hydrogels formed via crosslinking of multivalent DAT-sOEG 10 kDa by mTyr catalysis. Compared to model reactions, investigation of netpoints in DAT(T)-sOEG hydrogels is difficult on the one side due to the low relative amount of junctions/netpoints compared to OEG chains. On the other side, polymer networks are difficult to analyze e.g. by chromatographic methods due to their insolubility. Solubilization of the structures forming netpoints may in principle be realized by degradation of OEG segments, which can be fulfilled by an oxidative process.[176-179] However, this may potentially result in an undesired change of netpoint structure as a consequence of the harsh conditions. Herein, hydrolysis of the amide bonds connecting sOEG- $\text{NH}_2$  and tyrosine-derived end groups, involved in crosslinks, was chosen, as depicted in Fig. 35. Basic hydrolysis at elevated temperature (7.5 N NaOH, 70 °C, 4 days) was selected, since lower temperature conditions (7.5 N HCl, 37 °C, 10 days) did not lead to substantial network hydrolysis.

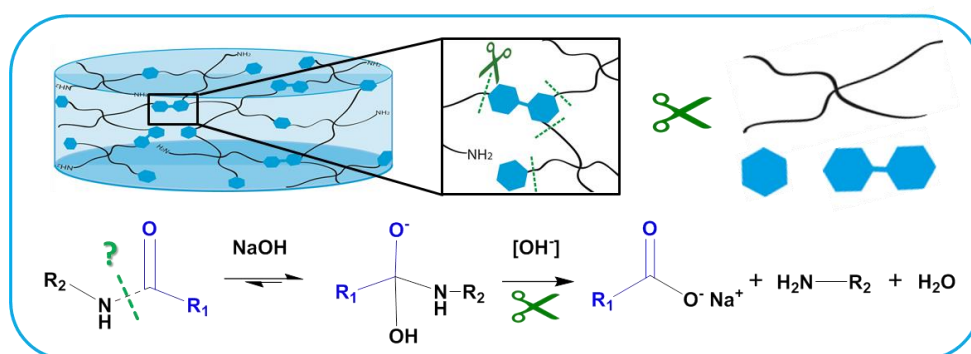


Figure 35: Concept of alkaline hydrolysis of DAT-sOEG hydrogels.

As products, sOEG- $\text{NH}_2$ , free DAT and derivatives thereof (blue hexagon) as well as the study subject, moieties corresponding to former netpoints based on DAT-derived catechols and quinones (illustrated as coupled blue hexagones) are expected.

Upon alkaline treatment of previously extracted and swollen hydrogels from DAT-sOEG 10 kDa (Fig. 36, step 1), no complete network solubilization could be observed. A total weight loss of 55% was calculated from the dried residual hydrogel sample (after step 4 in Fig. 36). A light brown color of the partially hydrolyzed gels was noted, which supported the observation of an incomplete netpoint cleavage. Accordingly, in the medium, a low absolute amounts of solubilized structures originating from netpoints were expected. It should be noted that the simultaneously produced free chains OEG show good solubility in almost all solvents, while a challenging solubility profile was expected for the structures that served as netpoints. This assumption is supported by reports for compounds with similar structures, [165] which was expected to make the separation of both fractions and analysis of the netpoint structures challenging.

The collapsed residual hydrogel was swollen and extensively washed in water and the water-soluble fraction was added to the supernatant fraction collected after alkaline treatment (Fig. 36, step 4). To assure that no cleaved components, which are not water-soluble, remain in the hydrogel, it was then extracted with organic solvents (ether, ethyl acetate, dichloromethane and methanol) (step 3 in Fig. 36). Since those organic phases exhibited no absorption at 280 nm, it was concluded that no additional structures corresponding to netpoints can be removed from the material. In principle, this may suggest an absence of solubility in the organic media, a complete extraction of all soluble materials in the aqueous phase (Fig. 36, steps 4 or 5), or a persistent covalent coupling of some colored components to the hydrogel network structure. Upon neutralization of the supernatant, a soluble fraction (fr\_1) and a precipitate (fr\_2) were isolated (step 6 in Fig. 36). The insoluble fraction fr\_2 was deduced to consist of NaCl as well as phenolic and catecholic derivatives and oligomers, which are dissociated and thus far better soluble in alkaline conditions (DAT-phenol  $pK_a \sim 10$ ).

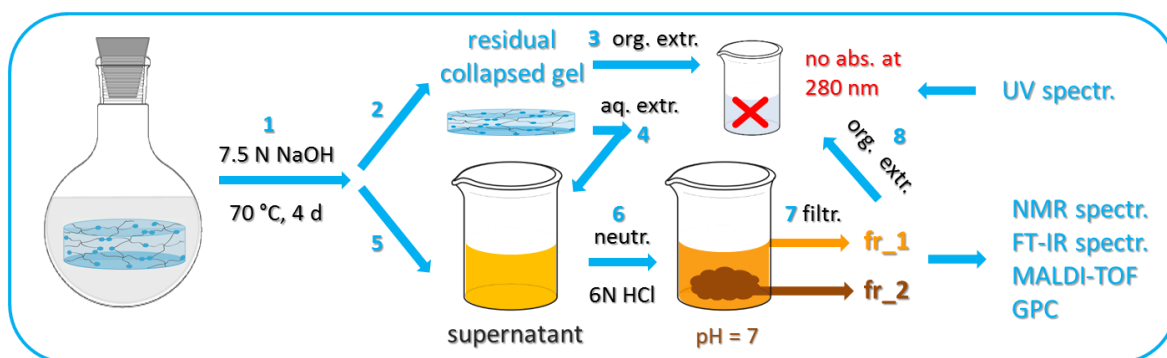
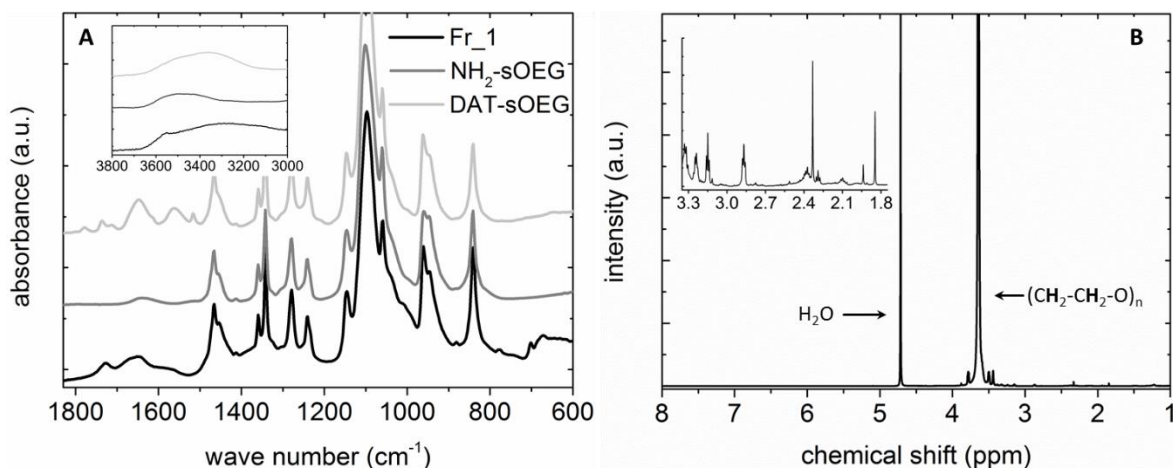


Figure 36: Scheme of the hydrolysate investigation procedure

basic treatment of swollen hydrogel (1), separation of the residual collapsed hydrogel (2) and the supernatant (5). The residual hydrogel was extracted in organic solvent (3) and swollen and washed intensively in water (4). The supernatant was separated into two fractions by neutralization (6) and filtration (7) of the resultant precipitate, fr<sub>2</sub> from the insoluble fraction, fr<sub>1</sub>

No netpoints could be extracted from the aqueous supernatant (fr<sub>1</sub>, Fig. 4) into an organic phase (ether, ethyl acetate or dichloromethane, step 8 in Fig. 4), as screened by UV absorbance measured at 280 nm. Spectroscopic analysis of the aqueous supernatant revealed that fr<sub>1</sub> contained mainly OEG, as confirmed by the peak at 3.65 ppm in <sup>1</sup>H-NMR spectrum (Fig. 37A). The structure was confirmed by the OEG characteristic bands in FT-IR spectrum (Fig. 37B). Apparently, primary amines as end groups of OEG in fr<sub>1</sub> could be excluded according to <sup>1</sup>H-NMR investigation, since no peak was found at 2.6 ppm ( $\alpha$ -methylene to NH<sub>2</sub> in precursors). This leads to the conclusion that other reactions than the intended amide cleavage has taken place. Instead, the <sup>1</sup>H-NMR signals at 3.15 and 2.87 ppm could possibly be assigned to methylene groups of esters or alcohols, respectively, which might be newly created end groups from alkaline hydrolysis. Furthermore, signals of stretching vibration of carbonyls at 1730 cm<sup>-1</sup> was detected by FT-IR in fr<sub>1</sub>, indicating the presence of carbonic acids or aldehydes, probably involved in H-bridges or conjugation with double bonds. The broad band with a shoulder at 3555 cm<sup>-1</sup> and center at 3280 cm<sup>-1</sup> (inset of Fig. 37A) may represent free and H-bonded OH groups, as typical for alcohols and carbonic acids, respectively. A similar conclusion can be made for fr<sub>2</sub>, exhibiting a peak centered at 3420 cm<sup>-1</sup>, see Fig. 39A.



**Figure 37: Spectroscopic analysis of fr\_1 (black):**

*FT-IR spectra, compared to NH<sub>2</sub>-sOEG (grey) and the hydrogel precursor DAT-sOEG 10 kDa (light grey) (A) and <sup>1</sup>H-NMR spectrum (B). Fr\_1 is the water-soluble fraction at neutral pH of the supernatant that results from alkali treatment of DAT-sOEG hydrogels.*

The investigation of fr\_1 gave a hint for unexpected reactions during the alkaline treatment of the hydrogel. The analysis suggested OEG degradation, leading to OEG fragments with terminal alcohol groups from OEG intra-chain scission, as well as OEG with terminal aldehyde, carboxylic or lactone functionalities due to oxidation of OEG side groups. Although performing the alkaline hydrolysis experiment under N<sub>2</sub> atmosphere in a closed system, dissolved oxygen in combination with elevated temperature might have triggered OEG degradation. These findings may be supported by literature on PEG degradation products by oxidative cleavage [177, 178] and additional experiments being performed: Shorter OEG fragments were found by MALDI-ToF. GPC analysis of fr\_1 corroborated the presence of OEG oligomers, as demonstrated by the detected peaks at elution volume > 5.1 mL, while non-degraded DAT-sOEG 10 kDa was eluted at ~5.1 ml (Fig. 38). The fractions with lower molecular weight (i.e. higher elution volume) exhibited no absorption at 280 nm, which supports that these species had no DAT end groups.

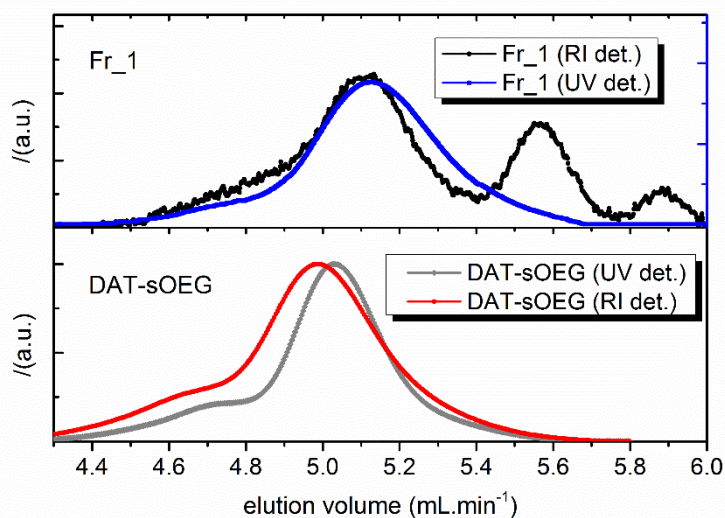


**Figure 38:** GPC elugram of fr\_1 (above) and the hydrogel precursor DAT-sOEG 10 kDa (below), measured in DMF.

The elution profile of both analytes was recorded by RI (refractive index) and UV detector, measuring the absorption at 280 nm. The exact calculation of  $M_n$  and  $M_w$  by universal calibration for fr\_1 was not possible, since the product was not completely solubilized in DMF. The signal of RI detector (black axis, left) above was 1.5 times magnified with respect to UV signal (blue axis, right).

As discussed above, the structures corresponding to netpoints were expected in fr\_2 (Fig. 36). It was assumed that netpoint structures isolated by hydrolysis of DAT-sOEG hydrogel would be of similar chemical composition compared to those detected in model reactions reported above (Ch. 5.2-5.5 and 5.7). To verify this assumption, DAT ester was incubated with mTyr in PBS for 48h and the FT-IR spectrum was compared to the FT-IR spectrum of fr\_2 (both measured in dry state) (Fig. 39A). The vibration patterns of fr\_2 showed poor structural resemblance of a DAT ester crosslinked by mTyr. This may suggest that the structures of interest corresponding to netpoints were not detectable in this fraction as well. The FT-IR spectrum of fr\_2 had some similarities to the IR spectra of dicarboxylates, such as muconic, maleic, oxalic and glyoxylic acids, found to be the main degradation products of catechols.[180] The broad band with maximum at  $3420\text{ cm}^{-1}$ , characteristic for OH vibrations and formed H-bridges, [180] was similar in intensity and form as found in glyoxylic and oxalic acid. The latter acids also exhibit a band near  $1640\text{ cm}^{-1}$ , which could be assigned to the asymmetric vibration of O-C-O functional groups.[180] The band at  $1640\text{ cm}^{-1}$  could also give a hint on the presence of unsaturated hydrocarbon derivatives, found in muconic and maleic acid. However, the absence of a carbonyl band in the region of  $1700\text{ cm}^{-1}$  indicated that the four named species and the respective  $\gamma$ -lactone derivatives thereof [181] were probably not present in fr\_2. Also, the

most intensive band centered at  $1035\text{ cm}^{-1}$  was not found in this intensity in any of the analyzed structures of degradation products of a model catechol.[180] The intensive band centered at  $1035\text{ cm}^{-1}$ , where usually O-H and C-O vibrations are detected, and the weak band at  $2925\text{ cm}^{-1}$  denote that fr\_2 may probably be composed of short-chained alcohols or ethers. The broad bands imply overlapping of vibrations. Also, the presence of crystallites in the sample, e.g. NaCl, may have affected the recording of the FT-IR spectrum by strong scattering phenomena.

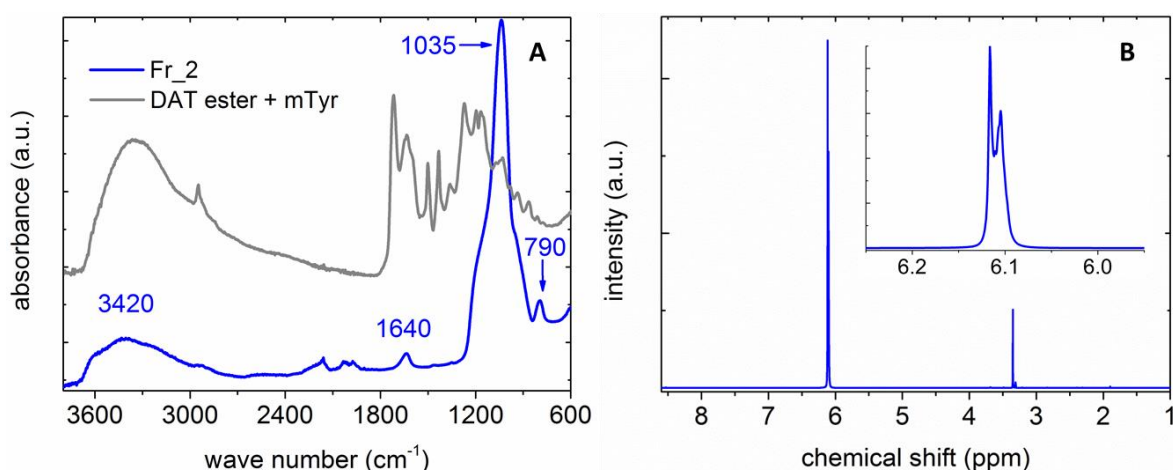


Figure 39: FT-IR and NMR analysis of fr\_2 (blue):

A) FT-IR spectrum compared to DAT ester after treatment with mTyr (grey); B)  $^1\text{H-NMR}$  spectrum of fr\_2 in  $\text{MeOH-d}_4$ . Fr\_2 is the precipitate isolated from the supernatant obtained after alkali treatment of a hydrogel from DAT-sOEG and subsequent neutralization.

A partial dissolution of the precipitate in  $\text{MeOH-d}_4$  allowed recording of  $^1\text{H-NMR}$  spectrum (Fig. 39B), which exhibited a singlet at 3.35 ppm (methylene protons of OEG/ethers or terminal methoxy groups) and a signal at 6.11 ppm, possibly representing an  $\alpha,\beta$ -unsaturated dicarbonyl derivative. A mixture of different compounds in fr\_2 is assumed, which makes an assignment of FT-IR and NMR signals to defined structures impossible.

The absence of aromatic and quinoid compounds and oligomers derived thereof in all analyzed fractions seemed surprising. Oxidative aromatic ring cleavage for phenol, catechol or *o*-quinone derivatives was typically achieved by strong oxidative agents, such as  $\text{H}_2\text{O}_2$ , [182, 183] ozone [180] or by metal catalysts (Fe, [184, 185] Cu or Pb [186]), but not by the conditions described here. However, hydrolysis of hydrogel-entrapped mTyr may have led to the release of Cu in catalytic amounts. The above reaction could also be initiated by free radicals. Catechol oligomerization initiated by autooxidation at  $\text{pH}>8$

bases on the formation of semiquinone radicals. The redox potential for the one-electron transfer is over five times lower at basic pH compared to physiological conditions (98 mV at pH 11 and 530 mV at pH 7).[187] Therefore, *o*-diphenol oxidation is much more probable in the selected conditions of hydrogel basic treatment. Furthermore, phenolates can generate superoxide radicals ( $O_2^{\cdot-}$ ) from oxygen in basic conditions in presence of metal catalysts.[188-190] The free radical initiation combined with the conditions applied during hydrolysis could explain the observed numerous degradation products. Further investigations regarding the degradation mechanism and the composition of the fractions were beyond the scope of this work.

Conclusively, hydrolysis in alkali led to a destruction of netpoints and is not suited for structure analysis of DAT-sOEG based hydrogels. Due to the susceptibility of catechols and quinones to oxidations, also acidic treatment may lead to an undesired change of netpoints structure. Also, enzymatic amide cleavage would require complete enzyme permeability through the network mesh and face challenges in terms of peptidases accessibility to the relevant cleavable amides next to sterically demanding DAT-derived units. Therefore, the attempt to mirror the netpoint structure by model reactions of polymeric substrates with mTyr, leading to soluble analytes (Ch. 5.2 to 5.7) proved more promising to investigate netpoint chemical properties.

## 5.9 Summary and rationale for selection of hydrogel precursors

---

Investigation of structure and functionality of netpoint, being formed from DAT derivatives by mTyr-mediated reactions was addressed by hydrolysis of DAT-sOEG networks and by model reactions. While analysis of the solubilized networks revealed netpoint decomposition and OEG degradation at the selected conditions, knowledge on netpoint structure and functionality could be acquired by studying the reaction of monofunctional mTyr substrates, i.e. DAT, DAT ester and DAT-IOEG<sub>OMe</sub>/DAT-ImOEG<sub>OMe</sub>. A formation of precipitates was observed during mTyr catalyzed reactions of DAT and DAT ester as an evidence of low solubility of formed oligomers. Distinct crosslinking intermediates, i.e. *o*-diphenols, *o*-quinones and  $\alpha,\beta$ -dehydrocatechols as end groups of IOEG<sub>OMe</sub> 10 kDa, were speculated to be formed based on characterization of model

reactions by UV-Vis spectroscopy. The catalysis of DAT-IOEG<sub>OMe</sub> 10 kDa oxidation by mTyr was faster when applying higher enzyme amounts. UV-Vis analysis provided evidence that the reactions may proceed further beyond the studied 24 h. FT-IR demonstrated that the aromatic groups are oxidized to quinonoid structures. NMR indicated *o*-diphenols as well as *o*-quinones to be involved in the netpoint formation process and confirmed the expected heterogeneity of the formed netpoints. From reactions of DAT ester, oligomers were proposed to consist predominantly from mono- and diphenols and a low number of quinone species, as characterized by exact assignment of theoretical adduct masses to *m/z* values, detected by MALDI-ToF. Investigation of netpoint functionality by MALDI-ToF resulted in detection of oligomers with 6 to 11 repeating units from DAT and DAT ester, respectively. In contrast, MALDI-ToF analysis of products formed from DAT-IOEG<sub>OMe</sub> 10 kDa could only detect ionized dimers and few trimers rather than multimers, possibly due to a lack of susceptibility to ionization. For narrowly distributed DAT-ImOEG<sub>OMe</sub> 2 kDa, a quantitative conversion by mTyr was detected after 24h. Nucleophilic NH<sub>2</sub> as end groups seemed to partially involve in netpoints as indicated from reactions of mixtures of in NH<sub>2</sub>-ImOEG<sub>OMe</sub> and DAT-ImOEG<sub>OMe</sub>. Despite the analysis of products formed from ImOEG<sub>OMe</sub> bearing DAT and NH<sub>2</sub> end groups by MALDI-ToF resulted only in low intensity peaks, this analysis suggests the presence of mono-, *o*-diphenols and *o*-quinones in the oligomer adducts, as well as the formation of Michael-type NH<sub>2</sub>-quinone adducts. A ratio of 40 to 50 mol% NH<sub>2</sub> as ImOEG<sub>OMe</sub> end groups (corresponding to a degree of DAT end group functionalization *d.f.* of 50 to 60 mol%) seemed to be optimal for netpoint formation. Therefore, tetrafunctional DAT(T)-sOEG with *d.f.* ~50-65 mol% were investigated as precursors for hydrogel formation in Ch. 6.

## 6 Synthesis and characterization of hydrogels from DAT- and DATT-sOEG crosslinked by mTyr catalysis

A covalent crosslinking of water-soluble oligomeric precursors is required in order to accomplish network stability over the required period relevant for controlled release of therapeutic compounds, which typically exceeds 1 week. Within Ch. 5, the crosslinking mechanism is investigated on the basis of model reactions with monofunctional telechels. Within this chapter, tetrafunctional branched, i.e. star-shaped oligo(ethylene glycol)s (sOEG), functionalized with DAT and DATT are investigated. The capacity of the different precursors to serve as precursors for mTyr-catalyzed hydrogel formation and the gelation kinetics of the formed networks are presented.

Selected hydrogels were characterized for their physicochemical properties including gel content, swelling capacity and mechanics in buffered solutions (Ch. 6.2.3 to 6.2.5). Spectroscopic techniques were applied to elucidate the chemical structure of the netpoints (Ch. 6.2.1 and 6.2.2) and the hydrogel molecular architecture, i.e. functional mesh size was explored by diffusion studies with FITC dextrans with different hydrodynamic diameters (Ch. 6.3). For hydrogels from DATT-sOEG, the influence of different degrees of DATT functionalization on the hydrogel structure and the resulting properties were studied (Ch. 6.1.2). Furthermore, the applicability of the hydrogels crosslinked by mTyr for the release of therapeutically relevant molecules was investigated (Ch. 6.4.2).

While polymers with comparable *d.f.* of 51 to 66 mol% were selected as starting materials for hydrogel synthesis (Ch. 6.2 to 6.4), almost quantitative conversion of the NH<sub>2</sub> end groups (90 mol%) could be achieved in the functionalization of DATT-sOEG 10 kDa. The influence of *d.f.*, i.e. amount of DATT as substrate, and side reactions between reactive *o*-quinone-derived intermediates and nucleophilic primary amines, discussed in Ch. 5, on the properties of DATT-sOEG networks is described in Ch. 6.1.2.

## 6.1 Parameters to control bulk hydrogel formation

For a systematic study of the gelation ability and the resulting mesh size of the hydrogel networks, precursors with three different molecular weights, i.e. 5, 10 and 20 kDa were investigated.

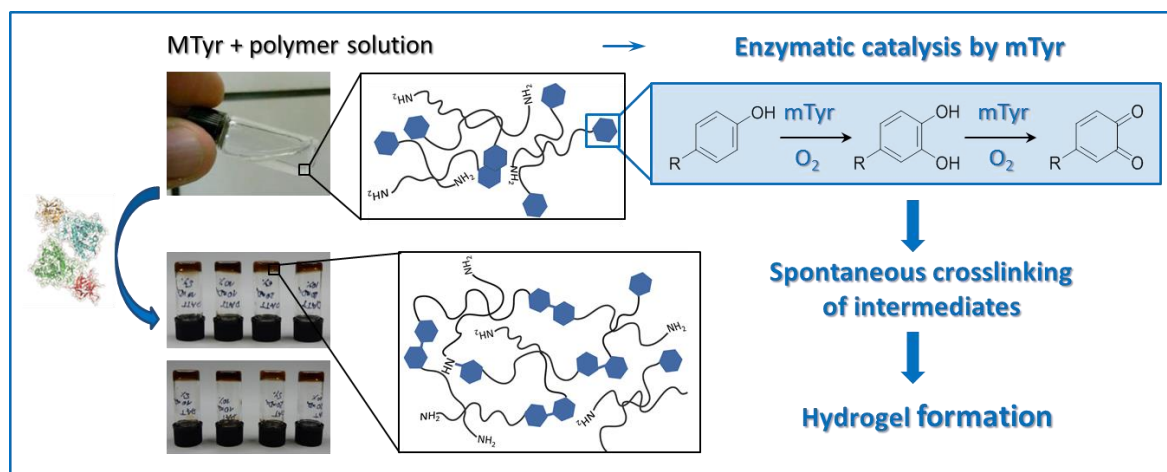


Figure 40: Hydrogel formation by enzymatic catalysis.

The crosslinking of soluble DAT-sOEG precursors by mTyr was demonstrated by sample solidification and the formation of chromophoric netpoints.

Fig. 40 illustrates the formation of semi-solid networks from transparent polymer solutions by mTyr catalyzed crosslinking of sOEG telechelic groups. The gelation is physically characterized by the change from liquid to solid state of matter. The tube tilting method, used here, recorded the instant time point when the macroscopic flow of a sample stopped. The capacity of the different precursors to form hydrogels, as screened by tube tilting, is summarized in Table 7. Hydrogels were successfully formed from DAT(T)-sOEG with  $M_n$  of 10 and 20 kDa within < 16h. Precursors with  $M_n$  of 5 kDa did not form networks in all cases. For instance, DATT-sOEG 5 kDa precursors were oxidized by mTyr (obvious as brown color) but the limited network mobility of shorter arms compared to sOEG  $M_n$  of 10 and 20 kDa led to insufficient number of intermolecular crosslinks for a hydrogel formation with a low mTyr concentration, or inhomogeneous structure (lumps) in presence of  $mTyr \geq 500 \text{ U}\cdot\text{mL}^{-1}$ . These hydrogels were not investigated further. In contrast, DAT-sOEG 5 kDa provided hydrogels by mTyr catalysis.

Table 7: Screening of precursor capacity to serve as precursors for hydrogel synthesis by biocatalysis with mTyr. The hydrogel formation was confirmed by tube tilting.

	DAT-sOEG			DATT-sOEG		
	5	10	20	5	10	20
$M_n$ (kDa)	5	10	20	5	10	20
Substr. conc. in gel (mM)	21.4	11.2	5.0	21.3	11.8	4.7
mTyr conc. ( $\text{U}\cdot\text{mL}^{-1}$ )	250	✓	✓	✗	✓	✓
	2500	✓	✓	✓	✓	✓

✓ hydrogels gelation within 16h ✓ gelation within 16h ✗ no gelation within 24h

This observation, together with the instability and soft nature of gels from DAT-sOEG 5 kDa (handling was often difficult since samples tend to break) may probably indicate the necessity of a minimum precursor length for hydrogel formation. Single amino acids tend to oligomerize into particles rather than coherent polymer networks (as previously observed, see Ch. 5.4). Moreover, the amphiphilicity of DAT(T)-sOEG renders the polymers surfactant-like behavior due to molecular organization based on aromatic stacking and hydrogen bonds, as reported before.[127, 128] Therefore, increased aromatic interactions between DAT(T) groups may result in micelle-like organization of the precursors, making the aromatic groups unavailable for enzymatic conversion.

### 6.1.1 Control on gelation kinetics by precursor properties and mTyr concentration

Within this chapter, the influence of sOEG molecular weight  $M_n$ , substituent (DAT or DATT)-sOEG and mTyr concentration on the gelation kinetics were investigated. The precursors with  $M_n$  10 and 20 kDa successfully formed hydrogels, when mixed with mTyr in concentrations from 50 to 1000  $\text{U}\cdot\text{mL}^{-1}$ . Selected hydrogels were investigated by rheology in order to determine the gelation time,  $t_{\text{gel}}$  on the molecular level. Small amplitude oscillatory rheology, applied here enables dynamic measurements of sample behavior with minimal interference to the chemical process,[191] which was realized here by application of low amplitude and frequency of oscillation ( $f = 1 \text{ s}^{-1}$ ,  $\gamma = 0.1\%$ ). The cone-plate geometry ensured a constantly distributed shear rate within the whole gap, i.e. analyzed sample.

In the beginning of the oscillatory rheological analysis of hydrogel formation, viscous modulus ( $G''$ ) is higher than the elastic modulus ( $G'$ ), which is a result of the predominant viscous nature of precursor solutions. Initially, an induction period was observed, during which  $G'$  and the complex viscosity  $\eta^*$  increased gradually. The following steep increase in  $G'$  and  $\eta^*$  demonstrated the onset of network formation, as illustrated for  $\eta^*$  in Fig. 41, which is associated with the formation of elastically effective covalent netpoints. Within the third region,  $G'$  levels off as a consequence of minimal crosslinking rate due to the reduction in the number of mobile chains, which are accessible for further netpoint formation.[192]

Macroscopically, the gelation coincidences with sample solidification, i.e. state of matter changes from liquid to semi-solid. On the molecular level, the gel point is defined as the timepoint, at which the viscoelasticity of the hydrogels is dominated by their elastic properties, which in some cases coincidences with crossover of  $G'$  and  $G''$  in rheological studies,[191, 193] being the most often used methodology to determine gel point/ $t_{gel}$ .

In these experiments, most initial  $G'$  and  $G''$  of were low (below 0.05 Pa) and a high deviation between the  $G'$  and  $G''$  values, measured in the course of time was observed. As a result,  $G'/G''$  crossover points were detected in some cases, which were far before a substantial increase of  $G'$  and  $\eta^*$ . The latter were considered to be an artefact due to the low rheometer sensitivity in this range, so the  $G'/G''$  crossover could not be applied for  $t_{gel}$  determination. However, the complex viscosity, being a function of the shear modulus is an alternative parameter to describe the evolution of rheological properties during hydrogel formation. The frequency-dependent dynamic viscosity was found to represent best the exact gel points and was verified together with the loss tangent,  $\tan \delta$  for systems, for which  $G'/G''$  crossover was not applicable for  $t_{gel}$  determination.[191, 194] Here,  $\eta^*$  was evaluated at fixed frequency instead, which was identical for all investigated hydrogels.  $T_{gel}$  as a function of  $\eta^*$  was determined by extrapolation of the region, where the steepest viscosity increase was observed, as illustrated in Fig. 41.

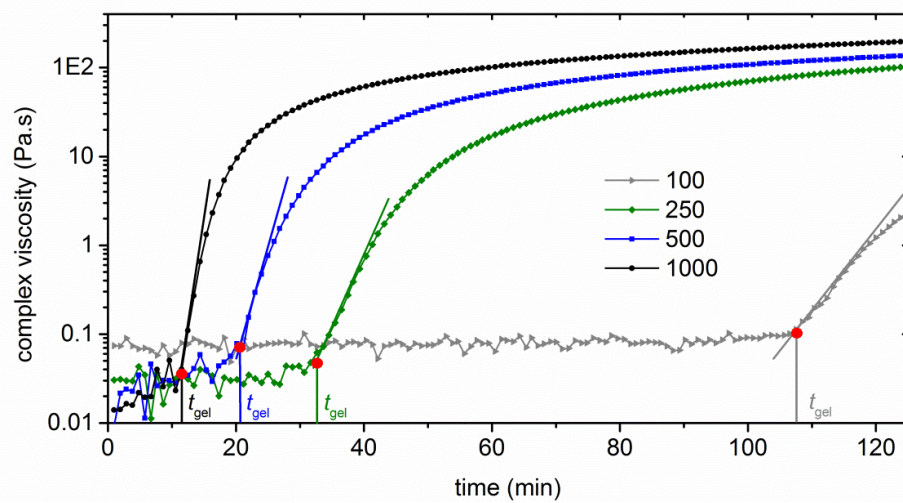


**Figure 41: Gel time determination by rheology:**

Rheogram visualizing the complex viscosity  $\eta^*$  of DAT-sOEG (5 wt%) during gelation with different concentrations of mTyr: 100 (grey), 250 (green), 500 (blue) and 1000  $\text{U}\cdot\text{mL}^{-1}$  (black). The methodology for determination of the gelation time  $t_{gel}$  (red crossover point of tangents) is demonstrated for the exemplary samples.

In the next steps, the effect of enzyme concentration on gelation kinetics should be evaluated. For all investigated precursors, the gelation time decreased substantially down to  $\sim 5$  min with increasing the enzyme concentration, as summarized in Fig. 42. This can be assigned to faster DAT(T) oxidation and netpoint formation in presence of higher catalyst amounts. A clear tendency is the reduction of the gelation time with increasing the prepolymer molecular weight, which may be a consequence of the higher chain flexibility of the precursor arms with increasing molecular weight. For macromolecular precursors with  $M_n$  of 10 kDa, DAT as a functional group leads to a slightly faster gelation compared to DATT (inter- and intramolecular netpoints are formed more slowly in DATT-sOEG 10 kDa).

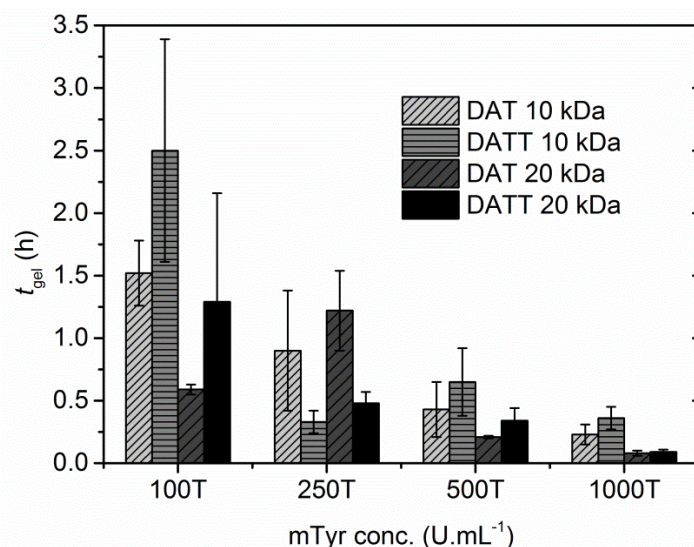


**Figure 42: Summary of the gelation time**

$t_{gel}$  of hydrogels, as determined by rheology:  $t_{gel}$  of hydrogels from DAT- and DATT-sOEG precursors (5 wt%) with  $M_n$  10 and 20 kDa crosslinked in the presence of different mTyr concentrations (100, 250, 500 and 1000 U·mL<sup>-1</sup>) at 25 °C, as determined by oscillatory rheology ( $n \geq 3$ ,  $\bar{x} \pm SD$ ).

The gelation time was also dependent on polymer concentration, as studied for DAT-sOEG 10 kDa: gelation in 2.5 wt% polymer solution was faster compared to solutions with 5 wt% polymer. Increasing polymer concentration to 10 wt% dramatically retarded gelation, indicating hindered diffusion of enzyme in solutions with increasing viscosity. A polymer concentration of 5 wt% was selected for the further investigations, focusing on the properties of preformed hydrogels (Ch. 6.2 to 6.3).

### 6.1.2 Influence of degree of DATT functionalization on hydrogel properties

Another approach to influence hydrogel molecular structure is to increase the amount of crosslinkable groups by increase in sOEG  $d.f.$  In case of mTyr mediated tyrosine oxidation, the formed quinone species involve in two types of reactions: coupling between different oxidized DAT derivatives and nucleophilic quinone coupling to alkylamines, i.e. unfunctionalized sOEG end groups. Since the favored pathway and the influence of both types of adducts for crosslinking is still unclear, the effect of sOEG  $d.f.$ , degree of DATT end group functionalization on network properties was intriguing. Hydrogels from DATT-sOEG 10 kDa with  $d.f.$  66 and 90 mol% (further on abbreviated as DATT<sub>0.7</sub> and DATT<sub>0.9</sub>) were prepared and comprehensively characterized, as summarized in Table 8. Gels from DATT<sub>0.9</sub>-sOEG were formed much faster with low mTyr concentration

compared to DATT<sub>0.7</sub>-sOEG (e.g. 50 instead of 110 min for the respective networks with 250 U·mL<sup>-1</sup>). On increasing mTyr concentration to 500 and 1000 U·mL<sup>-1</sup>, the gelation time decreased to comparable values of respectively 35±5 and 10±5 min). The *G* values demonstrated that slightly higher DATT<sub>0.7</sub>-sOEG amount could be integrated into the covalent network, which verified the impact of quinone-amine couplings on the crosslinking mechanism. Swelling could be significantly decreased in DATT<sub>0.9</sub>-sOEG as expected considering the higher impact of hydrophobic DATT dipeptide mimetics with increasing *d.f.* The mechanical properties of DATT<sub>0.9</sub>-sOEG were similar to the respective gels from DATT<sub>0.7</sub>-sOEG, but showed higher deviations between the triplicates, which probably resulted from the varying amount of random intra- or intermolecular crosslinking of these precursors with higher end group functionalization. The average mesh size  $\xi$ , calculated according to Eq. 5 (Ch. 1.1.2), displayed marginal differences between networks from both precursors. Although hydrogels from DATT<sub>0.7</sub>-sOEG were superior to the respective gels from DATT<sub>0.9</sub>-sOEG in terms restricting FDex diffusion (data not shown), the differences were almost negligible.

Table 8: Properties of preformed hydrogels from DATT-sOEG 10 kDa with *d.f.* of 66 and 90 mol% (DATT<sub>0.7</sub> and DATT<sub>0.9</sub> respectively).

mTyr (U·mL <sup>-1</sup> )	<b>G (%)</b>		<b>Q (vol%) at 37 °C</b>		<b>G' (kPa) at 37 °C</b>		<b><math>\xi</math> (nm) at 37 °C</b>	
	100	500	100	500	100	500	100	500
DATT <sub>0.7</sub>	80 ± 2	78 ± 5	850 ± 10	880 ± 20	1.7 ± 0.3	2.1 ± 0.7	13.4 ± 1.2	12.8 ± 1.2
DATT <sub>0.9</sub>	72 ± 2	73 ± 1	800 ± 40	700 ± 25	1.7 ± 0.5	2.5 ± 1	13.8 ± 1.4	12.1 ± 1.5

Conclusively, increasing *d.f.* with DATT to almost quantitative end group conversion did not seem to result in substantially higher crosslinking density. Possible reason could be that the networks properties are determined by a low overall amount of netpoints (DATT-DATT as well as DATT-NH<sub>2</sub> adducts) and large numbers of dangling chains. The detailed characterization of hydrogels with similar *d.f.* and different *M<sub>n</sub>* is described in Ch. 6.2.3 to 6.3.

## 6.2 Physicochemical hydrogel characterization

Physicochemical properties of different hydrogels from DAT- and DATT-sOEG (crosslinked with two different mTyr concentrations, 100 and 500 U·mL<sup>-1</sup>) were comprehensively analyzed in order to conclude on the influence of different parameters on hydrogel network structure.

### 6.2.1 Hydrogel analysis by NMR spectroscopy

The hydrogels were also studied in the (semi)solid state by NMR after equilibrium swelling in D<sub>2</sub>O. The spectra in Fig. 43 illustrate few very broad signals. The most intensive signals could be attributed to proton signals of OEG segments, (signal maximum ca. 3.75 ppm) and H<sub>2</sub>O (ca. 4.5 ppm). However, signals in the range 6.9-7.4 ppm indicated on the presence of residual aromatic protons in DAT und DATT side groups.

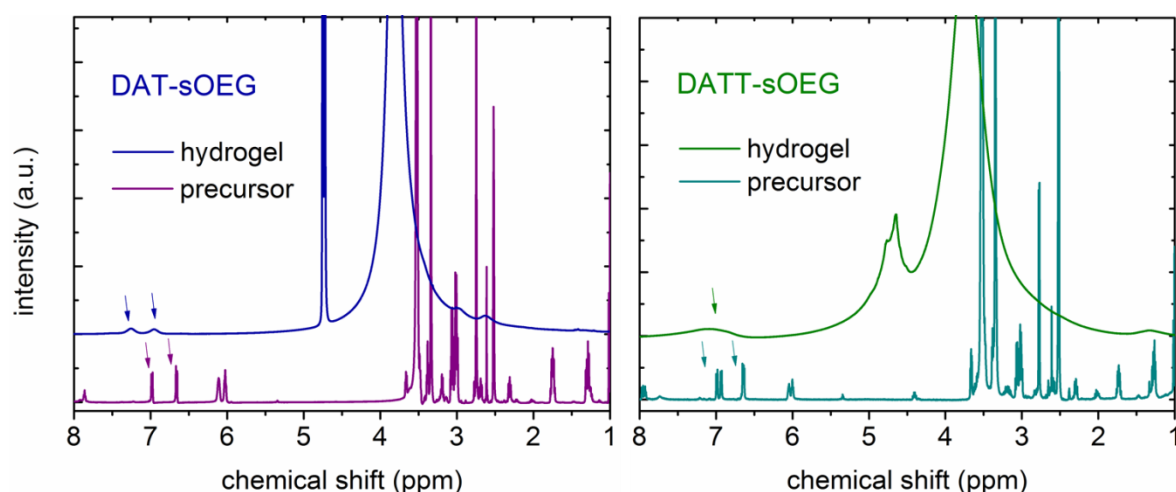


**Figure 43:** <sup>1</sup>H-NMR spectra of mTyr-crosslinked hydrogels from DAT- (–) and DATT-sOEG (–)

swollen in D<sub>2</sub>O to an equilibrium. The arrows underline the indicated presence of protons, found in the precursors (DAT– and DATT–). The high-field shift of the precursor spectra is due to the solvent effect (DMSO for precursors vs. D<sub>2</sub>O for the hydrogels).

Although the hydrogels from DATT-sOEG seemed to exhibit lower intensity of these signals, incomplete conversion of telechelic groups was demonstrated for both investigated hydrogels.

## 6.2.2 Hydrogel Analysis by FT-IR spectroscopy

Hydrogel networks are considered as one molecule with infinite molecular weight. Since hydrogels are insoluble, their molecular structure can be analyzed only in the solid state, after swelling in appropriate solvent, or drying. Extracted dried films of DAT-sOEG 10 kDa crosslinked by mTyr were investigated by FT-IR. The applied ATR technique is characterized by light penetration depths of several hundred nm to  $\mu\text{m}$  (typically  $1.7 \mu\text{m}$  characteristic for the applied diamond as ATR crystal material [195]). Therefore, not only information from the outer surface layer, but also from the underlying bulk is collected. Comparing the spectra (Fig. 44) of hydrogels, crosslinked by a low ( $100 \text{ U}\cdot\text{mL}^{-1}$ ) and high mTyr concentration ( $500 \text{ U}\cdot\text{mL}^{-1}$ ), to the previously shown oligomeric precursors (Ch. 4.2), a change in the region  $3600\text{-}3150 \text{ cm}^{-1}$  was observed. The shift of the broad plateau maximum to lower vibrational frequency (high  $\text{cm}^{-1}$ ) after crosslinking with higher mTyr amount may indicate O-H vibration in crosslinked phenolic compounds (requiring more energy to initiate molecular vibration) or the formation of hydrogen bonds. The most interesting spectral region is shown in the inset (Fig 44): In hydrogels, the amide I band is red-shifted ( $1650 \text{ cm}^{-1}$ ) and intensified. This change was interpreted to result from quinone moieties, formed by mTyr catalysis. Since the higher band intensity at  $1650 \text{ cm}^{-1}$  was found in hydrogels with  $500 \text{ U}\cdot\text{mL}^{-1}$  mTyr, higher conversion of telechelic groups in the respective hydrogels was concluded. The higher intensity of the band resulted from overlapping of the amide signal with C=C valence and C=O deformation vibrations, originating from quinones. The contribution from C=O stretching vibrations was rationalized, because carbonyl bands are usually very characteristic and intensive. The blue-shift of the ketone vibration (usually  $> 1690 \text{ cm}^{-1}$ ) may be a consequence of the conjunction of C=O with double bonds in *o*-quinones, as well as the presence of two adjacent ketone groups (enabling keto-enol tautomerie and formation of H-bridges in chelate form) [131], resulting in a blue shift. Similarly, the appearance of an intensive peak at around  $1650 \text{ cm}^{-1}$  was previously reported and attributed to quinone formation in other catechol-functionalized systems crosslinked by enzymatic [196] or non-enzymatic oxidation.[87, 171] The loss of aromatic character of DAT end groups to oxidized quinones after mTyr-mediated crosslinking is also supported by the disappearance of the peaks characteristic for aromatic combination vibrations ( $1780\text{-}1710 \text{ cm}^{-1}$ ) and C=C stretch at  $1616$  and  $1515 \text{ cm}^{-1}$  in hydrogels. Still, the peak at  $1515 \text{ cm}^{-1}$  was detected at low intensity

after hydrogel formation with low catalyst amount, indicating that some aromatic species (DAT or catechol formed after mTyr catalyzed hydroxylation) are still present in these hydrogels. Since the quinonoid groups are very reactive and unstable, it is expected that they represent the basis for crosslinks formed in the analyzed hydrogels, as discussed in detail in Ch. 5.

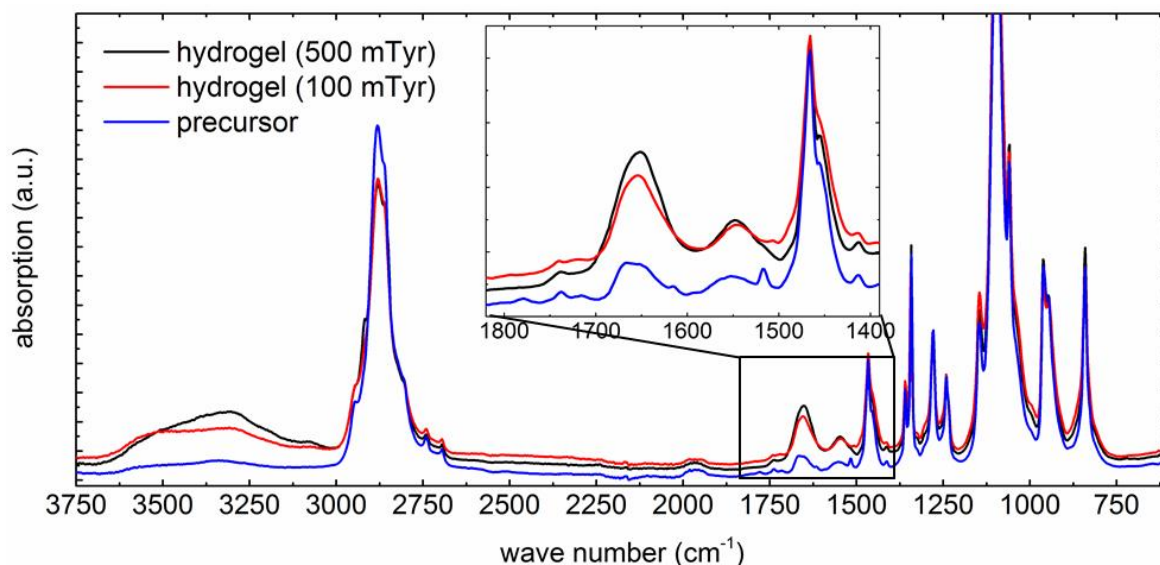


Figure 44: FT-IR spectra of dried hydrogel films crosslinked with 100 and 500 U·mL<sup>-1</sup> mTyr compared to the oligomeric precursor DAT-sOEG 10 kDa.

Further hypothetical netpoints in hydrogels, formed from precursors with unfunctionalized NH<sub>2</sub> end groups, may result from couplings of these nucleophiles to enzymatically activated DAT residues, as detailed in Ch. 5.1.2. Considering possible structural elements in quinone-amine adducts, the distinct regions of interest in FT-IR spectra include: (i) 3450-3300 cm<sup>-1</sup>, where N-H stretching vibrations in aromatic amines and imines are expected; [131] (ii) 1400-1250 cm<sup>-1</sup>, where stretching vibrations of C-N functionalities in unsaturated and aromatic amines are usually detected; [131, 197] (iii) 1690-1640 cm<sup>-1</sup>: characteristic peaks for -C=NR stretching vibrations in Schiff bases. [196, 198, 199] The first region is dominated by strong vibrations of H-bonded groups. Although differences in the band intensity and form between DAT-sOEG and hydrogels thereof were detected, one should be cautious in interpreting the presence of other functional groups within this broad band. C-N vibrations in the investigated networks would be covered by the strong signals of OEG segments. An interesting observation is the broadening of the band centered at 1650 cm<sup>-1</sup> in hydrogels crosslinked by 500 U·mL<sup>-1</sup>, where a slight shoulder at 1632 cm<sup>-1</sup> could be seen. This may indicate imine formation,

which may also explain the detected broad band at  $3080\text{ cm}^{-1}$  in these hydrogels, possibly associated to a C-H stretch in imines.

Another interesting region ( $900\text{-}600\text{ cm}^{-1}$ ) may give insight into the substitution pattern of aromatic DAT groups. However, no distinct differences between pure and crosslinked precursors could be found by FT-IR investigation, in contrast to the spectra of enzymatically oxidized model DAT-IOEG<sub>OMe</sub> precursor (see Ch. 5.3). Therefore, no direct evidence for netpoint formation could be found by FT-IR spectroscopy. The spectral changes in hydrogels clearly indicated quinone formation, finally leading to precursor crosslinking. Nevertheless, the low ratio of end groups to OEG, band overlapping and the presence of functionalities within complex mixtures made an unambiguous assignment of the bands to distinct functionalities difficult.

### 6.2.3 Gel content

The gel content  $G$  is a measure of the amount of precursor which is permanently incorporated by chemical or physical interaction into a network. Thus,  $G$  enables to estimate the effectivity of the crosslinking reaction. In this study,  $G$  of 70 to 80 % were achieved with similar values for DAT- and DATT-sOEG with 10 and 20 kDa (Table 9). For DAT-sOEG, crosslinking with a lower amount of mTyr ( $100\text{ U}\cdot\text{mL}^{-1}$ ) seemed to result in higher  $G$  and more homogeneous networks, demonstrated by the low standard deviation, as a result of the slower kinetics of netpoint formation. Hydrogels from DAT-sOEG with  $M_n$  of 5 kDa showed the lowest  $G$  ( $55 \pm 3\%$ ) when formed with  $100\text{ U}\cdot\text{mL}^{-1}$  mTyr due to limited chain flexibility. Functionalized oligomers of 5 kDa tend to form weaker, or no networks compared to prepolymers with higher molecular weight despite the substantially higher amount of DAT in solution. This phenomenon may indicate the importance of the balance of chain flexibility and steric hindrance for crosslinking in oligomers.

Table 9: Summary of the gel contents  $G$  of hydrogels from DAT- and DATT-sOEG with different  $M_n$ , crosslinked with 100 or 500 U·mL<sup>-1</sup> mTyr ( $n = 3$ ).

Polymer type	DAT-sOEG		DATT-sOEG	
	mTyr conc. (U·mL <sup>-1</sup> )		mTyr conc. (U·mL <sup>-1</sup> )	
$M_n$ (kDa)	100	500	100	500
5	55 ± 3	73 ± 6	n.d.	n.d.
10	77 ± 2	72 ± 12	80 ± 5	78 ± 2
20	77 ± 1	70 ± 3	76 ± 1	76 ± 0.3

A possible reason for the observed extent of non-incorporated DAT- and DATT-sOEG precursors could be on the one hand incomplete conversion of phenolic moieties by mTyr. On the other hand, it is unclear if all of the enzymatically converted DAT and DATT moieties may have formed crosslinks with adjacent functional groups.

#### 6.2.4 Analysis of swelling behavior

The degree of volumetric swelling  $Q$  is a property that reflects the netpoint density of networks. For hydrogels from DAT(T)-sOEG, crosslinked by mTyr, an equilibrium state of swelling was reached after 24 h at 37 °C. This was the case for both the uptake of water and PBS, where  $Q$  was similar. For all samples, higher enzyme concentration led to lower volumetric swelling as demonstrated in hydrogels with 500 U·mL<sup>-1</sup> compared to 100 U·mL<sup>-1</sup> mTyr, which is associated with a higher crosslinking density.

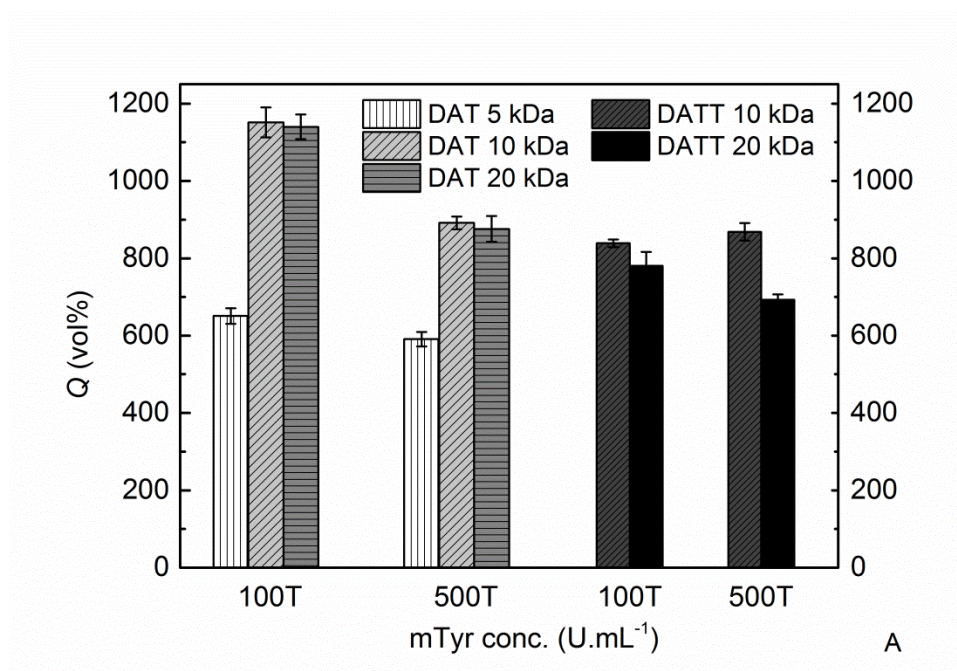


**Figure 45:** Summary of the equilibrium swelling of hydrogels from DAT(T)-sOEG crosslinked with mTyr (concentration 100 or 500 U·mL<sup>-1</sup>) at 37 °C in PBS. Precursors were varied by sOEG functional group (DAT/DATT) and  $M_n$ : DAT 5 kDa (white), DAT 10 kDa (light grey), DAT 20 kDa (middle grey), DATT 10 kDa (dark grey) and DATT 20 kDa (black). Values represent  $\bar{x} \pm SD$  ( $n=6$ ).

While  $Q$  was similar for hydrogels from DAT-sOEG with 10 and 20 kDa, when crosslinked with corresponding mTyr concentrations, samples with  $M_n$  of 5 kDa demonstrated substantially lower swelling (Fig. 45). Thus, this should be associated with the highest crosslinking density,  $v_c$  in these hydrogels. Also an effect from the increased influence of hydrophobic end groups with decreasing precursor  $M_n$ , i.e. length of hydrophilic segments can be expected. Hydrogels from DATT-sOEG demonstrated lower  $Q$  compared to DAT-sOEG, as a consequence of the higher hydrophobicity of DATT. Furthermore, resulting hydrogels may probably have a higher  $v_c$ , since DATT comprises two phenol moieties per end group, and thus contains more hypothetical active sites for crosslinking.

### 6.2.5 Mechanical properties described by rheology

The mechanical properties of hydrogels for biomedical application, e.g. to fill surgical cavities as medical implants, are important since most cells are functional only in an environment with stiffness similar to their natural surrounding tissues. Rheological characterization of the hydrogels before extraction, reflecting their mechanical properties as after *in situ* network formation, demonstrated lower elastic moduli compared to

extracted hydrogels. This fact is probably due to the softening effect of physically incorporated highly hydrated sOEG.

Mechanical testing of preformed hydrogels after extraction of soluble matter can provide knowledge on the molecular hydrogel structure, based on effective crosslinks, i.e. covalent and stable physical netpoints. The results from frequency sweeps showed for all samples linear storage moduli almost independent of the applied frequency over several orders of magnitude ( $G'$  values in accordance to values shown in Fig. 46), which is representative of solid-like hydrogel behavior [29] and accounts for hydrogel stability on applied mechanical stress and a terminated covalent crosslinking reaction.

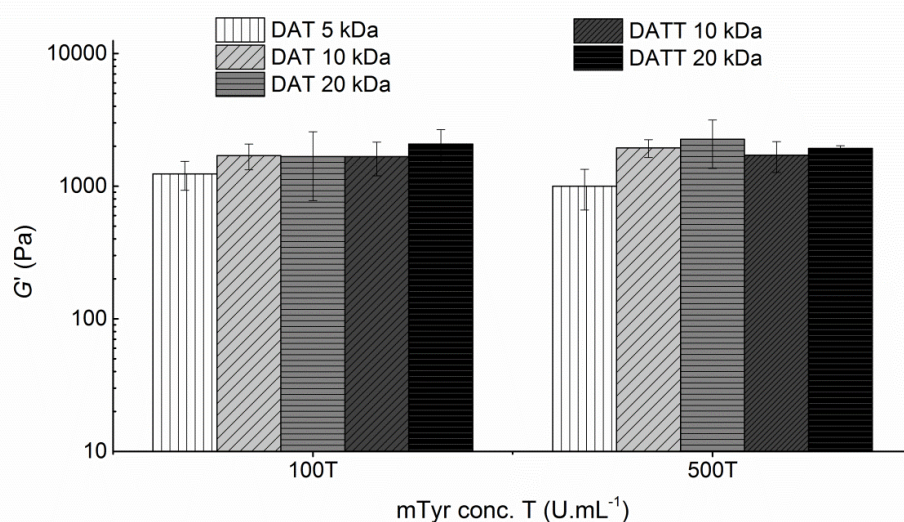


Figure 46: Summary of storage moduli  $G'$  of hydrogels from DAT- and DATT-sOEG with different  $M_n$ , crosslinked with mTyr, T (100 or 500 U.mL<sup>-1</sup>), as analyzed in rheological time sweeps at 37 °C ( $n \geq 3$ ).

Initially, the linear viscoelastic region of the hydrogels was determined by frequency and amplitude sweeps to identify suitable parameters for the further hydrogel investigations (here  $f = 1 \text{ s}^{-1}$ ,  $\gamma = 0.5\%$  selected). All following rheological studies were carried out within the range of linear viscoelasticity of the hydrogels, since there the networks structure is not disrupted and the response of the material is independent on the deformation. The investigated enzymatically crosslinked hydrogels demonstrated similar rigidity in the low kPa range from 1 to 1.5 kPa. In spite of their comparably low swelling, hydrogels from DAT-sOEG 5 kDa were softer (handling was difficult since samples tend to break) than the hydrogels from precursors with higher  $M_n$ . All other hydrogels demonstrated comparable elastic moduli independent on the end group and  $M_n$  (Fig. 46). The uncontrollable hydrogel mechanics may be an indication of ineffective crosslinking

reaction: the networks contain only few crosslinks and their elastic nature is dominated by OEG.

The determined elastic moduli  $G'$  can be used to correlate on the hydrogel molecular structure, i.e. the average mesh size  $\xi$ , basing on the rubber elasticity theory (Eq. 5). The theory considers the entropy loss, caused by the hindered movement of the swollen chains being deformed by oscillatory shear stress, as employed during rheological analysis of swollen hydrogels.[31]

**Table 10:** Mesh sizes  $\xi$  of hydrogels from DAT(T)-sOEG crosslinked with different concentrations of biocatalyst mTyr.  $\xi \pm$  standard deviation was calculated from the elastic moduli of hydrogels, determined by rheology at 37 °C ( $n \geq 3$ ).

Polymer type	$\xi$ (nm)			
	DAT-sOEG		DATT-sOEG	
	mTyr conc. (U·mL <sup>-1</sup> )		mTyr conc. (U·mL <sup>-1</sup> )	
$M_n$ (kDa)	100	500	100	500
5	15.2 ± 1.3 nm	16.5 ± 1.9 nm	n.d.*	n.d.*
10	13.6 ± 1.1 nm	13.1 ± 0.9 nm	13.4 ± 1.2 nm	12.8 ± 1.2 nm
20	13.4 ± 1.2 nm	12.8 ± 1.2 nm	13.5 ± 1.0 nm	13.1 ± 0.3 nm

\* *n.d.* – not determined

The determined values were all in a similar range between 12.8 and 15.2 nm, whereby crosslinking in presence of a higher mTyr amount resulted in smaller mesh sizes (Table 10). For DAT-sOEG gels, increase in  $M_n$  was inversely proportional to mesh size in spite of the decreasing amount of end groups as mTyr substrates. This interesting observation may result from the higher flexibility of OEG arms with increasing  $M_n$ , allowing for mTyr diffusion and encountering of other activated end groups for adduct formation. For hydrogels from DATT-sOEG,  $\xi$  were comparable to the  $\xi$  values of hydrogels from DAT-sOEG precursors with the respective  $M_n$  in contrast to the lower swelling of the former hydrogels (Ch. 6.2.4). Therefore, inter- as well as intramolecular junctions between DATT-sOEG chains may have been formed. The here determined  $\xi$  values, should be compared to the functional mesh size, determined experimentally for the hydrogels by diffusion of macromolecules, i.e. FITC dextran, described in the following Ch. 6.3.

## 6.3 Diffusion of FITC dextran and determination of functional mesh size

---

The average mesh size of hydrogels is a very important characteristic of network molecular structure. Moreover, the mesh size determines the mobility of molecules within hydrogels and the diffusion of solutes in- and outwards of the hydrogels, so it is a major factor towards application of hydrogels for delivery of cells or therapeutics.[34] It is known that  $D_0$  (diffusion coefficient in dilute aqueous solution) is constant in set environmental conditions, but markedly dependent on concentration in polymer solutions.[200] This effect is even more pronounced dependent on the molecular structure of crosslinked hydrogels, where the polymer chains are partially immobilized by the crosslinks and act as physical obstacles to the free solute diffusion. In case of release of macromolecules, the segment length between crosslinks,  $M_c$  determines the release kinetics and the overall hydrogel permeability dependent on the solute size.

Here, it was intended to determine a functional mesh size by investigating the diffusivity of molecules with different hydrodynamic diameters in hydrogels, and compare the estimated  $\xi$  to the values, discussed in Ch. 6.2.5. FITC labeled dextran (FDex\_  $M_n$  in kDa) was selected as a model neutral solute,[201, 202] which is available in different molecular weights and can be directly quantified by fluorescence spectrometry. The diffusion coefficient in the gels,  $D_g$  was experimentally determined by release studies with hydrogels from DAT and DATT functionalized sOEG with  $M_n$  of 5, 10 and 20 kDa, respectively and related to hydrogel structure.

A clear scaling effect in the enzymatically crosslinked hydrogels was demonstrated, as seen from the exemplary release experiment in Fig. 47. For all samples, the unhindered solute permeation was reduced with growing  $r_h$ , i.e. FDex  $M_n$ , resulting in release retention and decrease in the overall released fraction. The experimental data from quantification of FDex released amounts from all hydrogels resembled release kinetics dominated by diffusion, as exemplarily shown for hydrogels from DAT-sOEG 10 kDa in Fig. 47. The measured fractional release was fitted according to a power law, where  $M_t/M_\infty$  correlated to a square root time, as plausible based on the Fickian law of diffusion.[203] The diffusion coefficients  $D_g$  were calculated according to Eq. 8.[204, 205]

$$\frac{M_t}{M_\infty} \cong 4 \left( \frac{D_g t}{\pi l^2} \right)^{1/2} \quad (\text{Eq. 8})$$

Concerning the initial conditions for model application to the system, homogenous distribution and high solubility of the released compound in the hydrogel, as well as in the release medium, are typical for the experimental set-up. Furthermore, the diffusion law approximation (Eq. 8) is valid for slabs with plane sheet geometry and defined thickness  $l$  (here 0.25 cm), with homogenous solute distribution within the gel and concentration gradient only along the  $x$  axis (one hydrogel side contacting the release medium), releasing less than 60% of the payload in the initial stage (here 6 hours).[204, 205]

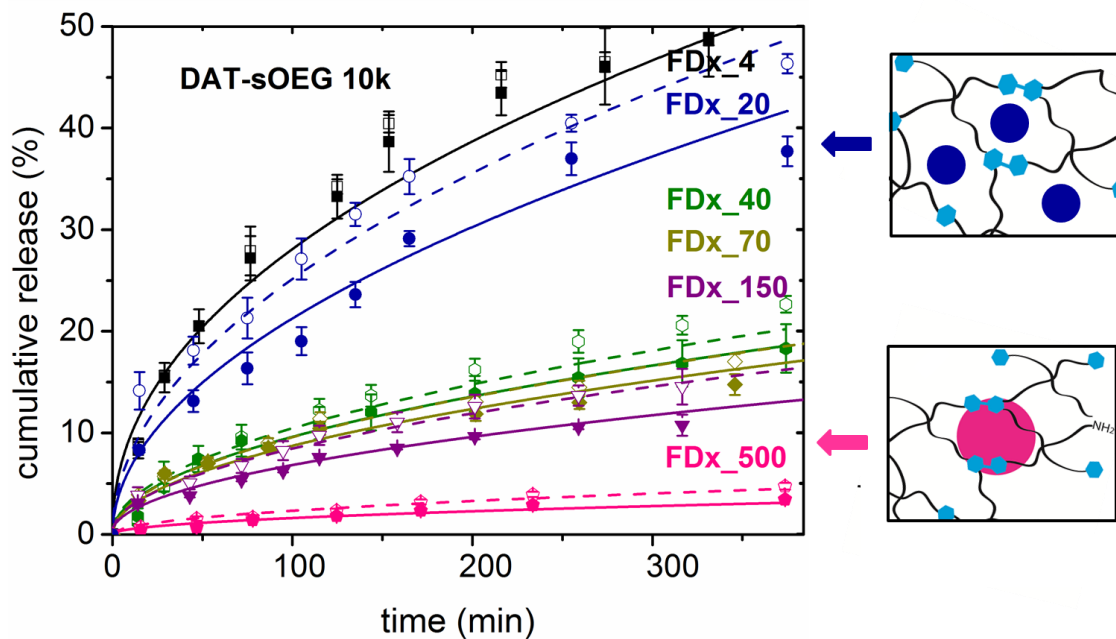


Figure 47: Cumulative release and theoretical data fit for the diffusion of FITC dextrans

with different  $M_n$  ( $FDx\_M_n$ ) from hydrogels from DAT-sOEG 10 kDa, crosslinked with a low (empty symbols and dashed line) and high mTyr concentration (solid symbols and solid line). The error bars show the standard deviation between FDx released amounts from different hydrogel samples ( $n=4$ ).

The experimental data (part of it shown in Fig. 47) correlated well with the theoretical fit, considering the  $R^2$  values from 0.99 to 0.93 for the most experimental curves. A purely diffusive mass transport of FDex could be concluded in some cases, when high  $R^2$  values, i.e. compatibility of the experimental data to the theoretical fit were observed. The release from hydrogels crosslinked with  $100 \text{ U}\cdot\text{mL}^{-1}$  was predicted better, which indicated a lower impact of physical interactions between the polymers and the loaded FDex on diffusive transport. For hydrogels with higher mTyr concentration, a higher crosslinking density was expected compared to respective hydrogels with lower mTyr concentration, as indicated in the previous experiments (Ch. 6.2.2 and 6.2.4). Therefore, polymer segments having stronger constrained chain mobility as part of the

network possibly had a higher obstruction effect on FDex diffusion, thus stronger interactions with the solute.

The discrepancy to the idealized diffusion-governed release can in some of the investigated hydrogels be explained in view of modelling the solute molecules as ideal solid spheres. Dextrans have linear structures, comprising ca. 5% short-chain branches,[206] so the  $r_h$ , calculated according to Stokes-Einstein equation, may not be representative of their actual size. Other effects interfering modelling the diffusion behavior are discussed below.

It was initially speculated that for FDex of very high molecular weight, a total retention in the hydrogel network may be found. The FDex molecular weight cut-off effect by the network mesh, serving as a diffusion barrier, was not demonstrated, leading to the conclusion that the mesh sizes of all hydrogels had a broad distribution with a maximum  $\xi$  above 30 nm, i.e.  $d_h$  of FDex\_500.[207] When assessing the overall hydrogel permeability, it has to be considered that FDex are highly polydispersed macromolecules with PDI values from 1.4 up to 2, as given by the supplier. Therefore, the release of the smaller fraction of FDex\_500 with  $d_h \ll 30$  nm probably leads to mesh size overestimation and experimental error when calculating  $D_g$ .[208]

In view of the experimentally determined diffusion coefficients (Fig. 48) for all investigated hydrogels, crosslinking with higher concentration led to higher diffusion restriction, as expected for hydrogels with higher crosslinking density, i.e. lower mesh size. The release retardation effect was anticipated to be stronger for hydrogels with more pronounced effect of the end groups, i.e. lower  $M_n$ . Instead, the highest diffusivity for all FDex was shown in hydrogels from DAT-sOEG 5 kDa compared to the respective gels from precursors with higher  $M_n$ . This fact was surprising considering the lower free volume resulting from the highest polymer ratio in swollen DAT-sOEG 5 kDa gels, as demonstrated in swelling experiments. The hydrogels from precursors with  $M_n$  of 10 and 20 kDa were very similar in terms of diffusive characteristics, when crosslinked with the same mTyr amount and probably had comparable mesh sizes. The reduction in FDex\_20 diffusivity in hydrogels  $D_g$  compared to  $D_0$  was higher than expected in all hydrogels, which indicate that these hydrogels had lower crosslinking density compared to the release experiments with the other dextrans, FDex. The varying reproducibility of hydrogel properties was already observed during the studies on gelation time and mechanical

properties. Therefore, the enzymatic crosslinking with mTyr seems to be very sensitive for other factors such as minor environmental temperature deviations, or oxygen supply during the crosslinking based on the contact area of the pregels with air.

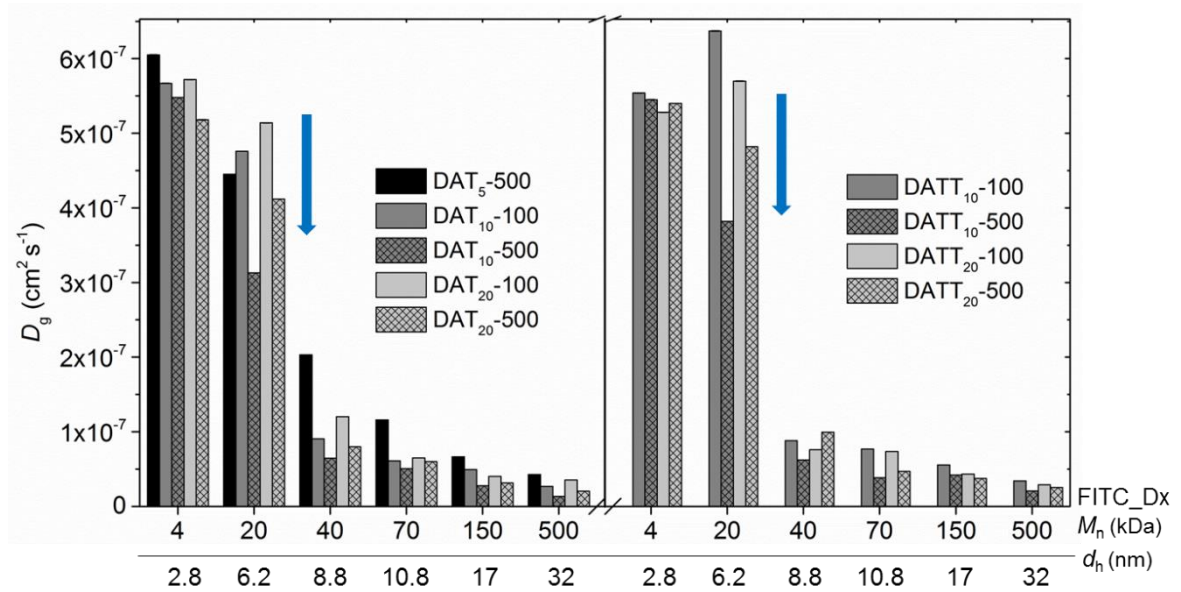


Figure 48: Diffusion coefficients  $D_g$  of FITC dextran (FDx) with different  $M_n$  in hydrogels from DAT(T)-SOEG precursors, crosslinked with 100 or 500  $\text{U}\cdot\text{mL}^{-1}$  mTyr ( $\text{DAT(T)}_{M_n}$ -mTyr concentration).

The standard deviation is not visible at this magnification.

Different models exist to describe the diffusion of solutes in hydrogels. The common feature is the attempt to relate on the diffusion behavior within different scale lengths of homogenous interactions between polymer chains and solutes. The most widely used models deal with correlating diffusion to the free volume in networks, physical obstruction by polymeric chains, increasing the solute diffusion path length or free volume, as well as thermodynamic effects caused by increase in frictional drag through polymer chains.[209, 210] Some of the theories relate the molecular structure based on solute partition ratios between hydrogel membranes and solution. The herein discussed release studies are not unconditionally applicable to conclude on partition ratios due to the short investigation times. Most commonly applied models propose exponential decrease of  $D_g/D_0$  with increasing  $r_h$ , [209] which could not properly describe the data due to outliers (two out of six FDex) from the overall exponential tendency. Considering the sieving effect of the polymer chains, Lustig and Peppas [211] described the correlation between the mesh size and the reduced solute diffusivity  $D_g/D_0$  by a combination between the free volume (represented by  $Q$ ) and obstruction theory, stating that permeability is realized only through the liquid-filled spaces in the network mesh. The probability of the solute to

encounter a succession of openings is approximated by  $p(r_s) = 1 - r_h/\xi$  [211], assuming a linear correlation between  $D_g/D_o$  and  $\xi$ . In other publications [23, 212], they stated a dependence of  $D_g/D_o$  on  $1 - (r_h^2/\xi^2)$ , which was found to represent the experimental data to some extent, but the correlation of the fits to the available data ( $R^2$  values below 0.8) was poor. One possible explanation is that only few values satisfy the prerequisite  $r_h \ll \xi$  to apply the above proposed theory. In case of the investigated hydrogels, a broad distribution of  $\xi$  was expected, where most of the meshes are estimated in the range around 9 - 11 nm, i.e.  $d_h$  FDex 40.[213] As visible in Fig. 48, a substantial decrease in FDex permeability was observed for  $M_n > 40$  kDa. Among the three  $D_g/D_o$  data points applicable to the model of Peppas and Lustig, one value,  $D_g$  of FDx\_20 seemed to be an outlier in the overall trend. Therefore, calculation of exact  $\xi$  values was not plausible. Moreover, the release experiments were performed to apply to release from injectable hydrogels. Therefore, extraction of uncrosslinked polymer (here up to 30 wt%) takes place concurrently to diffusion, which may affect the hydrodynamic drag of molecules. Moreover, potential swelling accompanied with mesh size increase of the hydrogels dependent on the polymer type may take place simultaneously to the release, which makes the diffusion process too complex to describe based on a theoretical approach.

The average mesh sizes of a network can be calculated basing on the hydrogel swelling thermodynamics, where  $\xi$  depends on  $v_{sw}^{-1/3}$  (Eq. 4), as postulated by Flory and Rehner. Hydrogels formed by crosslinking of oligomer end groups, and incomplete incorporation of the telechels into the network, as indicated by the characterization of DAT(T)-sOEG hydrogels, do not meet the requirements of idealized networks for using this model, as addressed in Ch. 1.1.2. This was already discussed above in view of the peculiar diffusivity in hydrogels from DAT-sOEG 5 kDa. The results from the here discussed  $\xi$  estimation indicated that crosslinking with the higher mTyr concentration led to higher crosslinking density compared to hydrogels crosslinked with  $100 \text{ U}\cdot\text{mL}^{-1}$  mTyr. All hydrogels comprising the same biocatalyst amount, except for the DAT-sOEG 5 kDa networks, which may contain lower amounts of crosslinks, had comparable molecular structure independent on precursor size (10 or 20 kDa) and end group substituent (DAT or DATT). The mesh sizes, calculated from rheological investigation, summarized in Table 10, Ch. 6.2.5 are somewhat higher than the estimated values discussed above, but a similar tendency was observed. The lower mesh sizes, estimated from the diffusion studies

experiments, may have resulted from additional effective netpoints by physical DAT(T)-sOEG incorporation in the unextracted hydrogels, subjected to release study here. Additional interactions of sOEG chains, such as entanglements, or aromatic clusters of unoxidized DAT(T) end groups may have contributed to lower  $M_c$  and  $\xi$  within these investigations. In contrast, the hydrogels studied in Ch. 6.2.5, were purified from non-covalently bound sOEG prior to rheological analysis.

## 6.4 Bulk hydrogels for release of bioactive molecules

### 6.4.1 Quantification of mTyr released from crosslinked hydrogels

One aspect in view of the potential *in vivo* applicability of enzymatically crosslinked hydrogels is if the catalyst can be removed from the hydrogels, since leaking out of an enzyme with residual activity in the surrounding tissue may cause undesired reactions with cells or metabolites, or cause immunological or toxic effects as a foreign protein. For injectable hydrogels, it may be desirable that mTyr remains entrapped within the hydrogel mesh, unless it can be previously washed out in case of implantation of preformed bulk hydrogels.

HPLC quantification of released mTyr (in the low  $\mu\text{g}$  range per mL hydrogel) after extensive washing of the hydrogels suggested that marginal amounts up to 12% of the employed catalyst could be released (Table 11). A higher percentage of the enzyme could be released from hydrogels crosslinked by the low enzyme concentration suggesting smaller average mesh size of these networks.

Table 11: Summary of relative amounts of mTyr extracted from DAT(T)-sOEG hydrogels crosslinked by mTyr catalysis ( $n = 3$ ).

Polymer type	DAT-sOEG		DATT-sOEG	
	mTyr conc. ( $\text{U}\cdot\text{mL}^{-1}$ )		mTyr conc. ( $\text{U}\cdot\text{mL}^{-1}$ )	
$M_n$ (kDa)	100	500	100	500
5	$10.5 \pm 2$	$4 \pm 0.4$	n.d.	n.d.
10	$11.5 \pm 9$	$4 \pm 0.4$	$8 \pm 1$	$5 \pm 0.1$
20	$8 \pm 1.5$	$6 \pm 1.8$	$10 \pm 0.2$	$5 \pm 0.1$

*n.d.* – not determined

mTyr is reported to have a globular structure and a  $r_h$  of 4.3 nm.[214] Surprisingly, the ratio of the released biocatalyst was slightly lower than the expected amount, as

extrapolated from the release of FDex<sub>40</sub> with comparable  $r_h$  of 4.4 nm. This may result from the globular protein structure compared to the linear randomly coiled dextran, which has higher mobility and flexibility to possibly fit through smaller mesh sizes. Another possibility, which was not previously addressed in literature and needs to be excluded in future investigations, is partial crosslinking of mTyr within the network.

### 6.4.2 Release of model bioactive compounds

To prove the stated mTyr selectivity and potential harm of the payload by the crosslinking reactions, tyrosine-free therapeutic peptides were studied. First, release studies were performed with octreotide, an inhibitor of growth hormone used in cancer therapy. However the released peptide could not be detected by the established HPLC method. Similar effect was observed for the antimicrobial peptide gramicidin S, which is characterized by stable cyclic structure. Incubating the peptides with mTyr revealed peptide degradation, as proven by HPLC and MALDI-ToF (Fig. 49A-B).[215] Contamination of commercial mTyr with peptidases was identified as the possible cause for peptide cleavage, and the peptide stability was retained in presence of protease inhibitors (Fig. 49D). However, the peptidase action seems to be vital for the activation of latent mTyr by proteolytic removal of active-center-blocking residues, as recently proven. [111] Various contaminants of mTyr after extraction from mushrooms, as detected here for industrially produced mTyr by SDS-PAGE (Fig. 49C) were also recently addressed in literature [112], emphasizing the importance of extensive purification of the enzyme intended to be used for biomaterial synthesis.

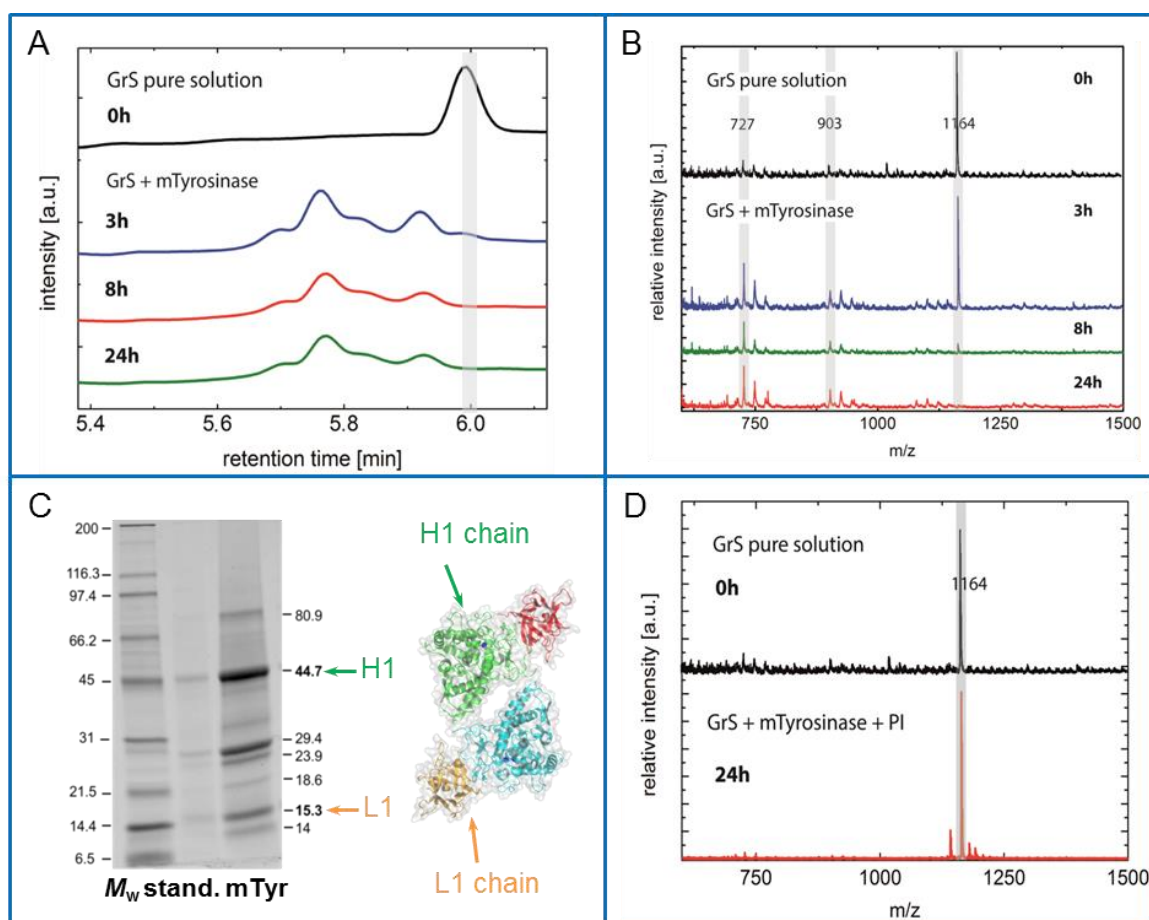


**Figure 49: Purity of mTyr affects the stability of therapeutic peptides.**

Chromatogram (A) and MALDI-ToF spectrum (B) of Gramicidin S, GrS, demonstrating the peptide degradation after incubation with mTyr at different time points. SDS-PAGE analysis of mTyr (C) revealed the presence of diverse contaminants beside the heavy (H) and light (L) chain of the tetrameric mTyr. The peptide stability was retained after addition of protease inhibitor (PI), as detected by MALDI-ToF (D). Figure adapted with permission from [215] © Materials Research Society 2015

Furthermore, heparin release from hydrogels formed with three different concentrations of DAT-sOEG 10 kDa and  $1000 \text{ U} \cdot \text{mL}^{-1}$  mTyr was investigated. The heparin molecular weight was determined by GPC analysis ( $M_w=47 \text{ kDa}$ ,  $M_n=36.2 \text{ kDa}$ ,  $\text{PDI}=1.3$ ). The heparin release kinetics from all hydrogels were conform with diffusion-controlled mass transport, as demonstrated by fitting of the initial timepoints in Fig. 50 (right) according to a power law, where the released amount is proportional to  $t^{-0.5}$ . Quantitative heparin release was achieved after 24 h, 32 h and 5 d from hydrogels with 1.8, 3.6 and 7.2 wt% DAT-sOEG respectively.

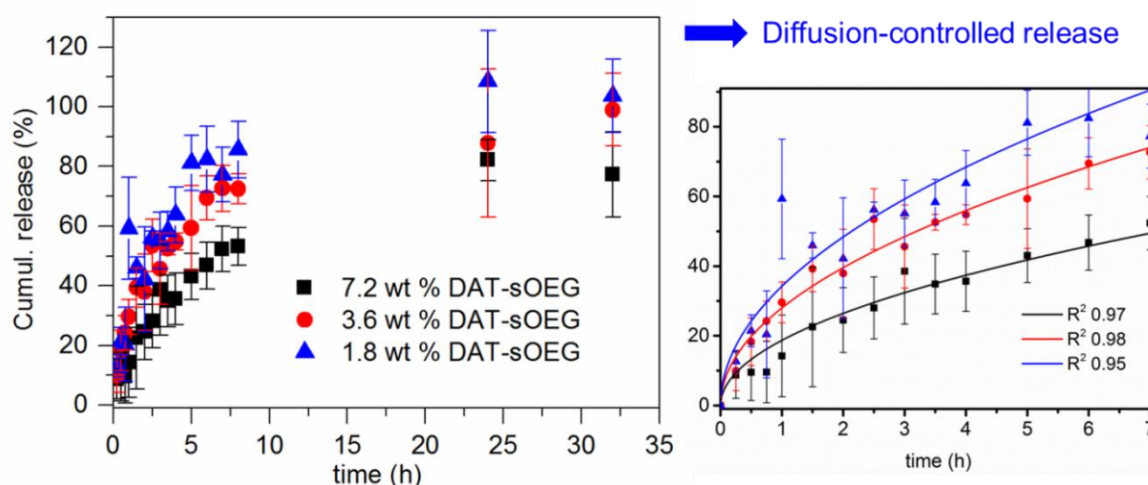


Figure 50: Release of heparin from hydrogels with varying DAT-sOEG 10 kDa precursor concentration. Error bars represent the standard deviation between the quantified heparin amounts released from different hydrogel samples ( $n=4$ ).

The retardation of the delivery rate with increasing polymer concentration indicated a decrease in the size of the openings in the molecular mesh and verified the tailorability of hydrogel structure by a substantial change in the amount of DAT as mTyr substrate, i.e. precursor concentration.

## 6.5 Summary

Within this chapter, the formation of hydrogels by mTyr mediated crosslinking reactions was demonstrated. Hydrogels could be synthesized from DAT(T)-sOEG telechels with varying  $M_n$  (5, 10 and 20 kDa), DATT-sOEG 5 kDa being an exception to this result. Gelation kinetics could be accelerated by increasing mTyr concentration from 2.5 h to 5 min. The gelation time decreased with increasing precursor  $M_n$ , which was surprising considering the decrease in amount of substrates DAT(T) as end groups. Equilibrium swelling was tailorable between 600 and 1200 vol% for most of the hydrogels. The lower  $Q$  for hydrogels from DAT-sOEG 5 kDa and DATT-sOEG 10 and 20 kDa indicated that the hydrogel swellability may have reflected the precursor hydrophobicity rather than the crosslinking density. All hydrogels exhibited similar mechanical properties ( $G'$  between 1 and 1.5 kPa), which were not systematically dependent on the precursor properties. The limited tailorability of hydrogel properties with increasing  $d.f.$  for DATT-sOEG 10 kDa indicated a potential low amount of crosslinks, which was confirmed by the incomplete

incorporation of precursors into all investigated networks ( $G$  up to 80%) and residual aromatic protons in hydrogels detected in  $^1\text{H-NMR}$ . In diffusion studies with FITC dextran of varying  $M_n$  on the other side, a strong decrease in the diffusion kinetics and permeability was observed with increasing solute size. Thereby, the diffusive properties of the investigated hydrogels indicated a decrease in the mesh size, when crosslinked with higher mTyr concentrations. All hydrogels demonstrated a molecular weight cutoff effect, lying at  $\sim 9\text{-}11$  nm, which however was biased by network defects and broad size distribution of the studied FITC dextrans. The release kinetics of heparin was governed by diffusion of the therapeutic macromolecule and could be controlled by increasing polymer concentration, which proved to be an effective approach to decrease the mesh size of hydrogels.



## 7 Conclusions and outlook

This study could demonstrate that DAT(T) are suitable substrates for mTyr-induced crosslinking reactions to build hydrogels with potential relevance for biomedical applications. The reaction principles and products formed by mTyr-initiated crosslinking reactions could be investigated in model studies with free and oligomer-bound DAT. The enzymatic catalysis enabled the synthesis of hydrogels from DAT(T)-sOEG with tailorable swelling characteristics, which enabled controllable diffusion of model and therapeutic macromolecules by variation of the concentration of enzyme and substrate/precursor. The experimental investigations allowed drawing following conclusions for the selected systems:

- The substrates were DAT and DATT were appropriate for the planned further investigations, as demonstrated in kinetic studies with mTyr. The oxidation efficiency of mTyr with the selected artificial substrates, lacking a free NH<sub>2</sub> in the side chain, was even threefold (DAT) to ninefold (DATT) increased compared to the natural phenolic substrate L-tyrosine.
- The enzymatic two-step oxidation of DAT-IOEG<sub>OMe</sub> as artificial mTyr substrate resulted in *o*-diphenol and *o*-quinone derivatives as reactive intermediates, which further involved in non-enzymatic crosslinking reactions and equally contributed to adduct formation in model reactions, as shown by NMR and UV-Vis spectroscopy. For a small molecular mTyr substrate, DAT methylester, the detected oligomeric products were heterogeneous in structure (NMR spectroscopy) and composed of *o*-diphenol, *o*-quinone and unoxidized DAT moieties, as proven by exact assignment of detected *m/z* to oligomer masses. Achieving high netpoint functionality by mTyr catalysis was possible, as oligomers with up to 11 repeating units were detected in model reactions with DAT methylester. Although there was evidence of di- and trimer formation from DAT-IOEG<sub>OMe</sub> 10 kDa, it could not be unequivocally concluded on the exact netpoint functionality of oligomeric substrates (DAT-IOEG<sub>OMe</sub> 10 kDa and DAT-ImOEG<sub>OMe</sub> 2 kDa) due to the limited ionization of products formed after mTyr catalysis, observed clearly in analyses of model reaction with DAT-ImOEG<sub>OMe</sub> 2 kDa by MALDI-ToF and ESI-MS. The hypothesized involvement of nucleophilic NH<sub>2</sub>

groups as into netpoint formation, initiated by mTyr mediated DAT oxidation, was indicated by MALDI-ToF analysis, which demonstrated marginal peaks of products preferentially formed by a Michael addition of  $\text{NH}_2$  to quinones rather than reacting to Schiff bases. These side products seemed to arise from a kinetically driven process, with the adduct formation from DAT derived intermediates being the favored crosslinking mechanism.

- The kinetics of enzymatic oxidation decreased in the sequence DAT > DAT-IOEG > DAT-sOEG and DATT > DATT-sOEG, as observed in kinetic investigations (MBTH assay, direct reaction monitoring by UV-Vis spectroscopy). The slower oxidation rate of DAT(T) on OEG attachment could be explained on the one side by a detrimental effect of the bulky highly hydrated oligomer chains causing steric hindrance for substrate interactions with the mTyr reactive center. On the other hand, the mTyr diffusivity in polymer solutions having higher viscosities compared to pure PBS was potentially decreased, which may have led to slower oxidation rate. The slow oxidation kinetics of polymeric substrates led to incomplete DAT(T) conversion, observed by NMR and MALDI-ToF, and was later confirmed by NMR characterization of swollen hydrogels, showing residual aromatic protons of DAT(T) end groups. Moreover, the fast spontaneous oligomerization of reactive intermediates, formed from mTyr catalyzed substrate oxidation, and the comparatively slow phenol hydroxylation being the rate-determining step in the enzymatic substrate activation, led to hydrogel formation preceding complete DAT(T) conversion resulting in restricted chain mobility, necessary for the formation of further netpoints. However, quantitative incorporation of end groups into netpoints was not necessary, as demonstrated by hydrogel formation from DAT(T)-sOEG precursors.
- Hydrogels could be formed from DAT(T)-sOEG 10 and 20 kDa in all cases. No network formation was observed for DATT-sOEG 5 kDa in contrast to DAT-sOEG 5 kDa, the latter showing very slow hydrogel formation and low gel contents (50 % when crosslinked with a low mTyr concentration), which indicated that a minimal size of precursors is needed for the formation of coherent networks. Surprisingly, the gelation time was reduced with increasing precursor  $M_n$ , although the substrate amount sinks in this order. The volumetric swelling  $Q$  could be controlled in the range 600 - 1200 vol% by the application of hydrogel precursors with varying end groups and

$M_n$ , as well as mTyr concentration. Networks from DAT-sOEG exhibited lower  $Q$ , when higher mTyr amounts were applied, and  $Q$  could be further reduced when DATT-sOEG with higher end group hydrophobicity was applied instead. Furthermore, the crosslinking densities of all hydrogels being crosslinked faster using higher biocatalyst amounts were higher, i.e. the networks exhibited smaller mesh sizes, as indicated by the decreased kinetics of FITC dextran diffusion in these cases. A systematic diffusion analysis of FITC dextrans with varying  $M_n$  (4 to 500 kDa) from enzymatically crosslinked DAT(T)-sOEG hydrogels showed a strong decrease in diffusive kinetics, as well as reduced hydrogel permeability of solutes with increasing sizes, which allowed estimation of a hydrogel mesh exclusion limit in the range 9 - 11 nm. The dependence of the diffusion coefficients from the average hydrogel mesh size could not be satisfactorily predicted by theoretical models, possibly resulting from an inhomogeneous network structure and broad FITC dextran size distribution. Furthermore, the release of heparin from DAT-sOEG 10 kDa hydrogels could be controlled by application of varying precursor concentrations. Therefore, a decrease of mesh size could be achieved by simultaneously increasing the substrate and precursor concentration.

- A higher crosslinking density was expected with decreasing precursor segment length, i.e.  $M_n$ . Nevertheless, some of the hydrogels properties ( $G'$ ,  $Q$  for DATT-sOEG hydrogels) could not be systematically controlled by increasing precursor  $M_n$ . In addition, the limited tailorability of hydrogel properties with increasing *d.f.* for DATT-sOEG 10 kDa (66 to 90 mol%) indicated a potential low amount of crosslinks, which was confirmed by the incomplete incorporation of precursors into the networks ( $G \leq 80\%$ ). An ineffective crosslinking may have resulted from kinetic and steric effects, as well as potential crowding of the hydrophobic aromatic DAT(T) residues in amphiphilic DAT(T)-sOEGs, making the substrates inaccessible for mTyr. This fact in addition to the complex chemical reactions, leading to a covalent network could explain the difficulty to establish a structure-property relationship for the investigated hydrogels in some cases.

Based on these scientific findings, the following aspects may be subject of future studies: (i) a detailed description of products from enzymatically initiated crosslinking reactions; (ii) increasing controllability of hydrogel properties; (iii) improving the potential of the investigated hydrogels for biomedical applications.

The systematic analysis of crosslinking reactions in model studies indicated the high complexity of the products, formed by mTyr catalyzed DAT oxidation, followed by various spontaneous cascade reactions. As recently reported, a detailed specification of various adducts could be achieved in model systems of small molecular compounds (catechol and propylamine), crosslinked by chemical oxidation in basic conditions, whereby the products were analyzed by various techniques after chromatographic separation.[173] These products however may not be representative of the adduct structures after mTyr catalysis with oligomeric substrates at physiological pH. Limited product ionization for oligomeric adducts hampered the mass spectrometric analyses within this work. Therefore, further investigation of DAT-ImOEG<sub>OMe</sub> as precursors in model reactions with mTyr may be conclusive on netpoint structure and functionality when the complex reaction mixtures are simplified by product separation and analysis, e.g. by coupling HPLC and GPC. By this means, also the contribution of side reactions, i.e. with NH<sub>2</sub> groups into the netpoint formation could be specified on by chromatographic quantification of the amount of reacted precursor after incubation with mTyr.

Moreover, a systematic variation of the properties of the hydrogels being a result of higher crosslinking density may be achieved by application of higher DAT(T)-sOEG precursor concentrations, e.g. 10 instead of 5 wt%, or by a combination of linear and branched precursor architectures. Since the slow crosslinking kinetics were identified as one of the potential causes of the ineffective hydrogel crosslinking, application of more potent recombinant tyrosinases with higher activity towards phenol oxidation [216, 217] compared to mTyr may lead to a higher impact of subsequent non-enzymatic reactions between the formed intermediates. In view of the potential application of the investigated hydrogels as drug releasing biomaterials, other aspects should be important in addition to mesh size control. Purification of commercial mTyr may be important with regard to undesired effects of impurities on contact with cells, or on the integrity of loaded peptides, demonstrated in this work.[215] Moreover, the synthesis of biocatalyst-free hydrogels may be important towards hydrogels intended to be injected. Therefore, a strategy to

immobilize mTyr in order to easily remove the enzyme after activation of the precursors would be particularly desirable. This approach was demonstrated successful for preparation of hydrogels by surface-bound hematin (porphyrin-derived macrocyclic iron complex) in presence of  $H_2O_2$  [218], but the approach may be more challenging for enzyme immobilization, since the coupling strategy needs to be suitable to preserve the enzyme tertiary structure, associated with its activity to initiate hydrogel formation.



## 8 Material and methods

### 8.1 Materials

Tyrosinase from mushroom, mTyr ( $1715 \text{ U}\cdot\text{mg}^{-1}$ ) was purchased from Sigma Aldrich Chemie GmbH, (Steinheim, Germany) and used without further purification. All experiments were performed with the same enzyme batch. DAT, DAT ester, *L*-tyrosine, *L*-DOPA, MBTH (Fluka analytical grade) and heparin (heparin sodium salt from porcine intestinal mucosa) were purchased from Sigma Aldrich Chemie GmbH (Steinheim, Germany). Oligomer precursors for functionalization, i.e. sOEG-NH<sub>2</sub>.HCl ( $M_n = 5, 10$  or  $20$  kDa) and NH<sub>2</sub>-lOEG<sub>OMe</sub> (Methoxy PEG Amine, HCl Salt,  $M_n = 2$  and  $10$  kDa) were obtained from Jen Kem Technology (Beijing, China) and the monodisperse oligomer NH<sub>2</sub>-l<sub>0</sub>OEG<sub>OMe</sub> (MeO-dPEG<sup>TM</sup>(48)-NH<sub>2</sub>) from Iris Biotech GmbH (Marktredwitz, Germany). FITC labeled dextrans (FITC-Dex) with  $M_n$  4, 20, 40, 70, 150 and 500 kDa were purchased from TdB Consultancy AB (Uppsala, Sweden). The solvents were of ACS grade, when used for synthesis and of HPLC grade for chromatographic purposes. All materials were used as received, instead otherwise specified.

### 8.2 Instrumental analysis of precursors, model reactions and hydrogels

Nuclear Magnetic Resonance (<sup>1</sup>H-NMR) spectra were recorded at room temperature on Avance DRX 500 MHz spectrometer (Bruker, Rheinstetten, Germany; software Topspin version 1.3) using deuterated dimethylsulfoxid, water, or methanol as solvents (deuterization  $\geq 99\%$ ), relaxation time 2 s. The analysis of the spectra was performed with ACD Labs Version 12.01 (the chemical shift of the solvent was used as reference). A relative error of 5% is expected for integration of peaks and calculation of *d.f.*

FT-IR-spectroscopy was performed at a Nicolet 6700 instrument (Thermo Scientific, Germany) with a diamond-ATR-unit (DuraSamplIR, Resultec, Garbsen) under the use of compressed dry air; at least 50 scans were recorded (resolution  $2 \text{ cm}^{-1}$ ).

MALDI-ToF mass spectra were measured using an ultrafleXtreme MALDI-TOF (Bruker, Bremen, Germany). 2,5-dihydroxybenzoic acid (DHB) dissolved in H<sub>2</sub>O/30%ACN+0.1% TFA was used as matrix (sample:matrix ratio 1:5 or 1:10). The spectra were obtained by laser irradiation at random spots throughout the target spot (average of 50 spectra for high signal-to-noise ratio).  $M_n$  was calculated by the software Polytools 1.0 (Bruker Daltonics).

UV-Vis spectroscopic analyses (Cary 50 Bio UV-Vis spectrophotometer, Varian, Victoria, Australia) were conducted from 200 to 800 nm at  $25 \pm 0.5$  °C (temperature control by thermostate connected to measurement cell). PBS/O<sub>2</sub> was used as reference, if not otherwise specified.

Multidetector GPC measurements were performed with DMF as eluent (0.005 wt% BHT as internal standard, flow rate  $0.25 \text{ mL} \cdot \text{min}^{-1}$  at 35 °C). The system was equipped with a precolumn (GRAM VS1,  $40 \times 4.6$  mm), two separation columns (GRAM 30Å 5091312 and GRAM 1000Å 71111, all from Polymer Standards Service GmbH (PSS), Mainz, Germany), an isocratic pump 980, an automatic injector 851-AS, LG 980-02 ternary gradient unit (both Jasco, Gross-Umstadt, Germany) and a degasser ERC-3315α (Ercatech AG, Berne, Switzerland). The detection was performed by a multiwavelength detector MD-910 (Jasco, Germany), a refractive index detector RI-930 (Shodex RI-101, USA), a miniDawn Tristar light scattering detector (Wyatt Technology Corporation, Santa Barbara, USA) and a differential viscometer  $\eta$ -1001 (WGE Dr. Bures, Dallgow-Doeberitz, Germany).

The LC-ESI-MS experiments were performed at an Acquity UPLC chromatographic system, coupled with an ESI-MS Q-TOF mass spectrometer (UPLC-Synapt G2-S HDMS, all from Waters Co., Milford, MA, US). The chromatographic system was equipped with an Acquity SDS pump and an Acquity AutoSampler (5  $\mu\text{L}$  injection volume) (all from Waters Co). The separation was performed on a C18 RP column (Zorbax Eclipse,  $3.5 \mu\text{m}$ ;  $150 \times 4.6$  mm, Agilent Technologies, Waldbronn, Germany) by a gradient elution with Water+0.1% formic acid (A) and ACN (B) (90-80% A within 1 min; 80-40% A within 20 min, to 100% B until 25 min, a flow rate of  $0.6 \text{ mL} \cdot \text{min}^{-1}$ ).

## 8.3 Precursor synthesis

### 8.3.1 Synthesis of monofunctionalized DAT-IOEG<sub>OMe</sub>

For the synthesis of DAT-IOEG<sub>OMe</sub> 10 kDa, NH<sub>2</sub>-IOEG<sub>OMe</sub> 10 kDa (2 g, 1 eq.) was dissolved in 20 mL NMP (fast dissolution at 40°C). DAT (70 mg, 2 eq.) was mixed with EDC·HCl (96 mg, 2.5 eq.), NHS (70 mg, 3 eq.) and DIPEA (75 µL, 4 eq.) in 20 mL NMP at 0°C and stirred for 1 hour. Afterwards, both solution are mixed and stirred at an ice bath for 17h. The reaction mixture was precipitated in cold hexane:ethylacetate 2:1 (v/v, 600 mL). The precipitate was washed with ethyl acetate. Subsequently, the polymer aqueous solution was dialyzed (Spectra/Por 3 membrane, MWCO 3.5 kDa, SpectrumLabs.com Spectrum Inc. Europe) against deionized water and freeze-dried. The degree of DAT functionalization, *d.f.* (here 87 mol%) was calculated by <sup>1</sup>H-NMR by relating the peak integrals of end group protons, i.e. the average areas of the aromatic (6.62 and 6.91 ppm) and side chain protons (2.5 and 2.87 ppm) of DAT and the area of the OMe protons (3.35 ppm).

To obtain DAT-IOEG<sub>OMe</sub> 2 kDa, DAT (200 mg, 1.2 eq.) was mixed with EDC·HCl (230 mg, 1.2 eq.), NHS (150 mg, 1.3 eq.) and DIPEA (142 µL, 1.5 eq.) in 10 mL anhydrous DCM at 0°C and stirred for 1 hour. A solution of poly(ethyleneglycol)methylether amine (NH<sub>2</sub>-IOEG<sub>OMe</sub>, M<sub>n</sub>~2 kDa 2 g, 1 eq.) in anhydrous dichloromethane (15 mL) was added dropwise and stirring was continued overnight while the mixture was allowed to reach room temperature. TLC analysis indicated full conversion of the OEG-amine (ninhydrin-test). The mixture was diluted with aqueous 1N HCl (80 mL) and CH<sub>2</sub>Cl<sub>2</sub> (30 mL). The layers were separated and the aqueous layer was extracted with CH<sub>2</sub>Cl<sub>2</sub> (5×30 mL). The combined organic layers were dried with Na<sub>2</sub>SO<sub>4</sub>, filtered and concentrated under reduced pressure. The obtained crude product (2.4 g) was filtered through basic Al<sub>2</sub>O<sub>3</sub> (Brockmann I, CH<sub>2</sub>Cl<sub>2</sub>/MeOH = 9:1) and dried under reduced pressure. Then, the product was further purified by RP-HPLC on a PS/DVB column, see Ch. 8.4. The degree of DAT functionalization, *d.f.* was calculated by <sup>1</sup>H-NMR by relating the peak integrals of end group protons, i.e. the average areas of the aromatic (6.62 and 6.91 ppm) and side chain protons (2.5 and 2.87 ppm) of DAT and the area of the OMe protons (3.35 ppm). The *d.f.* was 53 mol% before purification by HPLC and afterwards 78 mol%.

Monodisperse DAT-ImOEG<sub>OMe</sub> 2 kDa was synthesized applying another coupling chemistry: DAT (90 mg, 2.3 eq.), TBTU (190 mg, 2.5 eq.) and DIPEA (145  $\mu$ L, 3.5 eq.) were dissolved in 1.5 ml anhydrous DMF. After 5 min mixing, a solution of NH<sub>2</sub>-ImOEG<sub>OMe</sub> (500 mg, 1 eq.) in 2.5 ml anhydrous DMF was added and the coupling reaction was carried out under stirring for 3h. All reactions were performed under nitrogen protective atmosphere at room temperature. The solution was successively washed with saturated NaCl solution, 5% NaHCO<sub>3</sub>, 1 M HCl solution, and distilled water. The obtained crude product (82 mg) was filtered through basic Al<sub>2</sub>O<sub>3</sub> (Brockmann I, CH<sub>2</sub>Cl<sub>2</sub>/MeOH = 9:1) and dried under reduced pressure. The final product purification was performed by RP-HPLC on a C18/phenyl mixed stationary phase (see Ch. 8.4).

### 8.3.2 Synthesis of DAT- and DATT-sOEG

Desaminotyrosyltyrosine (DATT) was synthesized by a two-step procedure, as previously described.[219] The synthesis of DAT(T)-sOEG was performed according to an already reported protocol.[126] Shortly, for the synthesis of DAT(T)-sOEG 10 kDa, DAT (3.5 mmol, 582 mg) or DATT (3.5 mmol, 1.2 g), EDC-HCl (4 mmol, 770 mg), NHS (4.5 mmol, 520 mg) and DIPEA (6 mmol, 1.1 mL) were dissolved in 40 mL NMR and mixed at 0 °C for 1h, before adding NH<sub>2</sub>-sOEG (0.5 mmol, 5 g) in 40 mL NMP. The temperature was allowed to reach r.t. and the coupling reaction proceeded overnight for 17h. Afterwards, the crude product was precipitated in cold hexane:ethylacetate 1:1 (v/v, 800 mL) and left at 4 °C for at least 24h to complete the precipitation process. Then, the product was filtered and washed with ethylacetate before dissolving in water and free-drying to achieve the final product as a fine white powder. The degrees of DAT(T) functionalization (*d.f.*) of modified polymers were calculated by <sup>1</sup>H-NMR by relating the integrals of peaks corresponding to protons of the aromatic DAT groups ( $\delta$  = 6.6 and 6.9 ppm) or the  $\alpha$ -CH group of DATT ( $\delta$  = 4.4 ppm), and the CH<sub>2</sub> of the OEG repeating unit ( $\delta$  = 3.5 ppm).

## 8.4 Purification of monofunctional oligomers by RP-HPLC

---

DAT-ImOEG<sub>OMe</sub> and the products after mTyr catalysis were analyzed by analytical HPLC by an Agilent 1200 Infinity system (Agilent Technologies, Waldbronn, Germany)

with a reversed-phase (RP) column having a balanced ratio of C-18 and propylphenyl groups (Nucleodur Sphinx RP, 250 x 4 mm, particle size: 5  $\mu\text{m}$ ; Macherey-Nagel GmbH & Co. KG, Düren, Germany) and a H<sub>2</sub>O/ACN mobile phase (linear gradient 30% to 100% (v/v) ACN within 25 min, flow rate 1 mL·min<sup>-1</sup>).

Semi-preparative was carried out on a Prostar 701 HPLC system (Varian Deutschland GmbH, Germany). DAT-IOEG<sub>OMe</sub> 2 kDa was eluted on a PS/DVB (polystyrene/divinylbenzene) reversed-phase semi-preparative column (PLRP-S, pore size: 100 Å, particle size: 8  $\mu\text{m}$ ; 300 x 25 mm; Polymer laboratories, Church Stretton, UK) with a linear H<sub>2</sub>O/ACN gradient (10% to 90% (v/v) ACN within 25 min, flow rate 8 mL·min<sup>-1</sup>) and UV detection ( $\lambda = 254$  and 220 nm).

The monodisperse DAT-ImOEG<sub>OMe</sub> was purified on a semi-preparative RP column (balanced C-18 and propylphenyl groups, Nucleodur Sphinx RP, 250 x 21 mm, particle size: 5  $\mu\text{m}$ ; Macherey-Nagel GmbH & Co. KG, Düren, Germany) with a H<sub>2</sub>O/ACN mobile phase (linear gradient 30% to 100% (v/v) ACN, flow rate 7.5 mL·min<sup>-1</sup>). For DAT-ImOEG<sub>OMe</sub>, a purity  $\geq 94\%$  was achieved, with a purification yield of 57 mol% for the selected fraction.

## 8.5 Preparation of solutions

---

For all solutions, PBS saturated with O<sub>2</sub> (PBS/O<sub>2</sub>) was applied as solvent, unless otherwise specified. PBS buffer was prepared from 8.77 g NaCl, 1.03 g Na<sub>2</sub>HPO<sub>4</sub>·2H<sub>2</sub>O and 0.98 g NaH<sub>2</sub>PO<sub>4</sub>·2H<sub>2</sub>O dissolved in 1 L water and adjusted to pH 7.4. The PBS solution (50 mM) was adjusted at pH 7.4 and filtered sterile by membrane filter (0.2  $\mu\text{m}$  pore size; GE Healthcare life Science Whatman™, UK). The mTyr concentration is given in U·mL<sup>-1</sup>, using the activity unit, provided by the supplier (1 unit represented  $\Delta A_{280}$  of 0.001 per min at pH 6.5 and 25°C in a reaction mixture containing L-tyrosine; specific mTyr activity was 1715 U·mg<sup>-1</sup>).

## 8.6 Kinetic studies with mTyr

### 8.6.1 Dopachrome Assay

The monophenolase activity was measured in solutions, containing 1 mM *L*-tyrosine in PBS/O<sub>2</sub> (the solubility limit of the amino acid at the selected conditions), while 1 mM *L*-dopa solutions in PBS/O<sub>2</sub> were applied for the diphenolase activity investigations. The enzyme concentration in the dopachrome assay was set to 9.6 nM (calculated with mTyr  $M_w$  120 kDa). Spectrophotometric measurements were carried out at 25 °C in quartz precision cells with 1 cm light path (Hellma Analytics, Müllheim, Germany) on a Cary 50 Bio UV-Visible Spectrophotometer (Varian, Victoria, Australia). The absorption of dopachrome (molar absorption coefficient  $\epsilon_{475\text{nm}} = 3,700 \text{ M}^{-1}\cdot\text{cm}^{-1}$ ) was measured at 475 nm. For the pH study ( $n=6$ ), the pH of PBS/O<sub>2</sub> was adjusted to pH 5.5, 6.5, 7.0, and 7.4. For the analysis of the temperature effect on activity ( $n=6$ ), the enzyme and substrate solutions were pre-temperated (4 °C in a fridge, r.t. or 37 °C incubator). The spectrophotometer cuvette holder was also adjusted to the respective temperature prior to measurement. The storage stability of mTyr ( $n=6$ ) was investigated under different conditions. The freshly dissolved enzyme was compared to mTyr solution, stored for 6h at r. t., in a refrigerator at 4 °C (6 hours to 2 days), and after freezing and thawing of an enzyme aliquot.

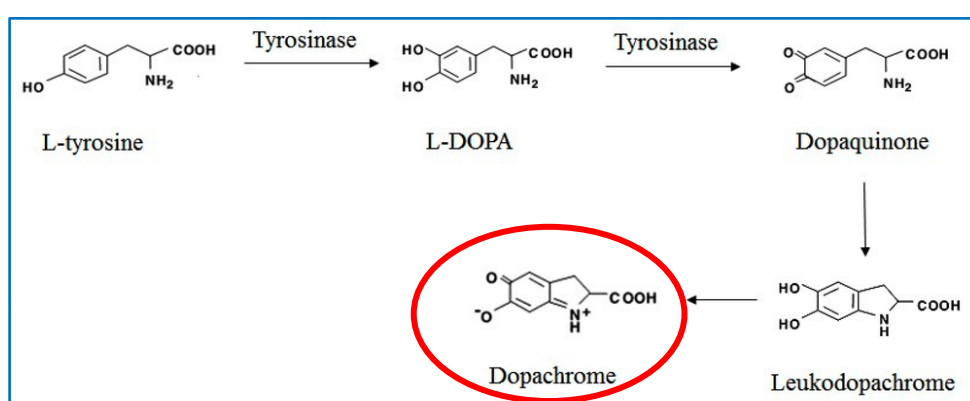


Figure 51: Scheme of the formation of dopachrome from *L*-tyrosine or *L*-dopa by tyrosinase catalysis.

The specific mTyr activity was calculated according to eq. 6, using the slope of the linear part of the curve ( $\Delta A/\Delta t$ ), which was determined using linear regression analysis with Excel ( $R^2$  0.996 to 0.999) and  $\epsilon_{475\text{nm}} = 3,700 \text{ M}^{-1}\cdot\text{cm}^{-1}$ .

$$\text{specific activity (U} \cdot \text{mg}^{-1}) = \frac{\Delta A \cdot V_S}{\Delta t \cdot d \cdot V_E \cdot c_E \cdot \epsilon} \quad (\text{Eq. 6})$$

## 8.6.2 MBTH Assay

First, MBTH was dissolved in PBS/O<sub>2</sub> with addition of 4% DMF (v/v), needed to solubilize the saturated reagent and the pigments formed by the action of mTyr during analysis. HCl addition of was necessary for complete MBTH dissolution, leading to pH =3.9-5. After adding the substrate solution, the pH of the resultant medium PBS/O<sub>2</sub>/2% DMF (v/v) was adjusted to pH 7. MTyr (5 nM) was added and the measurement ( $\Delta A_{505\text{ nm}}$ ) was started immediately at a Cary 50 Bio UV-Visible spectrophotometer (Varian, Victoria, Australia) with PMMA cells (light path 1 cm) (Brand GmbH, Wertheim, Germany). In all experiments, a saturated MBTH solution (6 mM) was applied and the MBTH concentration in the analyzed solution was present in at least 4fold excess with respect to the analyzed substrate. The experiments comparing DAT, DATT, *L*-tyrosine and *L*-dopa were carried out at substrate concentrations of 1 mM PBS/O<sub>2</sub>/2% DMF (v/v). The MBTH-quinone adduct was measured at  $\lambda$  505 nm until steady-state was achieved. Blanks samples without added mTyr (MBTH + substrate), as well as without substrate (MBTH + mTyr) did not show any increase in absorption over 20 min. The mTyr specific activity was calculated by Eq. 6. The absorption coefficient  $\epsilon_{505\text{ nm}}$  was 40,000 M<sup>-1</sup>·cm<sup>-1</sup> [143] and the slope of the curve ( $\Delta A/\Delta t$ ) was determined using linear regression analysis within Excel ( $R^2$  0.995 to 0.999 for the linear fits).

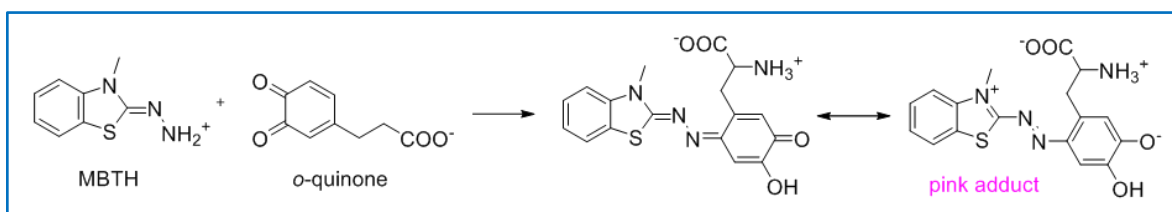


**Figure 52:** Scheme of the proposed reaction mechanism of MBTH assay.

*The enzymatically produced o-quinone reacts to a pink MBTH-quinone adduct, which was measured in the mTyr kinetic investigations.*

For analysis of mTyr kinetics according to the Michaelis-Menten formalism, the substrates DAT and DATT were dissolved at varying concentrations (0.1–2 mM). All other parameters were identical. The data analysis by non-linear fit to Eq. 7 was computed by Origin 9.0.0 (hyperbolic function) according to the Marquard-Levenberg algorithm.

For the MBTH study with polymeric substrates, DAT(T)-sOEG were dissolved in PBS/O<sub>2</sub>/2% DMF (v/v) at a final substrate concentration of 2 mM (oligomer stock solutions were 5fold diluted to final concentrations 8.77 mg·mL<sup>-1</sup> DAT-sOEG 10 kDa and 8.47 mg·mL<sup>-1</sup> DATT-sOEG 10 kDa). The absorption at 505nm nm was monitored for 60 min. For

DAT-sOEG 10 kDa, a steady-state was reached after 20 min, while for DATT-sOEG 10 kDa the absorbance increased for 35 min, before the reaction reaching equilibrium.

## 8.7 Model reaction solution for structural analyses

---

### 8.7.1 UV spectroscopic analysis

To study the formation of different products absorbing light in the UV and visible region, linear DAT monofunctionalized oligo(ethylene glycol) (DAT-IOEG<sub>OMe</sub>,  $M_n$  10 kDa, *d.f.* = 87 mol%) was dissolved in PBS, saturated with O<sub>2</sub> at pH 7.4 and mixed with a mTyr stock solution in PBS/O<sub>2</sub> at a volume ratio of 1:1. For the different experiments, different oligomer and mTyr concentrations were used, as referred in Ch. 5.2: DAT-IOEG 6.25 mg·mL<sup>-1</sup> (0.6 mM DAT) or DAT-sOEG 1 mg·mL<sup>-1</sup> (*d.f.* 64 mol%, 2.4 mM DAT) were equally mixed with 500 U·mL<sup>-1</sup> mTyr. The model reactions were monitored directly after mTyr addition by UV-Vis spectroscopy. In another study, 50 mg·mL<sup>-1</sup> DAT-IOEG<sub>OMe</sub> (4.7 mM DAT) incubated with 100 and 500 U·mL<sup>-1</sup> mTyr, the solutions were 50fold diluted before measurement. The absorption spectra were measured at different time points in the range between  $\lambda$  200 nm and 800 nm at 25 °C in quartz precision cells ( $d = 1$  cm, Hellma, Mühlheim, Germany) on a Cary 50 Bio UV-Visible Spectrophotometer (Varian, Victoria, Australia).

### 8.7.2 NMR

DAT (3 mg·mL<sup>-1</sup>) or DAT-IOEG<sub>OMe</sub> ( $M_n$  2 kDa, 5 wt%) were mixed with mTyr (1000 U·mL<sup>-1</sup>) and dissolved in D<sub>2</sub>O, saturated with O<sub>2</sub>. The solutions were directly subjected to NMR analysis. The precipitate, formed from DAT + mTyr after 28h was collected by centrifugation and partially solubilized in D<sub>2</sub>O, mixed with 50  $\mu$ L NaOD or MeOH-d<sub>4</sub>. DAT ester (2 mg·mL<sup>-1</sup>) and mTyr were dissolved in H<sub>2</sub>O. The reaction mixtures were freeze-dried at defined timepoints and analyzed by NMR after being partially dissolved in MeOH-d<sub>4</sub>.

### 8.7.3 MALDI-ToF

DAT-IOEG<sub>OMe</sub> ( $M_n$  10 kDa, 5 wt%), mixed with mTyr (500 U·mL<sup>-1</sup>) in PBS/O<sub>2</sub> and analyzed by MALDI-ToF after 2 and 8h. Purified DAT-ImOEG<sub>OMe</sub> 2 kDa was incubated with mTyr (1000 U·mL<sup>-1</sup>) in PBS/O<sub>2</sub> at an oligomer concentration of 5 mg·mL<sup>-1</sup> (2.2 mM DAT) and investigated by MALDI-ToF after 1, 8 and 24h. In a further study, DAT-ImOEG<sub>OMe</sub> was mixed with varying amount of NH<sub>2</sub>-ImOEG<sub>OMe</sub> 2 kDa corresponding to DAT to NH<sub>2</sub> molar ratios of 9:1, 6:4, 5:5, 3:7 and 1:9 (overall concentration of oligomer end groups 2.2 mM) and incubated with mTyr (1000 U·mL<sup>-1</sup>) as described above. The MALDI-ToF measurement was performed after 24h, as described above.

### 8.7.4 HPLC and LC-MS analysis

Purified DAT-ImOEG<sub>OMe</sub> 2 kDa was incubated with mTyr (1000 U·mL<sup>-1</sup>) in PBS/O<sub>2</sub> at an oligomer concentration of 5 mg·mL<sup>-1</sup> (2.2 mM DAT) and investigated by HPLC or LC-MS. The HPLC investigation was carried out on an Agilent 1200 Infinity system with a RP-column (C-18/propylphenyl mixed phase) with H<sub>2</sub>O and ACN as mobile phases, applying the same gradient elution as reported in Ch. 9.4.

## 8.8 Hydrogel synthesis

---

Hydrogel films were prepared/ synthesized in petri dishes by mixing a precursor solution (10 wt%) with an equal amount of mTyr stock solution (200 or 1000 U·mL<sup>-1</sup> respectively). The pregel solutions were sealed with parafilm and kept at r.t. under mild agitation (55 rpm) overnight to ensure complete crosslinking. Hydrogels (20 different compositions) were dried and extracted as described below, for analysis of  $G$ ,  $Q$  and mechanical properties.

## 8.9 Hydrogel characterization methods

### 8.9.1 Gelation kinetics

The gelation kinetics of the pre-polymer solutions was analyzed by oscillatory rheological experiments using a Physica MCR 301 rheometer (Anton Paar GmbH, Ostfildern-Scharnhausen, Germany) at 25 °C using a cone-plate geometry with a diameter of 25 mm. The applied oscillatory frequency and amplitude were kept very low ( $f = 1$  Hz,  $\gamma = 0.1\%$ ) to minimize external impact on the crosslinking reaction. Solutions of DAT- and DATT-sOEG in PBS/O<sub>2</sub> were mixed with equal amount of a mTyr solution and immediately loaded and analysed by rheology (resulting polymer and mTyr concentration 5 wt% and 100, 250, 500 and 1000 U·mL<sup>-1</sup>,  $n = 3$ ). The samples were covered with dodecane in order to exclude artifacts associated with water evaporation during the long-term experiments. The gelation time,  $t_{gel}$ , was determined by the crossover of the extrapolated  $\eta^*$  (tangent) at the steepest increase and the x axis, time.

### 8.9.2 Gel content

For analyzing the gel content, dried hydrogel films ( $n=3$ ) were weighed to obtain  $m_0$  and extracted at r.t. under agitation first in PBS, then in water for 24 hours with frequent exchange of the washing medium. Then, the hydrogels were freeze-dried and weighted to obtain  $m_{ex}$ .  $G$  was calculated according to Eq. 2

$$G \text{ (wt\%)} = \frac{m_{ex}}{m_0} \cdot 100 \quad (\text{Eq. 1})$$

### 8.9.3 Swelling

The volumetric degree of swelling  $Q$  was determined according to Eq. 2. Hydrogels ( $n=6$ ) were first extracted, then swollen in PBS at 37 °C for 24 h, blotted carefully on filter paper to remove water from the hydrogel surface and weighed to obtain equilibrium swelling mass  $m_{sw}$ . The samples were freeze-dried and weighed ( $m_d$ ).

$$Q \text{ (vol\%)} = 1 + \rho_p \left( \frac{m_{sw}}{m_d \cdot \rho_s} - \frac{1}{\rho_s} \right) \cdot 100 \quad (\text{Eq. 2})$$

The density of the dry polymer networks  $\rho_p$  was determined with an Ultra Pycnometer (Quantachrome, Odelzhausen, Germany) at r.t. using a measurement cell with a calibration volume of 1.0725 cm<sup>3</sup>. The density of PBS,  $\rho_s$  was 1.0052 g·cm<sup>-3</sup>.

### 8.9.4 Rheology

Hydrogels were synthesized in petri dishes ( $d=50$  mm), extracted and swollen in PBS as described above, and analyzed via a plate-plate geometry ( $d=25$  mm) at 37 °C with solvent trap using the rheometer, named above (Physica MCR 301, Anton Paar GmbH, Germany). The hydrogels were placed between the two plates with a gap of 1.4- 1.7 mm. A constant normal force of 0.1 Pa was applied. A solvent trap protected the samples from water evaporation. The linear viscoelastic region was determined at 37 °C by frequency ( $f=0.05$ -50 Hz at fixed  $\gamma=0.05\%$ ) and amplitude ( $\gamma=0.01$ -100% at fixed  $f=1$  Hz) sweep measurements. Hydrogels ( $n\geq 3$ ) were further analysed by time sweeps in the linear viscoelastic region ( $f=1$  Hz and  $\gamma=0.1\%$ ) for 30 min.

### 8.9.5 FITC Dextran release

Solutions of different polymeric precursors (end conc.in the gel 5 wt%) and mTyr (end conc. 100 or 500 U·mL<sup>-1</sup>) in PBS, pH 7.4 were mixed with FITC-Dex ( $M_n$  4, 20, 40, 70, 150 and 500 kDa, 1 mg·mL<sup>-1</sup>, 50  $\mu$ g per gel), in a 96 well plate and allowed to gel overnight in the absence of light ( $n=4$ , gel thickness 0.25 cm). The release was investigated at 37 °C under mild agitation and light absence. An aliquot of the release medium (100  $\mu$ L out of 250  $\mu$ L PBS, pH 7.4) was exchanged with fresh buffer solution at defined time points, and the emission was immediately measured (excitation/emission wavelengths 490/520 nm) at an Infinite 200Pro fluorescence spectrometer (Tecan Trading AG, Switzerland). FITC-Dex was quantified by the linear correlation between the emission intensity and concentration of standard FITC-Dex solutions of the respective  $M_n$ . The concentration of the standard FITC-Dex solutions were within the range, in which a linear relationship between the concentration and the fluorescence signal is verified.[220] The measured release curves were fitted to a power function according to the proposed diffusion model by Origin 9.0.0.

### 8.9.6 Tyrosinase extraction

The released amount of tyrosinase was quantified in the extracts of hydrogel films after extensive washing in PBS for 5 days, with frequent medium exchange ( $n=2$ ). The extraction solutions were freeze-dried for up-concentration, hydrolyzed in acidic environment (excess 7.5 N HCl at 115 °C for 12 h (PMC block heater, Germany)) and neutralized. Subsequently, the resulting amino acids were subjected to HPLC analysis on a C18 column (Zorbax Eclipse, 3.5 $\mu$ m; 150x4.6mm, Agilent Technologies, Waldbronn, Germany) with pre-column derivatization using 50  $\mu$ L sample and 50  $\mu$ L *o*-phthaldialdehyde (10 mg·mL<sup>-1</sup> in MeOH/borate buffer (90/10, v/v)). MeOH/ACN/H<sub>2</sub>O (45/45/10, v/v) was used as mobile phase (35 °C, 1 mL min<sup>-1</sup>) with fluorescence detection (ex. 335 nm, em. 450 nm). The sample quantification was performed by standard calibration with hydrolyzed mTyr solutions of known concentrations. The calculated values are mean values from two independent samples, quantified according to the average amounts of 5 selected amino acids (aspartic acid, glutamic acid, serine, alanine, cysteine) with elution times, well separated from the peaks, corresponding to polymer end groups.

### 8.9.7 Heparin release studies

DAT-sOEG 10 kDa, mTyr and heparin were dissolved in PBS. The solutions were mixed to final concentrations of 7.2, 3.6 and 1.8 wt% oligomeric precursor, 1000 U·mL<sup>-1</sup> enzyme and 500  $\mu$ g heparin per gel and pipetted in the middle of a 24-well plate (the surrounding empty wells were filled with water bidest. to prevent hydrogel drying). Pregel solution were allowed to gel overnight under mild shaking at r.t. The release study was started by applying 700  $\mu$ L PBS as a release medium and proceeded at 37 °C under mild shaking. At defined timepoints, 100  $\mu$ L of the release medium were withdrawn and exchanged with fresh PBS. For quantification of the released heparin, the collected supernatants were hydrolyzed in 0.2 mL 6 N HCl for 1 h at 105 °C. After the hydrolyzed samples cooled to r.t., 0.2 mL 6 M potassium acetate was added. Then, 0.1 mL 5 % (w/v) NaNO<sub>2</sub> was added to the unstoppered sample containers on an ice bath and 30 min later, 0.1 mL 12.5 % (w/v) ammonium sulfamate. The samples were then mixed with 0.2 mL 0.8 % (w/v) 3,5-diaminobenzoic acid dihydrochloride and incubated at 37 °C for 1 h

for color development. The solution was centrifuged after addition of 0.04 mL concentrated HCl. The supernatant was diluted five-fold before measuring the fluorescence was measured at an Infinite M200 Pro (Tecan Deutschland GmbH, Crailsheim, Germany) spectrophotometer (excitation/emission wavelengths 422/514 nm).

## 8.10 Statistics and error evaluation

---

Reported values are given as the mean value  $\pm$  standard deviation (*SD*), if not otherwise mentioned. The mean value  $\bar{x}$  is defined as the numerical average of all measured values within a data set and calculated according to Eq. 9, where  $n$  is the number of data points and  $x_i$  denotes the different measured values:

$$\bar{x} = \frac{1}{n} \sum_{i=1}^n x_i \quad (\text{Eq. 9})$$

The standard deviation (*SD*) describes the spread of the individual values  $x_i$  about its mean in a data set, and can be determined according to Eq. 10, where  $s$  is the standard deviation:

$$s = \sqrt{\frac{\sum_{i=1}^n (x_i - \bar{x})^2}{n-1}} \quad (\text{Eq. 10})$$



## 9 Abstract/Zusammenfassung

### 9.1 Abstract

---

Enzyme-catalyzed reactions are a possible alternative approach for the generation of hydrogels for biomedical applications, whereby the specificity of enzymatic reactions as well as the crosslinking in mild and cytocompatible conditions are evaluated as particularly advantageous. In this doctoral thesis, a basic understanding of the principles of enzymatically induced network synthesis should be established, whereby tyrosinase (mTyr) was selected as a physiologically relevant enzyme. The work has been developed based on the hypothesis that DAT(T) is a suitable alternative substrate for mTyr and applying DAT(T) as a functional group of hydrophilic telechels allows the generation of hydrogels with systematically controllable properties. In the first part, the suitability of free dissolved DAT (T) as a substrate for mTyr should be tested and various (model) precursors of DAT (T) -functional oligoethylene glycol synthesized. In the second step, mechanistic aspects of the tyrosinase catalyzed cross-linking of linear, monofunctionalized model precursors should be studied in order to decipher the reaction pathways and the nature of the formed network points as well as the involved chemical species. In the third step, the application potential of the cross-linking reactions for the synthesis of hydrogels from star-shaped telechelics should be demonstrated, whereby a comprehensive understanding of the complex system should be achieved by a systematic analysis of physicochemical properties, network structures and diffusion-controlled release of bioactive macromolecules.

The selected substrates DAT and DATT showed a threefold (DAT) or ninefold (DATT) higher mTyr activity compared to the natural phenolic substrate *L*-tyrosine in kinetic studies, which confirmed the suitability of the substrates for the studies planned here. To elucidate the reaction mechanism, which consists of an enzyme catalyzed reaction of DAT(T) to reactive species with subsequent spontaneous crosslinking, by means of soluble reaction products, DAT monofunctionalized oligomers (DAT-IOEG<sub>OMe</sub> 10 kDa and 2 kDa, respectively) were synthesized and employed in model reactions. Thereby, *o*-diphenol and *o*-quinone groups have been identified as enzymatically produced reaction intermediates

for the reaction of free and oligomer bound DAT by UV-Vis as well as NMR spectroscopy. An increase in signals characteristic of *o*-quinonoid structures, with a decrease in the aromatic character of DAT end groups, was also detected by FT-IR spectroscopy of DAT-IOEG<sub>OMe</sub> 2 kDa. By exact assignment of the *m/z* detected by MALDI-ToF, catechols, *o*-quinones, as well as monophenols for the first time, were identified as the building blocks of the oligomers formed from DAT and DAT methyl ester as the result of mTyr catalysis. In addition, the conversion of DAT ester oligomers with up to 11 repeating units could be detected by MALDI-ToF, which is an indication of the theoretically possible high network functionalities by enzyme catalysis. On the other hand, dimers and a few trimers were demonstrated from DAT-IOEG<sub>OMe</sub> 10 kDa by mTyr catalyzed reactions, suggesting a steric hindrance by the bulky strongly hydrated OEG chains, or a lack of product ionization. MALDI-ToF and developed HPLC-ESI-MS methods showed that narrowly distributed DAT-ImOEGOMe 2 kDa alone and in mixtures with NH<sub>2</sub>-ImOEGOMe react quantitatively within <24 h, indicating the possible involvement of primary amines in non-enzymatic polymerisation of the reactive intermediates.

Furthermore, hydrogels from 4-arm sOEG precursors were prepared by varying the end group (DAT or DATT), the molecular weight,  $M_n$  (5, 10 or 20 kDa) and the amount of substrate, represented by the degree of precursor functionalization. (60 and 90 mol% in the case of DATT-sOEG 10 kDa), as well as the concentration of the biocatalyst mTyr. The gel time of DAT(T)-sOEG hydrogels could be significantly reduced from 2.5 h to 5 min by the use of different enzyme concentrations. While for DAT-sOEG the gelation time decreased with increasing  $M_n$  or substrate quantity in the solution, no hydrogels could be formed by mTyr catalysis by DATT-sOEG 5 kDa. The enzymatic reaction kinetics followed the sequence free DAT > DAT-IOEG > DAT-sOEG, as determined by UV-Vis spectroscopy. NMR spectroscopic detection of non-oxidized aromatic DAT and DATT end groups in swollen hydrogels confirmed that there was no quantitative conversion of the substrate and was necessary to form hydrogels. Kinetic and steric phenomena, as well as competitive physical interactions could also be the relative

Furthermore, hydrogels from 4-arm sOEG precursors were prepared by varying the end group (DAT or DATT), the molecular weight,  $M_n$  (5, 10 or 20 kDa) and the amount of substrate, represented by the degree of precursor functionalization. (60 and 90 mol% in the case of DATT-sOEG 10 kDa), as well as the concentration of the biocatalyst mTyr. The

gelation time of DAT(T)-sOEG hydrogels could be significantly reduced from 2.5 h to 5 min by using different enzyme concentrations. While for DAT-sOEG the gelation time decreased with increasing  $M_n$  or substrate amount in solution, no hydrogels could be formed by mTyr catalysis by DATT-sOEG 5 kDa. The enzymatic reaction kinetics followed the sequence free DAT > DAT-IOEG > DAT-sOEG, as determined by UV-Vis spectroscopy. NMR spectroscopic detection of non-oxidized aromatic DAT and DATT end groups in swollen hydrogels confirmed that no quantitative conversion of the substrate took place, which however was not necessary for hydrogel formation. Kinetic and steric phenomena as well as competitive physical interactions could also explain the relatively low gel contents (up to 80%), as well as the hydrogel mechanics, which were controllable to a small extent (elastic moduli 1-2 kPa). However, swelling studies showed a systematic change in the hydrogel properties (swelling between 1200 and 650 vol%), whereby higher mTyr concentrations reduced the swelling of DAT-sOEG hydrogels. In addition, diffusion studies with FITC-dextran with systematically varied molecular weights allowed proved a systematic change of mesh sizes (9-11 nm) of the hydrogels, which could be estimated by a scaling model. In an application example for the release of heparin as a therapeutic macromolecule with hydrogels from DAT-sOEG 10 kDa, it was finally clarified that the network properties enabled both quantitative release and control of the release kinetics. Therefore, the hydrogels investigated herein have potential to be applied as matrices for controlled drug release.



## 9.2 Zusammenfassung

---

Enzym-katalysierte Umsetzungen sind ein möglicher alternativer Ansatz zur Erzeugung von Hydrogelen für biomedizinische Anwendungen, wobei die Spezifität von enzymatischen Reaktionen sowie die Vernetzung in milden und zytokompatiblen Bedingungen als besonders vorteilhaft bewertet werden. In dieser Doktorarbeit sollte ein grundlegendes Verständnis für die Prinzipien der enzymatisch induzierten Netzwerksynthese etabliert werden, wobei Tyrosinase (mTyr) als physiologisch relevantes Enzym ausgewählt wurde. Die Arbeit wurde ausgehend von der Hypothese entwickelt, dass DAT(T) ein geeignetes alternatives Substrat für Tyr ist und als funktionelle Gruppe von hydrophilen Telechelen die Erzeugung von Hydrogelen mit systematisch kontrollierbaren Eigenschaften ermöglicht. Im ersten Teil der Arbeit sollte die Eignung von frei gelöstem DAT(T) als Substrat für mTyr erprobt und verschiedene (Model-)Präkursor aus DAT(T)-funktionalisiertem Oligoethylenglycol synthetisiert werden. Im zweiten Schritt sollten mechanistische Aspekte der Tyrosinase katalysierten Vernetzung von linearen, monofunktionalisierten Modellpräkursoren studiert werden um die Reaktionswege und Art der gebildeten Netzpunkte sowie beteiligten chemischen Spezies zu entschlüsseln. Im dritten Schritt sollte das Anwendungspotential der Vernetzungsreaktionen für die Synthese von Hydrogelen aus sternförmigen Telechele aufgezeigt werden, wobei ein umfangreiches Verständnis des komplexen Systems durch eine systematische Analyse von physikochemischen Eigenschaften, Netzwerkstrukturen und der diffusionskontrollierten Freisetzung von bioaktiven Makromolekülen erzielt werden sollte.

Die ausgewählten Substrate DAT und DATT zeigten eine dreifach (DAT) bzw. neunfach (DATT) höhere mTyr Aktivität verglichen mit dem natürlichen phenolischen Substrat *L*-Tyrosin in kinetischen Untersuchungen, was die Eignung der Substrate für die hier geplanten Untersuchungen bestätigte. Um den Reaktionsmechanismus, der aus einer enzymkatalysierten Umsetzung von DAT(T) zu reaktiven Spezies mit nachgeschalteter spontaner Vernetzung besteht, anhand von löslichen Reaktionsprodukten detaillierter zu verstehen, wurden im Folgenden DAT monofunktionalisierte Oligomere (DAT-IOEG<sub>OMe</sub> 10 kDa bzw. 2kDa) erzeugt und in Modellreaktionen eingesetzt. So konnten *o*-Diphenol

und *o*-Chinon Gruppen als enzymatisch produzierten Reaktionsintermediate der Umsetzung von freiem und oligomergebundenen DAT gleichermaßen durch UV-Vis- und NMR-Spektroskopie identifiziert werden. Ein Anstieg von Signalen, die für *o*-chinonoiden Strukturen charakteristisch sind, unter Abnahme des aromatischen Charakters von DAT Endgruppen, wurde auch durch FT-IR spektroskopische Untersuchung von DAT-IOEG<sub>OMe</sub> 2 kDa nachgewiesen. Durch genaue Zuordnung der durch MALDI-ToF detektierten *m/z* wurden Catechole, *o*-Chinone, sowie erstmalig auch Monophenole als Bausteine der Oligomere identifiziert, die aus DAT und DAT Methylester als Resultat der mTyr Katalyse entstanden sind. Darüber hinaus konnten bei Umsetzung von DAT Ester Oligomere mit bis zu 11 Wiederholungseinheiten durch MALDI-ToF nachgewiesen werden konnten, was einen Hinweis auf theoretisch mögliche hohe Netzpunktfunktionalitäten durch Enzymkatalyse darstellt. Hingegen waren bei der mTyr katalysierte Umsetzung von DAT-IOEG<sub>OMe</sub> 10 kDa Dimere und wenige Trimere nachweisbar, was auf eine sterische Hinderung durch die sperrigen stark hydratisierten OEG Ketten hindeutet, oder auf mangelnde Produktionisierung zurückgeführt werden kann. MALDI-ToF- und entwickelte HPLC-ESI-MS Methoden zeigten, dass eng verteiltes DAT-ImOEG<sub>OMe</sub> 2 kDa alleine sowie in Mischungen mit NH<sub>2</sub>-ImOEG<sub>OMe</sub> quantitativ innerhalb < 24 h reagiert, wobei Hinweise auf eine mögliche Beteiligung von primären Aminen an der nichtenzymatischen Polymerisierung der reaktiven Intermediate bestehen.

Ferner wurden Hydrogele aus 4-Arm sOEG Präkursor unter Variation der Endgruppe (DAT oder DATT), des Molekulargewichts,  $M_n$  (5, 10 oder 20 kDa) und der Substratmenge, repräsentiert durch den Fuktionalisierungsgrad *d.f.* (60 und 90 mol% im Falle von DATT-sOEG 10 kDa) der Präkursors, sowie der Konzentration des Biokatalysators mTyr hergestellt. Die Gelierzeit von DAT(T)-sOEG Hydrogelen konnte durch die Verwendung von verschiedenen Enzymkonzentrationen erheblich von 2,5 h auf 5 min herabgesetzt werden. Während bei DAT-sOEG die Gelierzeit mit steigendem  $M_n$  beziehungsweise Substratmenge in der Lösung sank, konnten von DATT-sOEG 5 kDa keine Hydrogele durch mTyr Katalyse geformt werden. Die enzymatische Umsetzungskinetik folgte der Reihung freies DAT > DAT-IOEG > DAT-sOEG, wie durch UV-Vis spektroskopische festgestellt wurde. NMR spektroskopische Detektion von nicht oxidierten aromatischen DAT und DATT Endgruppen in gequollenen Hydrogelen bestätigten dass keine quantitative Umsetzung der Substrate erfolgt und zur Ausbildung von Hydrogelen

erforderlich ist. Kinetische und sterische Phänomene, sowie kompetitive physikalische Wechselwirkungen könnten auch die relativ geringen Gelgehalte (bis zu 80%) sowie die in einem geringen Umfang steuerbare Mechanik der Hydrogele (Elastizitätsmodule 1-2 kPa) erklären. Gleichwohl zeigten Quellungsuntersuchungen eine systematische Veränderung der Hydrogel-Eigenschaften (Quellung zwischen 1200 und 650 vol%), wobei u.a. höheren mTyr Konzentrationen die Quellung von DAT-sOEG Hydrogelen reduzierten. Diffusionsstudien mit FITC-Dextran mit systematisch variiertem Molekulargewicht erlaubten darüber hinaus, unter Anwendung eines Skalierungsmodells die anvisierte Veränderung von Maschenweiten (9-11 nm) der Hydrogele nachzuweisen. In einem Anwendungsbeispiel zur Freisetzung von Heparin als therapeutisches Makromolekül mit Hydrogelen aus DAT-sOEG 10 kDa wurde abschließend verdeutlicht, dass sowohl eine quantitative Freisetzung als auch eine Steuerung der Freisetzungskinetik anhand Netzwerkeigenschaften erzielt werden kann. Daher haben die hier untersuchten Hydrogele ein Potential zur Anwendung als Matrices für die kontrollierte Wirkstofffreisetzung.



# Appendices

## I. Peer reviewed publications

---

1. Racheva, M., Julich-Gruner, K., Nöchel, U., Neffe, A., Wischke, C., & Lendlein, A. (2013) *Influence of Drying Procedures on Network Formation and Properties of Hydrogels from Functionalized Gelatin* Macromol Symp. **334** (1)2013, 24–32.
2. Racheva, M., Romero, O., Julich-Gruner, K., Ulrich, A., Wischke, C., & Lendlein, A. (2015). *Purity of mushroom tyrosinase as a biocatalyst for biomaterial synthesis affects the stability of therapeutic peptides*. MRS Proc., **1718**, 85-90.
3. Racheva, Bähr, Wischke et al. *Surface immobilization strategies for tyrosinase as biocatalyst applicable to polymer network synthesis* (working title) (MRS Adv, submission planned May 2017).
4. Neffe, A., Wischke, C., Racheva, M. (2013) *Progress in biopolymer-based biomaterials and their application in controlled drug delivery* Exp Rev Med Dev. **10**,(6) 813-833.

## II. References

---

1. Brannon-Peppas, L., *Preparation and Characterization of Crosslinked Hydrophilic Networks*. Studies in Polymer Science, 1990. **8**: p. 45-66.
2. Flory, P.J., *Statistical Mechanics of Swelling of Network Structures*. The Journal of Chemical Physics, 1950. **18**(1): p. 108-111.
3. Hoffman, A.S., *Hydrogels for biomedical applications*. Advanced Drug Delivery Reviews, 2002. **54**(1): p. 3-12.
4. Sun, T.L., et al., *Physical hydrogels composed of polyampholytes demonstrate high toughness and viscoelasticity*. Nat Mater, 2013. **12**(10): p. 932-937.
5. Gombotz, W.R. and S.F. Wee, *Protein release from alginate matrices*. Advanced Drug Delivery Reviews, 2012. **64**, **Supplement**: p. 194-205.
6. Kuo, C.K. and P.X. Ma, *Ionically crosslinked alginate hydrogels as scaffolds for tissue engineering: Part 1. Structure, gelation rate and mechanical properties*. Biomaterials, 2001. **22**(6): p. 511-521.
7. Appel, E.A., et al., *Ultrahigh-Water-Content Supramolecular Hydrogels Exhibiting Multistimuli Responsiveness*. Journal of the American Chemical Society, 2012. **134**(28): p. 11767-11773.
8. Li, J., et al., *Self-assembled supramolecular hydrogels formed by biodegradable PEO–PHB–PEO triblock copolymers and  $\alpha$ -cyclodextrin for controlled drug delivery*. Biomaterials, 2006. **27**(22): p. 4132-4140.

9. Berg Jeremy M , T., John L and Stryer Lubert *Biochemistry*. 5 ed. 2002, New York: W H Freeman.
10. Holloway, J.L., A.M. Lowman, and G.R. Palmese, *The role of crystallization and phase separation in the formation of physically cross-linked PVA hydrogels*. *Soft Matter*, 2013. **9**(3): p. 826-833.
11. Stauffer, S.R. and N.A. Peppast, *Poly(vinyl alcohol) hydrogels prepared by freezing-thawing cyclic processing*. *Polymer*, 1992. **33**(18): p. 3932-3936.
12. Zhang, X.-Z., D.-Q. Wu, and C.-C. Chu, *Synthesis, characterization and controlled drug release of thermosensitive IPN–PNIPAAm hydrogels*. *Biomaterials*, 2004. **25**(17): p. 3793-3805.
13. Liu, R., M. Fraylich, and B.R. Saunders, *Thermoresponsive copolymers: from fundamental studies to applications*. *Colloid and Polymer Science*, 2009. **287**(6): p. 627-643.
14. Djabourov, M., J. Leblond, and P. Papon, *Gelation of aqueous gelatin solutions. I. Structural investigation*. *J. Phys. France*, 1988. **49**(2): p. 319-332.
15. GC, N., B. LJ, and C. RJ., *Mechanism of in vitro collagen fibril assembly. Kinetic and morphological studies*. *The Journal of Biological Chemistry*, 1986. **261**: p. 12290 - 12299.
16. Birk, D.E., *Type V collagen: heterotypic type I/IV collagen interactions in the regulation of fibril assembly*. *Micron*, 2001. **32**(3): p. 223-237.
17. Xiang, Y. and D. Chen, *Preparation of a novel pH-responsive silver nanoparticle/poly(HEMA–PEGMA–MAA) composite hydrogel*. *European Polymer Journal*, 2007. **43**(10): p. 4178-4187.
18. Balk, M., et al., *Architected Shape-Memory Hydrogels with Switching Segments Based on Oligo( $\epsilon$ -caprolactone)*. *MRS Advances*, 2016. **1**(27): p. 2011-2017.
19. Drumheller, P.D. and J.A. Hubbell, *Densely crosslinked polymer networks of poly(ethylene glycol) in trimethylolpropane triacrylate for cell-adhesion-resistant surfaces*. *Journal of Biomedical Materials Research*, 1995. **29**(2): p. 207-215.
20. Hild, G., *Model networks based on 'endlinking' processes: synthesis, structure and properties*. *Progress in Polymer Science*, 1998. **23**(6): p. 1019-1149.
21. Elliott, J.E., J.W. Anseth, and C.N. Bowman, *Kinetic modeling of the effect of solvent concentration on primary cyclization during polymerization of multifunctional monomers*. *Chemical Engineering Science*, 2001. **56**(10): p. 3173-3184.
22. Hild, G., *Interpretation of equilibrium swelling data on model networks using affine and 'phantom' network models*. *Polymer*, 1997. **38**(13): p. 3279-3293.
23. Peppas, N.A. and S.R. Lustig, *The Role of Cross-links, Entanglements, and Relaxations of the Macromolecular Carrier in the Diffusional Release of Biologically Active Materials*. *Annals of the New York Academy of Sciences*, 1985. **446**(1): p. 26-40.
24. Lin, C.C. and K.S. Anseth, *PEG hydrogels for the controlled release of biomolecules in regenerative medicine*. *Pharm Res*, 2009. **26**(3): p. 631-43.
25. Flory, P.J., *Phase Equilibria in Solutions of Rod-Like Particles*. *Proceedings of the Royal Society of London. Series A. Mathematical and Physical Sciences*, 1956. **234**(1196): p. 73-89.
26. Peppas, N.A., et al., *Hydrogels in pharmaceutical formulations*. *European Journal of Pharmaceutics and Biopharmaceutics*, 2000. **50**(1): p. 27-46.

27. Hakala, R.A., et al., *Photo-Cross-Linked Biodegradable Poly(Ester Anhydride) Networks Prepared from Alkenylsuccinic Anhydride Functionalized Poly( $\epsilon$ -caprolactone) Precursors*. *Biomacromolecules*, 2011. **12**(7): p. 2806-2814.
28. Yan, C. and D.J. Pochan, *Rheological properties of peptide-based hydrogels for biomedical and other applications*. *Chemical Society Reviews*, 2010. **39**(9): p. 3528-3540.
29. Stokes, J.R. and W.J. Frith, *Rheology of gelling and yielding soft matter systems*. *Soft Matter*, 2008. **4**(6): p. 1133-1140.
30. Flory, P.J., *Molecular Theory of Rubber Elasticity*. *Polym J*, 1985. **17**(1): p. 1-12.
31. Flory, P.J. and J.R. Jr., *Statistical Mechanics of Cross-Linked Polymer Networks I. Rubberlike Elasticity*. *The Journal of Chemical Physics*, 1943. **11**(11): p. 512-520.
32. Welzel, P.B., et al., *Modulating Biofunctional starPEG Heparin Hydrogels by Varying Size and Ratio of the Constituents*. *Polymers*, 2011. **3**(1): p. 602.
33. Rubinstein, M., *Polymer physics—The ugly duckling story: Will polymer physics ever become a part of "proper" physics?* *Journal of Polymer Science Part B: Polymer Physics*, 2010. **48**(24): p. 2548-2551.
34. Peppas, N.A., et al., *Hydrogels in Biology and Medicine: From Molecular Principles to Bionanotechnology*. *Advanced Materials*, 2006. **18**(11): p. 1345-1360.
35. Zohuriaan-Mehr, M.J., et al., *Advances in non-hygienic applications of superabsorbent hydrogel materials*. *Journal of Materials Science*, 2010. **45**(21): p. 5711-5735.
36. Kabiri, K., et al., *Superabsorbent hydrogel composites and nanocomposites: A review*. *Polymer Composites*, 2011. **32**(2): p. 277-289.
37. Boateng, J.S., et al., *Wound healing dressings and drug delivery systems: A review*. *Journal of Pharmaceutical Sciences*, 2008. **97**(8): p. 2892-2923.
38. Censi, R., et al., *Hydrogels for protein delivery in tissue engineering*. *Journal of Controlled Release*, 2012. **161**(2): p. 680-692.
39. Thiele, J., et al., *25th Anniversary Article: Designer Hydrogels for Cell Cultures: A Materials Selection Guide*. *Advanced Materials*, 2014. **26**(1): p. 125-148.
40. Marklein, R.A. and J.A. Burdick, *Controlling Stem Cell Fate with Material Design*. *Advanced Materials*, 2010. **22**(2): p. 175-189.
41. Hoare, T.R. and D.S. Kohane, *Hydrogels in drug delivery: Progress and challenges*. *Polymer*, 2008. **49**(8): p. 1993-2007.
42. McKenzie, M., et al., *Hydrogel-Based Drug Delivery Systems for Poorly Water-Soluble Drugs*. *Molecules*, 2015. **20**(11): p. 19705.
43. Vashist, A., et al., *Recent advances in hydrogel based drug delivery systems for the human body*. *Journal of Materials Chemistry B*, 2014. **2**(2): p. 147-166.
44. Buwalda, S.J., T. Vermonden, and W.E. Hennink, *Hydrogels for Therapeutic Delivery: Current Developments and Future Directions*. *Biomacromolecules*, 2017. **18**(2): p. 316-330.
45. Vermonden, T., R. Censi, and W.E. Hennink, *Hydrogels for Protein Delivery*. *Chemical Reviews*, 2012. **112**(5): p. 2853-2888.
46. Neffe, A.T., et al., *Progress in biopolymer-based biomaterials and their application in controlled drug delivery*. *Expert Review of Medical Devices*, 2013. **10**(6): p. 813-833.
47. Moreira Teixeira, L.S., et al., *Enzyme-catalyzed crosslinkable hydrogels: Emerging strategies for tissue engineering*. *Biomaterials*, 2012. **33**(5): p. 1281-1290.
48. Benkovic, S.J. and S. Hammes-Schiffer, *A Perspective on Enzyme Catalysis*. *Science*, 2003. **301**(5637): p. 1196-1202.

49. Albertsson, A.-C. and R.K. Srivastava, *Recent developments in enzyme-catalyzed ring-opening polymerization*. *Advanced Drug Delivery Reviews*, 2008. **60**(9): p. 1077-1093.
50. Veisi, H., et al., *Chemoselective hydration of nitriles to amides using hydrated ionic liquid (IL) tetrabutylammonium hydroxide (TBAH) as a green catalyst*. *RSC Advances*, 2015. **5**(9): p. 6365-6371.
51. Michrowska, A., et al., *A green catalyst for green chemistry: Synthesis and application of an olefin metathesis catalyst bearing a quaternary ammonium group*. *Green Chemistry*, 2006. **8**(8): p. 685-688.
52. Thomas, S.M., R. DiCosimo, and V. Nagarajan, *Biocatalysis: applications and potentials for the chemical industry*. *Trends in Biotechnology*, 2002. **20**(6): p. 238-242.
53. Schmid, A., et al., *Industrial biocatalysis today and tomorrow*. *Nature*, 2001. **409**(6817): p. 258-268.
54. Bornscheuer, U.T., *Biocatalysis: Successfully Crossing Boundaries*. *Angewandte Chemie International Edition*, 2016. **55**(14): p. 4372-4373.
55. Drepper, T., et al., *Novel biocatalysts for white biotechnology*. *Biotechnology Journal*, 2006. **1**(7-8): p. 777-786.
56. Kumar, A. and S. Singh, *Directed evolution: tailoring biocatalysts for industrial applications*. *Critical Reviews in Biotechnology*, 2013. **33**(4): p. 365-378.
57. Wells, A. and H.-P. Meyer, *Biocatalysis as a Strategic Green Technology for the Chemical Industry*. *ChemCatChem*, 2014. **6**(4): p. 918-920.
58. Choi, J.-M., S.-S. Han, and H.-S. Kim, *Industrial applications of enzyme biocatalysis: Current status and future aspects*. *Biotechnology Advances*, 2015. **33**(7): p. 1443-1454.
59. Rasor, J.P. and E. Voss, *Enzyme-catalyzed processes in pharmaceutical industry*. *Applied Catalysis A: General*, 2001. **221**(1-2): p. 145-158.
60. Uyama, H. and S. Kobayashi, *Enzyme-catalyzed polymerization to functional polymers*. *Journal of Molecular Catalysis B: Enzymatic*, 2002. **19-20**: p. 117-127.
61. Zavada, S., T. Battsengel, and T. Scott, *Radical-Mediated Enzymatic Polymerizations*. *International Journal of Molecular Sciences*, 2016. **17**(2): p. 195.
62. Yang, Y., et al., *Chemoenzymatic synthesis of polymeric materials using lipases as catalysts: A review*. *Biotechnology Advances*, 2014. **32**(3): p. 642-651.
63. Matsumoto, K.i. and S. Taguchi, *Enzyme and metabolic engineering for the production of novel biopolymers: crossover of biological and chemical processes*. *Current Opinion in Biotechnology*, 2013. **24**(6): p. 1054-1060.
64. Sen, S. and J. Puskas, *Green Polymer Chemistry: Enzyme Catalysis for Polymer Functionalization*. *Molecules*, 2015. **20**(5): p. 9358.
65. Gübitz, G.M. and A.C. Paulo, *New substrates for reliable enzymes: enzymatic modification of polymers*. *Current Opinion in Biotechnology*, 2003. **14**(6): p. 577-582.
66. Bode, F., et al., *Enzymatically Cross-Linked Tilapia Gelatin Hydrogels: Physical, Chemical, and Hybrid Networks*. *Biomacromolecules*, 2011. **12**(10): p. 3741-3752.
67. Mariniello, L., et al., *Transglutaminase-mediated macromolecular assembly: production of conjugates for food and pharmaceutical applications*. *Amino Acids*, 2014. **46**(3): p. 767-776.

68. Yung, C.W., et al., *Transglutaminase crosslinked gelatin as a tissue engineering scaffold*. Journal of Biomedical Materials Research Part A, 2007. **83A**(4): p. 1039-1046.
69. Sperinde, J.J. and L.G. Griffith, *Control and Prediction of Gelation Kinetics in Enzymatically Cross-Linked Poly(ethylene glycol) Hydrogels*. Macromolecules, 2000. **33**(15): p. 5476-5480.
70. Sperinde, J.J. and L.G. Griffith, *Synthesis and Characterization of Enzymatically-Cross-Linked Poly(ethylene glycol) Hydrogels*. Macromolecules, 1997. **30**(18): p. 5255-5264.
71. Davis, N.E., et al., *Modular enzymatically crosslinked protein polymer hydrogels for in situ gelation*. Biomaterials, 2010. **31**(28): p. 7288-7297.
72. Kurisawa, M., et al., *Injectable enzymatically crosslinked hydrogel system with independent tuning of mechanical strength and gelation rate for drug delivery and tissue engineering*. Journal of Materials Chemistry, 2010. **20**(26): p. 5371-5375.
73. Ren, C.D., et al., *Liposomal delivery of horseradish peroxidase for thermally triggered injectable hyaluronic acid-tyramine hydrogel scaffolds*. Journal of Materials Chemistry B, 2015. **3**(23): p. 4663-4670.
74. Lee, F., J.E. Chung, and M. Kurisawa, *An injectable hyaluronic acid-tyramine hydrogel system for protein delivery*. Journal of Controlled Release, 2009. **134**(3): p. 186-193.
75. Xu, K., et al., *Hyaluronidase-incorporated hyaluronic acid-tyramine hydrogels for the sustained release of trastuzumab*. Journal of Controlled Release, 2015. **216**: p. 47-55.
76. Jin, R., C. Lin, and A. Cao, *Enzyme-mediated fast injectable hydrogels based on chitosan-glycolic acid/tyrosine: preparation, characterization, and chondrocyte culture*. Polymer Chemistry, 2014. **5**(2): p. 391-398.
77. Loebel, C., et al., *Cross-Linking Chemistry of Tyramine-Modified Hyaluronan Hydrogels Alters Mesenchymal Stem Cell Early Attachment and Behavior*. Biomacromolecules, 2017. **18**(3): p. 855-864.
78. Wang, L.-S., et al., *Injectable biodegradable hydrogels with tunable mechanical properties for the stimulation of neurogenic differentiation of human mesenchymal stem cells in 3D culture*. Biomaterials, 2010. **31**(6): p. 1148-1157.
79. Yu, F., et al., *An injectable hyaluronic acid/PEG hydrogel for cartilage tissue engineering formed by integrating enzymatic crosslinking and Diels-Alder "click chemistry"*. Polymer Chemistry, 2014. **5**(3): p. 1082-1090.
80. Abu-Hakmeh, A., et al., *Sequential gelation of tyramine-substituted hyaluronic acid hydrogels enhances mechanical integrity and cell viability*. Medical & Biological Engineering & Computing, 2016. **54**(12): p. 1893-1902.
81. Wei, Q., et al., *Printable hybrid hydrogel by dual enzymatic polymerization with superactivity*. Chemical Science, 2016. **7**(4): p. 2748-2752.
82. Roberts, J.J., et al., *A comparative study of enzyme initiators for crosslinking phenol-functionalized hydrogels for cell encapsulation*. Biomaterials Research, 2016. **20**(1): p. 30.
83. Burzio, L.A. and J.H. Waite, *Reactivity of peptidyl-tyrosine to hydroxylation and cross-linking*. Protein Science, 2001. **10**(4): p. 735-740.
84. Selinheimo, E., et al., *Formation of Protein-Oligosaccharide Conjugates by Laccase and Tyrosinase*. Journal of Agricultural and Food Chemistry, 2008. **56**(9): p. 3118-3128.

85. Lee, S.H., et al., *Enzyme-mediated cross-linking of pluronic copolymer micelles for injectable and in situ forming hydrogels*. *Acta Biomater*, 2011. **7**.
86. Jin, R., B. Lou, and C. Lin, *Tyrosinase-mediated in situ forming hydrogels from biodegradable chondroitin sulfate–tyramine conjugates*. *Polymer International*, 2013. **62**(3): p. 353-361.
87. Fisher, O.Z., et al., *Melanin-like hydrogels derived from gallic macromers*. *Adv Mater*, 2012. **24**(22): p. 3032-6.
88. Das, S., et al., *Bioprintable, cell-laden silk fibroin–gelatin hydrogel supporting multilineage differentiation of stem cells for fabrication of three-dimensional tissue constructs*. *Acta Biomaterialia*, 2015. **11**: p. 233-246.
89. Taddei, P., et al., *Silk Fibroin/Gelatin Blend Films Crosslinked with Enzymes for Biomedical Applications*. *Macromolecular Bioscience*, 2013. **13**(11): p. 1492-1510.
90. Chen, T., et al., *Enzyme-catalyzed gel formation of gelatin and chitosan: potential for in situ applications*. *Biomaterials*, 2003. **24**(17): p. 2831-2841.
91. Wu, L.-Q., W.E. Bentley, and G.F. Payne, *Biofabrication with biopolymers and enzymes: Potential for constructing scaffolds from soft matter*. *Int J Artif Organs*, 2011. **34**(2): p. 215-224.
92. Gao, J., et al., *Dual enzymes regulate the molecular self-assembly of tetra-peptide derivatives*. *Soft Matter*, 2011. **7**(21): p. 10443-10448.
93. Waite, J.H., *Nature's underwater adhesive specialist*. *International Journal of Adhesion and Adhesives*, 1987. **7**(1): p. 9-14.
94. Lee, B.P., et al., *Mussel-Inspired Adhesives and Coatings*. *Annual Review of Materials Research*, 2011. **41**(1): p. 99-132.
95. Kim, B.J., et al., *Mussel-Mimetic Protein-Based Adhesive Hydrogel*. *Biomacromolecules*, 2014. **15**(5): p. 1579-1585.
96. Chan Choi, Y., et al., *Human gelatin tissue-adhesive hydrogels prepared by enzyme-mediated biosynthesis of DOPA and Fe<sup>3+</sup> ion crosslinking*. *Journal of Materials Chemistry B*, 2014. **2**(2): p. 201-209.
97. Liu, H.-Y., et al., *Enzyme-mediated stiffening hydrogels for probing activation of pancreatic stellate cells*. *Acta Biomaterialia*, 2017. **48**: p. 258-269.
98. Li, Y., et al., *An enzyme-assisted nanoparticle crosslinking approach to enhance the mechanical strength of peptide-based supramolecular hydrogels*. *Chemical Communications*, 2013. **49**(77): p. 8653-8655.
99. Borrmann, A., et al., *Strain-Promoted Oxidation-Controlled Cyclooctyne–1,2-Quinone Cycloaddition (SPOCQ) for Fast and Activatable Protein Conjugation*. *Bioconjugate Chemistry*, 2015. **26**(2): p. 257-261.
100. Jonker, A.M., et al., *A Fast and Activatable Cross-Linking Strategy for Hydrogel Formation*. *Advanced Materials*, 2015. **27**(7): p. 1235-1240.
101. Le Thi, P., et al., *In situ forming gelatin hydrogels by dual-enzymatic cross-linking for enhanced tissue adhesiveness*. *Journal of Materials Chemistry B*, 2017. **5**(4): p. 757-764.
102. Wang, Y., et al., *Microbial Transglutaminase and Tyrosinase Modified Gelatin-Chitosan Material*. *Soft Materials*, 2015. **13**(1): p. 32-38.
103. da Silva, M.A., et al., *Enzymatically Cross-Linked Gelatin/Chitosan Hydrogels: Tuning Gel Properties and Cellular Response*. *Macromolecular Bioscience*, 2014. **14**(6): p. 817-830.
104. Mayer, A.M., *Polyphenol oxidases in plants and fungi: Going places? A review*. *Phytochemistry*, 2006. **67**(21): p. 2318-2331.

105. Gorman, M.J. and Y. Arakane, *Tyrosine hydroxylase is required for cuticle sclerotization and pigmentation in Tribolium castaneum*. *Insect biochemistry and molecular biology*, 2010. **40**(3): p. 267-273.
106. Andersen, S.O., *Insect cuticular sclerotization: A review*. *Insect Biochemistry and Molecular Biology*, 2010. **40**(3): p. 166-178.
107. Galko, M.J. and M.A. Krasnow, *Cellular and Genetic Analysis of Wound Healing in Drosophila Larvae*. *PLOS Biology*, 2004. **2**(8): p. e239.
108. Dadachova, E. and A. Casadevall, *Ionizing radiation: how fungi cope, adapt, and exploit with the help of melanin*. *Current Opinion in Microbiology*, 2008. **11**(6): p. 525-531.
109. Ju, K.-Y., et al., *Bioinspired Polymerization of Dopamine to Generate Melanin-Like Nanoparticles Having an Excellent Free-Radical-Scavenging Property*. *Biomacromolecules*, 2011. **12**(3): p. 625-632.
110. van Gelder, C.W.G., W.H. Flurkey, and H.J. Wichers, *Sequence and structural features of plant and fungal tyrosinases*. *Phytochemistry*, 1997. **45**(7): p. 1309-1323.
111. Mauracher, S.G., et al., *Latent and active abPPO<sub>4</sub> mushroom tyrosinase cocrystallized with hexatungstotellurate(VI) in a single crystal*. *Acta Crystallogr D Biol Crystallogr*, 2014. **70**(Pt 9): p. 2301-15.
112. Mauracher, S.G., et al., *High level protein-purification allows the unambiguous polypeptide determination of latent isoform PPO<sub>4</sub> of mushroom tyrosinase*. *Phytochemistry*, 2014. **2014 v.99**: p. pp. 14-25.
113. Ismaya, W.T., et al., *Crystallization and preliminary X-ray crystallographic analysis of tyrosinase from the mushroom Agaricus bisporus*. *Acta Crystallographica Section F*, 2011. **67**(5): p. 575-578.
114. Weijn, A., et al., *Melanin biosynthesis pathway in Agaricus bisporus mushrooms*. *Fungal Genetics and Biology*, 2013. **55**: p. 42-53.
115. Ismaya, W.T., et al., *Crystal Structure of Agaricus bisporus Mushroom Tyrosinase: Identity of the Tetramer Subunits and Interaction with Tropolone*. *Biochemistry*, 2011. **50**(24): p. 5477-5486.
116. Ismaya, W.T., et al., *The light subunit of mushroom Agaricus bisporus tyrosinase: Its biological characteristics and implications*. *International Journal of Biological Macromolecules*, 2017. **102**: p. 308-314.
117. ISMAYA, W., et al., *In Silico Study to Develop a Lectin-Like Protein from Mushroom Agaricus bisporus for Pharmaceutical Application*. *Scientia Pharmaceutica*, 2016. **84**(1): p. 203.
118. Ramsden, C.A. and P.A. Riley, *Tyrosinase: The four oxidation states of the active site and their relevance to enzymatic activation, oxidation and inactivation*. *Bioorganic & Medicinal Chemistry*, 2014. **22**(8): p. 2388-2395.
119. Fenoll, L.G., et al., *Unification for the Expression of the Monophenolase and Diphenolase Activities of Tyrosinase*. *IUBMB Life*, 2002. **54**(3): p. 137-141.
120. Decker, H., T. Schweikardt, and F. Tuczec, *The First Crystal Structure of Tyrosinase: All Questions Answered?* *Angewandte Chemie International Edition*, 2006. **45**(28): p. 4546-4550.
121. Chang, T.-S., *An Updated Review of Tyrosinase Inhibitors*. *International Journal of Molecular Sciences*, 2009. **10**(6): p. 2440.
122. Naish-Byfield, S. and P.A. Riley, *Oxidation of monohydric phenol substrates by tyrosinase. An oximetric study*. *Biochem J*, 1992. **288 ( Pt 1)**: p. 63-7.

123. Naish-Byfield, S. and P.A. Riley, *Tyrosinase Autoactivation and the Problem of the Lag Period*. Pigment Cell Research, 1998. **11**(3): p. 127-133.
124. Land, E.J., C.A. Ramsden, and P.A. Riley, *Tyrosinase Autoactivation and the Chemistry of ortho-Quinone Amines*. Accounts of Chemical Research, 2003. **36**(5): p. 300-308.
125. Riley, P.A., *The great DOPA mystery: the source and significance of DOPA in phase I melanogenesis*. Cell Mol Biol (Noisy-le-grand), 1999. **45**(7): p. 951-60.
126. Julich-Gruner, K.K., A.T. Neffe, and A. Lendlein, *Synthesis and characterization of oligo(ethylene glycol)s functionalized with desaminotyrosine or desaminotyrosyltyrosine*. J Appl Biomater Funct Mater, 2013. **10**(3): p. 170-176.
127. Julich-Gruner, K.K., et al., *Synthesis and characterization of star-shaped oligo(ethylene glycol) with tyrosine derived moieties under variation of their molecular weight*. Clin Hemorheol Microcirc, 2015. **60**(1): p. 13-23.
128. Brunacci, N., et al., *Influence of surfactants on depsipeptide submicron particle formation*. European journal of pharmaceutics and biopharmaceutics : official journal of Arbeitsgemeinschaft fur Pharmazeutische Verfahrenstechnik e.V, 2016.
129. Romero-Vargas Castrillón, S., et al., *Amine enrichment and poly(ethylene glycol) (PEG) surface modification of thin-film composite forward osmosis membranes for organic fouling control*. Journal of Membrane Science, 2014. **450**: p. 331-339.
130. *SDBS National Institute of Adv Industr Sci and Techn (AIST), Japan*. <http://sdfs.db.aist.go.jp>.
131. M., H., et al., *Spektroskopische Methoden in der organischen Chemie*. 8 edition ed. 2011: Thieme.
132. H., M., *The chemistry of melanin III. Mechanism of the oxidation of dihydroxyphenylalanine by tyrosinase*. The Journal of Biological Chemistry, 1948. **172** p. 83-99.
133. Ikehata, K. and J.A. Nicell, *Characterization of tyrosinase for the treatment of aqueous phenols*. Bioresource Technology, 2000. **74**(3): p. 191-199.
134. Duarte, L.T., et al. *Production and characterization of tyrosinase activity in Pycnoporus sanguineus CCT-4518 Crude extract*. in *Brazilian journal of microbiology*. 2012.
135. Paranjpe, P.S., M.S. Karve, and S.B. Padhye, *Characterization of tyrosinase and accompanying laccase from Amorphophallus campanulatus*. Indian Journal of Biochemistry and Biophysics (IJBB), 2003. **40**.
136. Makino, N. and H.S. Mason, *Reactivity of Oxytyrosinase toward Substrates*. The Journal of Biological Chemistry, 1973. **248**: p. 5731-5735.
137. Ros, J., J. Rodríguez-López, and F. García-Cánovas, *Tyrosinase: kinetic analysis of the transient phase and the steady state*. Biochimica et Biophysica Acta (BBA) - Protein Structure and Molecular Enzymology, 1994. **1204**(1): p. 33-42.
138. Rodriguezlopez, J.N., J. Escribano, and F. Garcia-canovas, *A Continuous Spectrophotometric Method for the Determination of Monophenolase Activity of Tyrosinase Using 3-Methyl-2-benzothiazolinone Hydrazone*. Analytical Biochemistry, 1994. **216**(1): p. 205-212.
139. Winder, A.J. and H. Harris, *New assays for the tyrosine hydroxylase and dopa oxidase activities of tyrosinase*. European Journal of Biochemistry, 1991. **198**(2): p. 317-326.
140. L., M. and M.M. L., *Die Kinetik der Invertinwirkung*. 1913.
141. Johnson, K.A. and R.S. Goody, *The Original Michaelis Constant: Translation of the 1913 Michaelis–Menten Paper*. Biochemistry, 2011. **50**(39): p. 8264-8269.

142. Lockridge, O. and B.N. La Du, *Comparison of atypical and usual human serum cholinesterase. Purification, number of active sites, substrate affinity, and turnover number*. Journal of Biological Chemistry, 1978. **253**(2): p. 361-366.
143. Espín, J.C., et al., *Kinetic characterization of the substrate specificity and mechanism of mushroom tyrosinase*. European Journal of Biochemistry, 2000. **267**(5): p. 1270-1279.
144. King, P.W., *Solubility of Oxygen in Water*. Colby College, Department of Chemistry, Maine, USA: <http://www.colby.edu/chemistry/CH331/O2%20Solubility.html>.
145. Yang, J., M.A. Cohen Stuart, and M. Kamperman, *Jack of all trades: versatile catechol crosslinking mechanisms*. Chemical Society Reviews, 2014. **43**(24): p. 8271-8298.
146. Haemers, S., G.J.M. Koper, and G. Frens, *Effect of Oxidation Rate on Cross-Linking of Mussel Adhesive Proteins*. Biomacromolecules, 2003. **4**(3): p. 632-640.
147. Waite, J.H. and A.C. Rice-Ficht, *Presclerotized eggshell protein from the liver fluke Fasciola hepatica*. Biochemistry, 1987. **26**(24): p. 7819-7825.
148. Miserez, A., D. Rubin, and J.H. Waite, *Cross-linking Chemistry of Squid Beak*. Journal of Biological Chemistry, 2010. **285**(49): p. 38115-38124.
149. Kramer, K.J., et al., *Oxidative conjugation of catechols with proteins in insect skeletal systems*. Tetrahedron, 2001. **57**(2): p. 385-392.
150. Rzepecki, L.M. and J.H. Waite, *A chromogenic assay for catecholoxidases based on the addition of l-proline to quinones*. Analytical Biochemistry, 1989. **179**(2): p. 375-381.
151. Sugumaran, M. and J.L. Bolton, *Laccase—and Not Tyrosinase—Is the Enzyme Responsible for Quinone Methide Production from 2,6-Dimethoxy-4-allyl Phenol*. Archives of Biochemistry and Biophysics, 1998. **353**(2): p. 207-212.
152. Rzepecki, L.M., T. Nagafuchi, and J.H. Waite,  *$\alpha,\beta$ -Dehydro-3,4-dihydroxyphenylalanine derivatives: Potential sclerotization intermediates in natural composite materials*. Archives of Biochemistry and Biophysics, 1991. **285**(1): p. 17-26.
153. Abebe, A., et al., *Reexamination of the mechanisms of oxidative transformation of the insect cuticular sclerotizing precursor, 1,2-dehydro-N-acetyldopamine*. Insect Biochemistry and Molecular Biology, 2010. **40**(9): p. 650-659.
154. Rzepecki, L.M. and J.H. Waite,  *$\alpha,\beta$ -Dehydro-3,4-dihydroxyphenylalanine derivatives: Rate and mechanism of formation*. Archives of Biochemistry and Biophysics, 1991. **285**(1): p. 27-36.
155. Lee, B.P., J.L. Dalsin, and P.B. Messersmith, *Synthesis and Gelation of DOPA-Modified Poly(ethylene glycol) Hydrogels*. Biomacromolecules, 2002. **3**(5): p. 1038-1047.
156. Sugumaran, M., *Unified Mechanism for Sclerotization of Insect Cuticle*. Advances in Insect Physiology, 1998. **27**: p. 229-334.
157. Albarran, G., et al., *Absorption Spectrum, Mass Spectrometric Properties, and Electronic Structure of 1,2-Benzoquinone*. The Journal of Physical Chemistry A, 2010. **114**(28): p. 7470-7478.
158. Waite, J.H., *Calculating extinction coefficients for enzymatically produced o-quinones*. Analytical Biochemistry, 1976. **75**(1): p. 211-218.
159. Andersen, S.O., et al., *Phenoloxidase catalyzed coupling of catechols. Identification of novel coupling products*. Biochimica et Biophysica Acta (BBA) - Protein Structure and Molecular Enzymology, 1992. **1118**(2): p. 134-138.

160. Wang, S.X., et al., *A crosslinked cofactor in lysyl oxidase: redox function for amino acid side chains*. *Science*, 1996. **273**(5278): p. 1078-84.
161. Bladon, P., *Spectroscopic identification of organic compounds*, by R. M. Silverstein and G. C. Bassler. *John Wiley and Sons Inc, New York and Chichester, Sussex*. 2nd Edition 1967. 256 pp. + x. £5.3.0d \$10.95, students edition £3.0.0. *Organic Magnetic Resonance*, 1969. **1**(3): p. 277-277.
162. Hollenstein, R. and W. Von Philipsborn, *<sup>13</sup>C- and <sup>1</sup>H-NMR. Spectra of ortho-benzoquinones. On the assignment problem in <sup>13</sup>C spectra*. *Helvetica Chimica Acta*, 1973. **56**(1): p. 320-322.
163. Yu, M., J. Hwang, and T.J. Deming, *Role of l-3,4-Dihydroxyphenylalanine in Mussel Adhesive Proteins*. *Journal of the American Chemical Society*, 1999. **121**(24): p. 5825-5826.
164. FENOLL, L.G., et al., *Deuterium isotope effect on the oxidation of monophenols and o-diphenols by tyrosinase*. *Biochemical Journal*, 2004. **380**(3): p. 643-650.
165. Prota, G., *Melanins and Melanogenesis*. Academic Press. 1992 San Diego: Elsevier
166. Ramsden, C.A. and P.A. Riley, *Studies of the competing rates of catechol oxidation and suicide inactivation of tyrosinase*. *Archive for Organic Chemistry*, 2010. **2010**(10): p. 248-254.
167. McDowell, L.M., et al., *Rotational Echo Double Resonance Detection of Cross-links Formed in Mussel Byssus under High-Flow Stress*. *Journal of Biological Chemistry*, 1999. **274**(29): p. 20293-20295.
168. Jee, J.-G., S.-J. Park, and H.-J. Kim, *Tyrosinase-induced cross-linking of tyrosine-containing peptides investigated by matrix-assisted laser desorption/ionization time-of-flight mass spectrometry*. *Rapid Communications in Mass Spectrometry*, 2000. **14**(16): p. 1563-1567.
169. Kobayashi, S. and H. Higashimura, *Oxidative polymerization of phenols revisited*. *Progress in Polymer Science*, 2003. **28**(6): p. 1015-1048.
170. Jeon, J.-R., J.-H. Kim, and Y.-S. Chang, *Enzymatic polymerization of plant-derived phenols for material-independent and multifunctional coating*. *Journal of Materials Chemistry B*, 2013. **1**(47): p. 6501-6509.
171. Wei, Q., et al., *Mussel-Inspired Dendritic Polymers as Universal Multifunctional Coatings*. *Angewandte Chemie International Edition*, 2014. **53**(43): p. 11650-11655.
172. Faure, E., et al., *Catechols as versatile platforms in polymer chemistry*. *Progress in Polymer Science*, 2013. **38**(1): p. 236-270.
173. Yang, J., et al., *Reaction Pathways in Catechol/Primary Amine Mixtures: A Window on Crosslinking Chemistry*. *PLOS ONE*, 2016. **11**(12): p. e0166490.
174. Hall, H.K., *Correlation of the Base Strengths of Amines<sup>1</sup>*. *Journal of the American Chemical Society*, 1957. **79**(20): p. 5441-5444.
175. Zhang, T., et al., *A sensitive mediator-free tyrosinase biosensor based on an inorganic-organic hybrid titania sol-gel matrix*. *Analytica Chimica Acta*, 2003. **489**(2): p. 199-206.
176. Han, S., C. Kim, and D. Kwon, *Thermal degradation of poly(ethyleneglycol)*. *Polymer Degradation and Stability*, 1995. **47**(2): p. 203-208.
177. Glastrup, J., *Degradation of polyethylene glycol. A study of the reaction mechanism in a model molecule: Tetraethylene glycol*. *Polymer Degradation and Stability*, 1996. **52**(3): p. 217-222.
178. Han, S., C. Kim, and D. Kwon, *Thermal/oxidative degradation and stabilization of polyethylene glycol*. *Polymer*, 1997. **38**(2): p. 317-323.

179. Lange, M., et al., *Surface Functionalization of Poly(ether imide) Membranes with Linear, Methylated Oligoglycerols for Reducing Thrombogenicity*. *Macromolecular Rapid Communications*, 2012. **33**(17): p. 1487-1492.
180. Pillar, E.A., R. Zhou, and M.I. Guzman, *Heterogeneous Oxidation of Catechol*. *The Journal of Physical Chemistry A*, 2015. **119**(41): p. 10349-10359.
181. Rockcliffe, D.A. and A.E. Martell, *Oxidation reactions of a macrocyclic dinuclear copper(I) dioxygen complex and a dinuclear copper(II) complex*. *Inorganic Chemistry*, 1993. **32**(14): p. 3143-3152.
182. Yalfani, M.S., et al., *Phenol degradation by Fenton's process using catalytic in situ generated hydrogen peroxide*. *Applied Catalysis B: Environmental*, 2009. **89**(3-4): p. 519-526.
183. Mandal, A., et al., *Removal of catechol from aqueous solution by advanced photo-oxidation process*. *Chemical Engineering Journal*, 2004. **102**(2): p. 203-208.
184. Ohkubo, K., K. Miyata, and S. Sakaki, *Catalytic dioxygen insertion and aromatic ring opening of 3,5-di-*t*-butyl-catechol by iron(II) complexes including nitrogen counter ligands*. *Journal of Molecular Catalysis*, 1982. **17**(1): p. 85-88.
185. Hitomi, Y., et al., *Catalytic oxygenative degradation of 4-chlorocatechol by a nonheme iron(III) complex—Mechanism and prevention of catechol ester formation*. *Journal of Molecular Catalysis A: Chemical*, 2005. **240**(1-2): p. 207-213.
186. Walsh, J.G., et al., *Studies in the oxidative ring-opening of catechols and *o*-benzoquinones. Lead tetraacetate versus the copper(I) chloride/pyridine/methanol system*. *Tetrahedron*, 1999. **55**(38): p. 11519-11536.
187. Wardman, P., *Reduction Potentials of One-Electron Couples Involving Free Radicals in Aqueous Solution*. *Journal of Physical and Chemical Reference Data*, 1989. **18**(4): p. 1637-1755.
188. Qiao, X., et al., *Investigation of formation of superoxide anion radical in DMSO by ESR: Part 1. Influence of Fe<sup>2+</sup> and Cu<sup>2+</sup>*. *Magnetic Resonance in Chemistry*, 2001. **39**(4): p. 207-211.
189. Sakihama, Y., et al., *Plant phenolic antioxidant and prooxidant activities: phenolics-induced oxidative damage mediated by metals in plants*. *Toxicology*, 2002. **177**(1): p. 67-80.
190. Tsuji, J. and H. Takayanagi, *Oxidative cleavage reactions of catechol and phenol to monoester of *cis,cis*-muconic acid with the oxidizing systems of O<sub>2</sub>/CuCl, KOH/CuCl<sub>2</sub>*. *Tetrahedron*, 1978. **34**(6): p. 641-644.
191. Bonino, C.A., et al., *Real-time in situ rheology of alginate hydrogel photocrosslinking*. *Soft Matter*, 2011. **7**(24): p. 11510-11517.
192. Bowman, C.N. and C.J. Kloxin, *Toward an enhanced understanding and implementation of photopolymerization reactions*. *AIChE Journal*, 2008. **54**(11): p. 2775-2795.
193. Tung, C.-Y.M. and P.J. Dynes, *Relationship between viscoelastic properties and gelation in thermosetting systems*. *Journal of Applied Polymer Science*, 1982. **27**(2): p. 569-574.
194. Winter, H.H., *Can the gel point of a cross-linking polymer be detected by the G' – G'' crossover?* *Polymer Engineering & Science*, 1987. **27**(22): p. 1698-1702.
195. Ryczkowski, J., *IR spectroscopy in catalysis*. *Catalysis Today*, 2001. **68**(4): p. 263-381.

196. Božič, M., S. Gorgieva, and V. Kokol, *Homogeneous and heterogeneous methods for laccase-mediated functionalization of chitosan by tannic acid and quercetin*. Carbohydrate polymers, 2012. **89**(3): p. 854-864.
197. Seo, J., et al., *The impact of environment and resonance effects on the site of protonation of aminobenzoic acid derivatives*. Physical Chemistry Chemical Physics, 2016. **18**(36): p. 25474-25482.
198. Marin, L., B. Simionescu, and M. Barboiu, *Imino-chitosan biodynamers*. Chemical Communications, 2012. **48**(70): p. 8778-8780.
199. Dragone, V., et al., *3D-printed devices for continuous-flow organic chemistry*. Beilstein Journal of Organic Chemistry, 2013. **9**: p. 951-959.
200. Masaro, L. and X.X. Zhu, *Physical models of diffusion for polymer solutions, gels and solids*. Progress in Polymer Science, 1999. **24**(5): p. 731-775.
201. Bohrer, M.P., G.D. Patterson, and P.J. Carroll, *Hindered diffusion of dextran and ficoll in microporous membranes*. Macromolecules, 1984. **17**(6): p. 1170-1173.
202. Hagel, V., T. Haraszti, and H. Boehm, *Diffusion and interaction in PEG-DA hydrogels*. Biointerphases, 2013. **8**(1): p. 36.
203. Crank, J., *The mathematics of diffusion*. 1975, Oxford: Oxford University Press.
204. Cellesi, F., N. Tirelli, and J.A. Hubbell, *Towards a fully-synthetic substitute of alginate: Development of a new process using thermal gelation and chemical cross-linking*. Biomaterials, 2004. **25**(21): p. 5115-5124.
205. Siepmann, J., *Modeling of diffusion controlled drug delivery*. Journal of controlled release, 2012. **v. 161**(no. 2): p. pp. 351-362-2012 v.161 no.2.
206. Larm, O., B. Lindberg, and S. Svensson, *Studies on the length of the side chains of the dextran elaborated by Leuconostoc mesenteroides NRRL B-512*. Carbohydrate Research, 1971. **20**(1): p. 39-48.
207. De Smedt, S.C., et al., *Structural information on hyaluronic acid solutions as studied by probe diffusion experiments*. Macromolecules, 1994. **27**(1): p. 141-146.
208. Yuan, W., et al., *Non-invasive measurement of solute permeability in cerebral microvessels of the rat*. Microvasc Res, 2009. **77**(2): p. 166-73.
209. Amsden, B., *Solute Diffusion within Hydrogels. Mechanisms and Models*. Macromolecules, 1998. **31**(23): p. 8382-8395.
210. Lin, C.C. and A.T. Metters, *Hydrogels in controlled release formulations: network design and mathematical modeling*. Adv Drug Deliv Rev, 2006. **58**(12-13): p. 1379-408.
211. Lustig, S.R. and N.A. Peppas, *Solute diffusion in swollen membranes. IX. Scaling laws for solute diffusion in gels*. Journal of Applied Polymer Science, 1988. **36**(4): p. 735-747.
212. Am Ende, M.T. and N.A. Peppas, *Transport of ionizable drugs and proteins in crosslinked poly(acrylic acid) and poly(acrylic acid-co-2-hydroxyethyl methacrylate) hydrogels. II. Diffusion and release studies*. Journal of Controlled Release, 1997. **48**(1): p. 47-56.
213. Nugent, L.J. and R.K. Jain, *Plasma pharmacokinetics and interstitial diffusion of macromolecules in a capillary bed*. American Journal of Physiology - Heart and Circulatory Physiology, 1984. **246**(1): p. H129-H137.
214. Sharma, R.C. and R. Ali, *Hydrodynamic properties of mushroom tyrosinase*. Phytochemistry, 1981. **20**(3): p. 399-401.

215. Racheva, M., et al., *Purity of mushroom tyrosinase as a biocatalyst for biomaterial synthesis affects the stability of therapeutic peptides*. MRS Proceedings, 2015. **1718**: p. 85-90.
216. Mattinen, M.-L., et al., *Oxidation of peptides and proteins by *Trichoderma reesei* and *Agaricus bisporus* tyrosinases*. Journal of Biotechnology, 2008. **133**(3): p. 395-402.
217. Hernández-Romero, D., A. Sanchez-Amat, and F. Solano, *A tyrosinase with an abnormally high tyrosine hydroxylase/dopa oxidase ratio*. FEBS Journal, 2006. **273**(2): p. 257-270.
218. Byun, E., J.H. Ryu, and H. Lee, *Catalyst-mediated yet catalyst-free hydrogels formed by interfacial chemical activation*. Chemical Communications, 2014. **50**(22): p. 2869-2872.
219. Zaupa, A., et al., *Influence of Tyrosine-Derived Moieties and Drying Conditions on the Formation of Helices in Gelatin*. Biomacromolecules, 2011. **12**(1): p. 75-81.
220. Braeckmans, K., et al., *Three-Dimensional Fluorescence Recovery after Photobleaching with the Confocal Scanning Laser Microscope*. Biophysical Journal, 2003. **85**(4): p. 2240-2252.

### III. Abbreviations & Symbols

---

ACN	acetonitrile
ATR	attenuated total reflectance
BHT	butylated hydroxytoluene
Ch.	Chapter
$D_o$	diffusion coefficient in water
$D_g$	diffusion coefficient in hydrogel
DAT	desaminotyrosine/3-(4-hydroxyphenyl) propionic acid
DATT	desaminotyrosyl tyrosine
DCM	dichlormethane
DMF	<i>N,N</i> -dimethylformamide
<i>d</i>	deuterated
<i>D</i>	diameter
dopa	dihydroxyphenyl alanine
EDC·HCl	1-Ethyl-3-(3-dimethylaminopropyl) carbodiimide hydrochloride
ESI	electrospray ionization
ESR	electron spin resonance
Edeoxy	enzyme mushroom tyrosinase in the <i>deoxy</i> state
Emet	enzyme mTyr in the <i>met</i> state
Eoxy	enzyme mTyr in the <i>oxy</i> state
Eq.	equation
eq.	equivalent
<i>f</i>	oscillation frequency in rheology
Fig.	figure

FT-	IR Fourier transformation infrared spectroscopy
$G$	gel content
$G'$	elastic/storage modulus
$G''$	viscous/loss modulus
GPC	gel permeation chromatography
$^1\text{H-NMR}$	spectroscopy Nuclear Magnet resonance
$K_M$	Michaelis-Menten constant
LC-ESI-MS	liquid chromatography coupled with mass spectrometry
IOEG =	linear oligo(ethylene glycol)
ImOEG =	linear monodisperse oligo(ethylene glycol)
$M$	$\text{mol}\cdot\text{L}^{-1}$
MALDI-ToF	matrix-assisted lased desorption ionization, equipped with a time-of-flight
MBTH $\text{z}$ -	Methyl-2-Benzothiazolinonehydrazone hydrochloride or Besthorns
MeOH	Methanol
Me(O)	Methyl or methoxy
$M_c$	average molecular weight between crosslinks
$M_n$	number-average molecular weight
$m_{sw}, m_d$	mass of hydrogel in the swollen and dry state, respectively
MS	mass spectrometry
mTyr	mushroom tyrosinase from <i>Agaricus bisporus</i>
$m/z$	ratio of masse to charge
$N_A$	Avogadro constant ( $6.022\cdot 10^{23} \text{ mol}^{-1}$ )
NHS	<i>N</i> -hydroxysuccinimide
NMP	<i>N</i> -Methylpyrrolidone
NMR	nuclear magnetic resonance
<i>o</i> -	<i>ortho</i>
OEG	oligo(ethylene glycol)
<i>p</i> -	<i>para</i>
PBS	phosphate buffered saline
PPO	polyphenol oxidase
$Q$	volumetric degree of swelling
$R$	universal gas constant ( $8.314 \text{ J}\cdot\text{mol}^{-1}\cdot\text{K}^{-1}$ )
$r_H$	hydrodynamic radius
RI	refractive index
RP-	HPLC reversed phase-high performance liquid chromatography
r.t.	room temperature, 25 °C
$SD$	standard deviation
sOEG	star-shaped, 4arm oligo(ethylene glycol)
TBTU	2-(1H-Benzotriazole-1-yl)-1,1,3,3-tetramethyluronium tetrafluoroborate
Tyr	tyrosinase
UV-Vis	ultraviolet-visual
$\nu_c$	crosslinking density

$V_{\max}$	maximal reaction velocity
$v_s$	versus
$v_{sw}$	polymer volume fraction in the swollen state
( $v/v$ )	volume per volume
( $w/v$ )	weight per volume
wt	weight
$\gamma$	amplitude in rheology
$\delta$	chemical shift
$\epsilon$	molar absorption coefficient
$\eta^*$	complex viscosity
$\lambda$	wavelength
$\xi$	mesh size
$\pi$	3.14159
$\rho$	density
$\tau$	lag phase during enzymatic hydroxylation of monophenols

## IV. List of Figures

---

Figure 1: A scheme of network structure and network structure-property relationship .....	2
Figure 2: Concepts for controlled release from hydrogels:.....	5
Figure 3: Scheme of the catalytic cycle of mTyr (A) and enzyme-substrate complexes (B). .....	13
Figure 4: Concept of the planned experimental work. ....	18
Figure 5: Applied approaches towards the synthesis of DAT-IOEG <sub>OMe</sub> and DAT-ImOEG <sub>OMe</sub> as model oligomeric mTyr substrates.....	22
Figure 6: MALDI-ToF spectrum of DAT-IOEG <sub>OMe</sub> 2 kDa after purification by RP-HPLC (stationary phase based on polystyrene and divinylbenzene polymeric beads). ....	23
Figure 7: Chromatograms of DAT-ImOEG <sub>OMe</sub> before (A) and after (B) semi-preparative purification .....	25
Figure 8: MALDI-ToF spectrum of purified DAT-ImOEG <sub>OMe</sub> 2 kDa. ....	25
Figure 9: Chemical structures of DAT- and DATT-sOEG. ....	26
Figure 10: FT-IR spectra of DAT-sOEG 5 kDa (black) compared to the unfunctionalized precursor (red). ....	27
Figure 11: Scheme of the enzymatic conversion of monophenols to <i>o</i> -quinones (monophenolase mTyr cycle) .....	29
Figure 12: Specific activity of mTyr towards L-tyrosine (blue bars) and L-dopa (grey bars), .....	31
Figure 13: Tyrosinase activity towards L-dopa (blue bars) and L-tyrosine (grey bars) .....	32
Figure 14: Structures of mTyr substrates: natural, i.e. L-tyrosine and L-dopa; and artificial, DAT and DATT. ....	33
Figure 15: Kinetics of mTyr catalysis and specific activity with L-tyrosine, L-dopa, DAT and DATT ....	34
Figure 16: Dependence of mTyr kinetics on substrate concentration and MM plots for DAT and DATT and determined kinetic constants: .....	35
Figure 17: Kinetics of mTyr catalyzed oxidation of DAT(T) and DAT(T)-functionalized sOEG: .....	37

Figure 18: Proposed reaction scheme for network formation from DAT-functionalized OEG by tyrosinase (TYR) catalysis, involving enzymatic and non-enzymatic pathway.....	40
Figure 19: Formation of <i>o</i> -semiquinone radicals during mTyr catalysis. ....	42
Figure 20: UV-Vis absorption spectra of linear and branched DAT-OEG, oxidized by mTyr vs time....	44
Figure 21: Wavelength of maximum absorption $\lambda_{\text{max}}$ of model catechols, quinones and crosslinks. ...	45
Figure 22: UV-Vis absorption spectra of DAT-IOEG <sub>OMe</sub> mixed with differing amounts mTyr vs time..	46
Figure 23: FT-IR spectra for monofunctional DAT-IOEGOMe 2 kDa incubated with mTyr vs the non-oxidized precursor .....	49
Figure 24: <sup>1</sup> H-NMR spectra of mushroom tyrosinase (Tyr, purple), DAT (black) and a mixture thereof in D <sub>2</sub> O incubated for 15 mins (red), as well as 28 hours (blue) in D <sub>2</sub> O. ....	53
Figure 25: <sup>1</sup> H-NMR spectra of DAT (black) and the water-insoluble fraction of the oligomers formed by incubation of DAT with mTyr (>28 h), dissolved in A) D <sub>2</sub> O/NaOD (blue) and B) MeOH-d <sub>4</sub> . ....	54
Figure 26: <sup>1</sup> H-NMR spectra of DAT ester before (black) and after incubation with mushroom tyrosinase (Tyr) for 15 min (blue), 5 h (green) und 48h (red), recorded in MeOH-d <sub>4</sub> . ....	55
Figure 27: <sup>1</sup> H-NMR spectra of DAT-IOEG <sub>OMe</sub> before (black) and after incubation with tyrosinase mTyr in D <sub>2</sub> O/O <sub>2</sub> for 24 h (blue) und 7 d (red). ....	56
Figure 28: Prediction of possibly detected masses in model reactions with DAT ester. ....	58
Figure 29: MALDI-ToF spectra of DAT (A) and DAT-ester (B) in presence of mTyr 48 hours after addition of the biocatalyst, The sets of peaks indicate the formation of oligomers with up to 6 (A) or 11 (B) repeating units. ....	59
Figure 30: MALDI-ToF of DAT-IOEG <sub>OMe</sub> 10 kDa, incubated with mTyr for 2 h (top) and 8h (bottom). .	61
Figure 31: MALDI-ToF spectra of purified DAT-ImOEG <sub>OMe</sub> 2 kDa, incubated with mTyr for 1h (grey), 8h (blue) and 24h (green) in comparison to the unmodified precursor DAT-ImOEG <sub>OMe</sub> 2 kDa (red) and unfunctionalized NH <sub>2</sub> - ImOEG <sub>OMe</sub> 2 kDa (purple). ....	63
Figure 32: HPLC chromatogram of DAT-ImOEG <sub>OMe</sub> before (top) and after 24h of incubation with mTyr (bottom). ....	65
Figure 33: LC-MS analysis of model reactions of DAT-IOEG <sub>OMe</sub> 2 kDa and mTyr: .....	66
Figure 34: MALDI-ToF spectra of mTyr catalyzed reaction of DAT-ImOEG <sub>OMe</sub> with NH <sub>2</sub> -ImOEG <sub>OMe</sub> after 24 h. ....	68
Figure 35: Concept of alkaline hydrolysis of DAT-sOEG hydrogels. ....	71
Figure 36: Scheme of the hydrolysate investigation procedure .....	73
Figure 37: Spectroscopic analysis of fr <sub>1</sub> (black):.....	74
Figure 38: GPC elugram of fr <sub>1</sub> (above) and the hydrogel precursor DAT-sOEG 10 kDa (below), measured in DMF. ....	75
Figure 39: FT-IR and NMR analysis of fr <sub>2</sub> (blue):.....	76
Figure 40: Hydrogel formation by enzymatic catalysis.....	80
Figure 41: Gel time determination by rheology:.....	83
Figure 42: Summary of the gelation time.....	84
Figure 43: <sup>1</sup> H-NMR spectra of mTyr-crosslinked hydrogels from DAT- (–) and DATT-sOEG (–) .....	86
Figure 44: FT-IR spectra of dried hydrogel films crosslinked with 100 and 500 U·mL <sup>-1</sup> mTyr compared to the oligomeric precursor DAT-sOEG 10 kDa. ....	88
Figure 45: Summary of the equilibrium swelling of hydrogels from DAT(T)-sOEG crosslinked with mTyr.....	91
Figure 46: Summary of storage moduli $G'$ of hydrogels from DAT- and DATT-sOEG with different $M_n$ , crosslinked with mTyr, T (100 or 500 U·mL <sup>-1</sup> ), as analyzed in rheological time sweeps at 37 °C (n≥3). 92	

Figure 47: Cumulative release and theoretical data fit for the diffusion of FITC dextrans .....	95
Figure 48: Diffusion coefficients $D_g$ of FITC dextran (FDx) with different $M_n$ in hydrogels from DAT(T)-sOEG precursors, crosslinked with 100 or 500 U·mL <sup>-1</sup> mTyr (DAT(T) <sub><math>M_n</math></sub> -mTyr concentration).....	97
Figure 49: Purity of mTyr affects the stability of therapeutic peptides.....	101
Figure 50: Release of heparin from hydrogels with varying DAT-sOEG 10 kDa precursor concentration. ....	102
Figure 51: Scheme of the formation of dopachrome from L-tyrosine or L-dopa by tyrosinase catalysis. ....	116
Figure 52: Scheme of the proposed reaction mechanism of MBTH assay. ....	117

## V. List of Tables

---

Table 1: Summary of characteristics of different synthesized DAT-IOEGOMe oligomers .....	22
Table 2: Summary of sOEG characteristics after DAT and DATT functionalization: $M_n$ measured by MALDI-ToF, given in parenthesis, degrees of DAT(T) functionalization. ....	28
Table 3: Structures of intermediates and netpoints, potentially formed after mTyr catalyzed crosslinking of DAT-IOEG <sub>OMe</sub> , and prediction of their <sup>1</sup> H-NMR signals in D <sub>2</sub> O.....	51
Table 4: Proposed structures of multimers of DAT ester in H <sub>2</sub> O/O <sub>2</sub> in presence of mTyr after 48h based on assignment of calculated and detected masses by MALDI-ToF in two independent measurements (1 and 2). ....	60
Table 5: Semi-quantitative estimation of NH <sub>2</sub> -ImOEG(24) <sub>OMe</sub> incorporation in netpoints after 24 h of mTyr incubation.....	69
Table 6: Proposed structures of dimers formed from DAT-ImOEG <sub>OMe</sub> + NH <sub>2</sub> -ImOEG <sub>OMe</sub> solutions by mTyr catalysis based on assignment of theoretically expected masses and detected m/z by MALDI-ToF. M = monophenol (DAT), D = <i>o</i> -diphenol, Q = <i>o</i> -quinone, MA = Michael addition. ....	70
Table 7: Screening of precursor capacity to serve as precursors for hydrogel synthesis by biocatalysis with mTyr. The hydrogel formation was confirmed by tube tilting. ....	81
Table 8: Properties of preformed hydrogels from DATT-sOEG 10 kDa with <i>d.f.</i> of 66 and 90 mol% (DATT <sub>0.7</sub> and DATT <sub>0.9</sub> respectively).....	85
Table 9: Summary of the gel contents $G$ of hydrogels from DAT- and DATT-sOEG with different $M_n$ , crosslinked with 100 or 500 U·mL <sup>-1</sup> mTyr ( $n = 3$ ).....	90
Table 10: Mesh sizes $\xi$ of hydrogels from DAT(T)-sOEG crosslinked with different concentrations of biocatalyst mTyr. $\xi \pm$ standard deviation was calculated from the elastic moduli of hydrogels, determined by rheology at 37 °C ( $n \geq 3$ ). ....	93
Table 11: Summary of relative amounts of mTyr extracted from DAT(T)-sOEG hydrogels crosslinked by mTyr catalysis ( $n = 3$ ). ....	99

## VI. Curriculum Vitae

---

For reasons of data protection, the curriculum vitae is not published in the electronic version.